PNC TN9410 96-140

Simulation of Crack Propagation in a Pre-Cracked Tube Subject to Thermal Cyclic Loading

January 1996

O-arai Engineering Center
Power Reactor and Nuclear Fuel Development Corporation

PNC TN9410 96-140
January, 1996

Simulation of Crack Propagation in a Pre-Cracked Tube Subject to Thermal Cyclic Loading

Sunil FELIX*

ABSTRACT

This study was undertaken to reproduce numerically crack propagation tests in a pre-cracked tube subject to thermal cyclic loading (radial temperature gradients varying with time).
The experimental tests simulated are part of the ATTF experimental program (Air cooled Thermal Transient Test Facility), carried out at OEC/PNC.
The simulation is performed using two techniques, the Energy Release Rate Method (or G-Theta Method), programmed in the Finite Element computer code CASTEM 2000 developped at CEA (FRANCE), and the Js Simpilified Method of the A-16 Appendix of the French RCCMR. It is then compared to experimental data and to numerical results obtained from PNC's Finite Element computer code FINAS.
From elastic and plastic Finite Element analysis, the G-Theta procedure and the Js Method allow us to obtain the evolution of the J-variation versus the crack length. Paris' law then leads to an evaluation of the crack length versus the number of cycles.
It is shown that the elastic prediction of crack growth using the G-Theta Method is close to FINAS' results, and very close to measured values. The plastic prediction using the Simplified Method is slightly better than the one using the G-Theta procedure, but both agree well with the experimental results. FINAS' predictions in the plastic case are better, but a different definition of the J-variation is used.
This study confirms that the G-Theta procedure of CASTEM 2000 and the Js-Method of the A-16 Appendix of the French RCCMR are in good agreement with PNC's simulation methods, and that they are well suited for crack propagation analysis in the case of thermal cyclic loading.

*International Fellow
O-arai Engineering Center, OEC/PNC
Advanced Technology Division
Structure and Material Research Section

公　開　資　料
PNC TN9410 96-140
1 9 9 6 年 1 月

繰り返し熱過渡を受ける予き裂付円筒のき裂進展シミュレーション

Sunil FELIX*

要　旨

この研究は繰り返し熱過渡を受ける（半径方向の温度分布が時間とともに変化する）予き裂付円筒のき裂進展を数値解析によって再現することを目的として実施した。

シミュレーションに用いた試験は動力炉・核燃料開発事業団大洗工学センターで実施されたATTF試験の一部である。

シミュレーションは2つの方法で行った。すなわち、エネルギー開放法とフランスのRCCMRの付録A-16のJ積分による簡易法である。前者はCEA（フランス）で開発された有限要素コードCASTEM2000を用いて行う。シミュレーション結果を、試験データ及び動力炉・核燃料開発事業団の有限要素コードFINASによる数値シミュレーション結果と比較した。

有限要素法による弾性解析及び塑性解析においてはG－θ法とJ積分による簡易法によりΔJとき裂長さの関係を得ることができる。次にParis則により繰り返し数とき裂長さの関係を得ることができる。

G－θ法を用いた弾性解析による予測では、FINAS に近い結果を得た。また、この結果は試験結果と非常によく再現した。簡易法を用いた塑性解析による予測結果はCASTEM2000を用いた結果よりもやや良好であったが、両者とも試験結果とよく一致した。塑性解析においてはFINASの結果の方が良好であったが、ΔJの定義が異なっている。

本研究により、CASTEM2000のG－θ法とフランスのRCCMRの付録A-16のJ積分簡易法は動力炉・核燃料開発事業団の数値解析法とよく一致すること、さらにこれらの方法は繰り返し熱応力下のき裂進展解析に有効であることが検証できた。

* 大洗工学センター 基盤技術開発部 構造・材料技術開発室
国際特別研究員

Table of Contents

List of Tables

List of Figures

I / Introduction

This work covers one part of the research program set up by OEC/PNC (JAPAN) for Fiscal Year 1995, namely step 1 of "Crack Propagation Analysis" (Part I.B) (see flow chart 1).

Its purpose is to apply two sets of numerical tools for the simulation of crack propagation.

The first one, programmed in the Finite Element computer code CASTEM 2000, allows the study of crack behaviour from the computation of various Fracture Mechanics parameters, such as the rate of energy release J, C*, etc ... In what follows, we shall refer to this first set of tools as the Energy Method, or the G-θ procedure.

The second set of tools, called the Simplified Methods, is an extension of the French RCCMR rules (A-16 Appendix of the RCCMR). It describes simplified methods to determine J, C*, and various other parameters, from elastic estimations corrected to account for the true non-linear behaviour of the material.

We used these tools to simulate thermal fatigue crack growth tests performed at OEC/PNC, on preflawed specimens.

In what follows, we shall describe :

. the basic principles on which are built CEA's numerical tools
. the experimental data avalaible at OEC/PNC
. the results and discussion of the simulation

II / Description of Crack Propagation Analysis

II.1 / The G-θ procedure

Its purpose is to compute the rate of energy release G in elastoplasticity and C* in creep.

We assume that the problem remains linear from a geometrical point of view (small displacements and small strains), and that the behaviour of the structure can be considered elastic non-linear. An elastoplastic behaviour can be considered non-linear elastic if the load applied to the cracked structure increases monotonously.

Basic principles of the G-θ procedure :

The rate of energy release G is defined as the decrease of potential energy Π during an increase dA of the crack area :

$$G = -\frac{d\Pi}{dA}$$

It can be shown that G is expressed as a boundary integral, defined around a domain surrounding the crack tip. Thus, G becomes equivalent to Rice's integral J :

$$J = \int_{\Gamma} W dx_2 - \vec{t}\frac{\partial \vec{U}}{\partial x_1} d\Gamma$$

where

$W = \int \sigma \; d\varepsilon_m$ is the energy density of mechanical strain

$\vec{t} = \bar{n}\sigma$ is the stress vector on the side perpandicular to the normal unit vector $\bar{n}$

$\frac{\partial \vec{U}}{\partial x_1} =$ displacement gradient vector in the direction of the crack

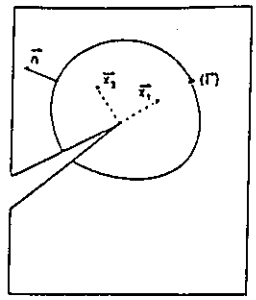

- Domain for the computation of Rice J-integral -

The final expression of G, programmed in CASTEM 2000, accounts for exterior forces close to the crack, thermal load, variation of mechanical properties with temperature, presence of an interface separating two different materials.
A detailed description of each of these terms and of the final expression of G programmed in CASTEM 2000 can be found in [1].

II.2 / The A-16 Simplified Method

The A-16 Appendix of the French RCCMR provides rules to study the nocivity of a flaw in a structure. These rules are based on Fracture Mechanics, and require :

. the identification of a flaw : it will be considered to be a crack
. the study of its initiation and propagation in the case of fatigue loading
. the study of its stability
. the study of its behaviour if creep has to be accounted for

Phenomena different from creep and fatigue are not considered.

As the experimental tests we have to simulate as a first stage only concern fatigue propagation, we shall now describe the different steps to be followed to apply the A-16 rules for crack propagation analysis. Such rules make up the Js Method [2].

The flow chart of the Js Method is given below :

- Flow Chart 1 -

Part I (Fiscal Year 1995)
Base Metal Samples and/or Weld Metal Samples

-I.A- Crack Initiation Analysis

Purpose :

Application of Local Methods :
Damage equations to determine Crack Initiation

Step 1 :

Simulation of a tensile creep test on a perfect (uncracked) sample

Step 2 :

Extension of step 1 to the case of cyclic loading (creep/fatigue) on a perfect sample

-I.B- Crack Propagation Analysis

Purpose :

Application of Energy and Simplified Methods to analyze crack propagation
Comparison with PNC's experimental data

Step 1 :

Simulation of cyclic/loading (creep/fatigue) on a pre-cracked sample

Part II (Fiscal Year 1996)
Extension of Part I to the Case of Welded Joints

- Flow Chart 2 -

General Algorithm of the

A-16 Appendix

Js Method

Principal : Calculate $\delta a = \frac{dA}{dN} =$ crack propagation per cycle

$= C \times \left[q_R \times \sqrt{E \times \Delta J} \right]^n$

C, n = coefficients of Paris' law

Problem : Evaluate q_R and ΔJ

Step 1 :

Perform a thermoelastic analysis on a whole cycle

Compute the nominal (far from the defect) elastic stresses ;

+ primary membrane stress ΔP_{mno}
+ primary bending stress ΔP_{bno}
+ secondary membrane stress ΔQ_{mno}
+ secondary bending stress ΔQ_{bno}

Step 2 :

Compute the nominal reference stress

$$\Delta\sigma_{noref} = f(\Delta P_{mno}, \Delta P_{bno}, \Delta Q_{mno}, \Delta Q_{bno})$$

Step 3 :

Compute the true nominal reference stress (Neuber' s hyperbola)

$$\Delta\sigma_{nor}$$

Step 4 :

Compute the first corrective factor KJ_1

$$KJ_1 = \left[\frac{\Delta\sigma_{nor}}{\Delta\sigma_{noref}} \right]^2$$

Step 5 :

Compute the shape factor q_R

$$q_R = \frac{1 - R/2}{1 - R} \quad if \quad R < 0$$

$$R = \frac{\min K_1}{\max K_1}$$

$$q_R = \frac{1}{1 - R} \quad if \quad R \geq 0$$

Step 6 :

Loop on all the cycles
(Computation of fatigue crack propagation)

Step 6a : Evaluate the stress intensity factor ΔK_1 from :
+ the elastic nominal stresses
+ the dimensions of the crack

Step 6b : Evaluate $\Delta J_{elastic} = \frac{\Delta K_1^2}{E^*}$

Step 6c : Compute the elastic stresses in the section of the flaw:
+ primary membrane stresses ΔP_{mdef}
+ primary bending stresses ΔP_{bdef}
+ secondary membrane stresses ΔQ_{mdef}
+ secondary bending stresses ΔQ_{bdef}

Step 6d : Compute the reference stress near the flaw

$$\Delta\sigma_{defref} = f(\Delta P_{mdef}, \Delta P_{bdef}, \Delta Q_{mdef}, \Delta Q_{bdef})$$

Step 6e : Compute the true reference stress near the flaw using Neuber' s rule (and the corresponding strain)

$$\Delta\sigma_{defr} \ , \ \Delta\varepsilon_{defr}$$

Step 6f : Compute the second corrective factor KJ_2

$$KJ_2 = \frac{E \ \Delta\varepsilon_{defr}}{\Delta\sigma_{defr}} + \Delta\Psi$$

$$\Delta\Psi = \frac{0.5\left[\Delta\sigma_{defr}\right]^2}{\Delta\sigma_{defr} + 4R_{0.002}^2}$$

Step 6g : Compute ΔJ

$$\Delta J = KJ_1 \times KJ_2 \times \Delta J_{elastic}$$

Step 6h : Compute the fatigue propagation using Paris'law

δa = Crack propagation rate

$$= C \times \left[q_R \times \sqrt{E \times \Delta J}\right]^n$$

Step 6i : Update the total crack length

$$a = a + \delta a$$

End of step 6, i.e. end of loop on the cycles

($R_{0.002}$ corresponds to the yield stress, taken as the stress that leads to a strain equal to 0.2%).

III / Description of the experimental data to be simulated

The experimental data to be simulated is obtained from the ATTF program (Air cooled Thermal Transient Test facility). This program includes various tests, among which the CPTT010 and CPTT102 tests, aimed at analyzing thermal fatigue crack growth on preflawed specimens.

. In these two series of tests, the specimens are made of forged type 304 Stainless Steel cylinders (300 mm long, 30 mm thick, 70 mm interior diametre), with an axisymetrical circumferential initial crack prepared by electric discharged machining on the inner surface. Various samples were manufactured, each one of them with one particular crack length. The different crack lengths obtained are :

a_0 = 1mm, 2mm, 3mm, 5mm, 9mm, 15mm, 20mm, 25mm

Each specimen is first gradually heated by an electrical furnace up to a temperature of 650 $^{\circ}C$, and then exposed to a cold transient by pressurized air. The air is blown into the cylinder for 90 s. After 210 s, the heating up process is restarted, and the whole body is then brought back uniformally to 650 $^{\circ}C$. A complete thermal cycle lasts 24 minutes. Crack size is measured by ultrasonic examination [3].
The temperature history observed during a whole cycle is shown on figure 1 (distances are measured from the inner surface of the tube, in the radial direction).
It is assumed that a non-linear temperature gradient exists in the thickness of the wall (radial direction), but that the temperature distribution does not depend on the z-coordinate (axial direction).

IV / Presentation of the numerical simulation

IV.I / Details about the use of the numerical tools

A / The G-θ procedure

The simulation carried out with the G-θ procedure is achieved by calculating the stress/strain field in the structure for each crack length. The results are then used for the determination of the J-integral by the G-θ procedure.

These two steps are performed in the elastic and plastic cases, using the Finite Element code CASTEM 2000.

This allows us to compute, for each crack length, the following quantity :

$$\Delta J = J_{max} - J_{min}$$

where

J_{max} = maximum value of J on a cycle
J_{min} = minimum value of J on a cycle

which leads to the relationship :

$$\Delta J = f(a_0)$$

where

a_0 = initial crack length

From the following equations

$$\frac{da}{dN} = C(\Delta J)^n \quad \text{(Paris' law)}$$

N = total number of cycles

a_i = crack length at cycle number i

$$= a_{i-1} + \frac{da}{dN}$$

$$= a_{i-1} + C\left[f(a_{i-1})\right]^n$$

we plot the crack length versus the number of cycles :

$$a = g(N)$$

The results are then compared to experimental data, and to numerical predictions got using OEC/PNC's Finite Element code FINAS.

B / The J_S Simplified Method

The J_S method only considers the case of a thermal gradient, linear in the wall thickness.
In what follows, we describe in detail the general steps given in the previous flow chart (see flow chart 2).

Assumption :

The temperature gradient is radial and linear in the wall thickness

Detail of each step of flow chart 2 :

Step 1 :

+ Thermoelastic Analysis performed on a whole cycle.
+ As the load is purely thermal, stresses are all secondary. They are made up of axial and circumferential components, each one being decomposed into membrane and bending parts.

Nominal Stresses :

+ axial bending stresses

$$\sigma_{no}Q_{1b} = \frac{E\,\alpha\,\Delta T}{2(1-\nu)}$$

+ axial membrane stresses

$$\sigma_{no}Q_{1m} = -\left[\frac{E\,\alpha\,\Delta T}{2(1-\nu)}\right]\left[\frac{t}{6\,r_i}\right]$$

+ circumferential bending stresses

$$\sigma_{no}Q_{2b} = \frac{E\,\alpha\,\Delta T}{2(1-\nu)}$$

+ circumferential membrane stresses

$$\sigma_{no}Q_{2m} = \left[\frac{E\,\alpha\,\Delta T}{2(1-\upsilon)}\right]\left[\frac{t}{3\,r_i}\right]$$

(The proof of these formula can be found in [4]).

Step 2 :

Computation of the reference stress

$$\sigma_{ref} = \underset{ti,tj\,cycle}{Max} \left| \overline{\sigma\,Q(t_i) \;-\; \sigma\,Q(t_j)} \right|$$

where

$\overline{\sigma\,Q(t_i)}$ = equivalent stress

$$\left(\overline{\sigma\,Q(t_i)}\right)^2 = \left(\sigma_{1m}^2 + \sigma_{2m}^2 - \sigma_{1m}\sigma_{2m}\right) + \left(\frac{2}{3}\right)^2 \left(\sigma_{1b}^2 + \sigma_{2b}^2 - \sigma_{1b}\sigma_{2b}\right) +$$

$$\frac{2}{3\sqrt{3}} \left| \sigma_{1m}\sigma_{1b} + \sigma_{2m}\sigma_{2b} - 0.5\left(\sigma_{1m}\sigma_{2b} - \sigma_{2m}\sigma_{1b}\right)\right|$$

= equivalent stresses used in shell elements. They allow to account for axial and circumferential components of membrane and bending stresses.

We select the times t_1 and t_2 in a cycle which verify the above maximum relation.

Step 3 :

Computation of the true nominal reference stresses to account for the non-linear behaviour of the material (Neuber's rule).

Step 4 :

Computation of the first corrective factor

Step 5 :

Computation of the cycle shape factor q_R

$$\min K_1 = 0 \Rightarrow R = 0 \Rightarrow q_R = 1$$

Step 6 :

Loop on the cycles

Step 6a-b :

No formula provide us with an expression for ΔK_1, corresponding to the dimensions of the tube studied. $\Delta J_{elastic}$ for crack length a_i is thus obtained from linear interpolation of $J_{elastic}$ between J_k and J_p $(a_k \le a_i \le a_p)$.

Step 6c :

Computation of elastic stresses near the defect :

+ axial membrane stresses :

$$\sigma_{def} Q_{1m} = -\left[\frac{E\,\alpha\,\Delta T}{2(1-\nu)}\right]\left[\frac{t}{6\,r_i}\right]$$

+ circumferential membrane stresses :

$$\sigma_{def}\, Q_{2m} = \left[\frac{E\,\alpha\,\Delta T}{2(1-\nu)}\right]\left[\frac{t}{3\,r_i}\right]$$

+ bending axial stresses :

$$\sigma_{def}\; Q_{1b} = \frac{6\; M_z^{EF}}{(t-a)^2}$$

$$M_z^{EF} = \textit{bending moment} = \int_{ligament} x\left[\sigma_{ZZ}(x) - \sigma_{ZZmean}^{ligament}\right]dx$$

+ bending circumferential stresses :

$$\sigma_{def}\; Q_{2b} = \frac{E\,\alpha\,\Delta T}{2(1-\nu)}$$

Step 6d :

Computation of the reference stress near the defect (same formula as in step 2)

Step 6e :

Computation of the true reference stress near the defect (Neuber's rule)

Step 6f :

Computation of the second corrective factor

Step 6g :

Computation of ΔJ

Step 6h :

Computation of $\frac{da}{dN}$

Step 6i :

Update of the final crack length a

End of step 6

IV.2 / Load applied to the structure

The temperature history obtained from heat transfer analysis on a whole cycle is shown on figure 1.

IV.3 / Mechanical characteristics used in the analysis

In both elastic and plastic analysis, the mechanical characteristics are allowed to vary with temperature. The characteristics are taken from the report published by OEC/PNC, in which is described the Finite Element simulation of tests CPTT010 and CPTT102 using FINAS [3].

Table 1 gives the mechanical characteristics used.

In the plastic case, the material is considered to follow a linear kinematic model.

IV.4 / Finite Element mesh used in the CASTEM 2000 simulation

For each crack length, a specific mesh is created. Figure 2a shows the mesh corresponding to a 15mm crack. Figure 2b is a zoom of the mesh around the crack tip P_f. The use of the $G-\theta$ procedure requires the definition of a domain around the crack tip. This domain is defined by the number of layers of elements around P_f. For comparison, FINAS' mesh is shown in figure 3.

Computation is performed in a 2-D axisymmetrical configuration.

The same boundary conditions are used as in FINAS :

+ $U_z\,(ligament) = 0$
+ *Same* U_z *displacement for all the nodes of the upper edge of the structure*

IV.5 / Results and discussion

A / Displacement results

Figures 4.a.1 to 4.h.1 (CASTEM 2000) show good agreement with figures 4.a.2 to 4.h.2 (FINAS) (Uz displacement of the crack in the elastic case).

The same conclusion can be reached in the elastoplastic case (figures 5.a.1 to 5.a.2 (CASTEM 2000) and figures 5.a.2 to 5.h.2 (FINAS)).

B / Stress/strain results

Stresses and strains are plotted versus time at a point A close to the crack tip. The location of this point is shown on the corresponding figures (distances are counted from the center of the tube). As CASTEM 2000's mesh is different from FINAS', the location of A is not exactly the same in both simulations.

Figures 6.a.1 to 6.h.1 (CASTEM 2000) and figures 6.a.2 to 6.h.2 (FINAS) show the stresses versus time in the elastic case, while figures 7 correspond to the elastoplastic one. In both cases, CASTEM 2000 and FINAS give very close results.

The same conclusion can be drawn from figures 8 (axial stress and strain histeresis curve).

C / ΔJ results

C.1 - The G-θ procedure

ΔJ is defined within a cycle as :

$$\Delta J = J_{max} - J_{min}$$

In the elastic case, the minimum and maximum values of stresses on the inner surface of the tube appear at 0s for the minimum value, and around 70s for the maximum value, as can be seen on the stress profiles (Figures 9.a.b.c)

The minimum and maximum values of the stress intensity factor K and of the $J_{elastic}$ integral thus appear at the same times (0 and 70 seconds). Therefore :

$$J_{min} = 0$$
$$\Delta J = J_{max} - J_{min}$$
$$\Delta J = J_{max}$$

Figures 10 give the J values throughout a cycle, for each crack length.
Figure 11 shows the curve ΔJ versus the initial crack length in elasticity.

In the plastic case, the high levels of plastic strains reached on the inner surface of the tube during loading ($t \leq 90s$) lead to very high compressive stresses during the unloading phase ($t \geq 90s$), as can be seen on figures 12a,b,c (figures 13,a,b,c represent the corresponding equivalent plastic strain).
Figures 12a,b,c show that the maximum value of stresses occurs around 60s, during loading, while the minimum value of stresses occurs around 120s (during unloading).
From 60s to 120s, the loading history is not monotonous. Although, from a theoretical point of view, it is not valid to calculate J on a whole cycle, we still computed its values for each crack length (see figures 14a,b), thus leading to J_{max} and J_{min} values. These curves distinctly show J_{max} at 60s and $J_{min} \leq 0$ (around 120s), with J_{min} negligible compared to J_{max}. It was then decided to consider $J_{min} = 0$ for the rest of the analysis.
Figure 14 also shows that throughout a cycle, the value of J does not depend on the number of layers of elements contained in the domain used to calculate it.
Therefore, in plasticity, the expression for ΔJ remains the same as in elasticity :

$$\Delta J = J_{max} - J_{min}$$
$$= J_{max}$$

Figure 15 shows ΔJ versus the initial crack length in plasticity.

C.2- The J_S Simplified Method

As described in II.2/, the simplified method allows the computation of the crack growth rate per cycle from the evaluation of a value of ΔJ, namely ΔJ_S.

Application of the previous algorithm leads to the computation of ΔJ_s at each cycle, which in turn allows us to plot the curve ΔJ_s versus the crack length (figure 16).

Figures 11, 15 and 16 show that $\Delta J_{elastic}(G-\theta)$ is higher than $\Delta J_{plastic}(G\text{–}\theta)$, which seems natural, as the elastic evaluation of stresses is higher than the plastic one ; it is also seen that $\Delta J_{plastic}(G\text{–}\theta)$ is very close to $\Delta J_{plastic}(A-16)$.

Figures 17a, b, c show $J_{plastic}$ for each crack length, calculated by $G-\theta$ and FINAS.

It has to be specified that FINAS' crack growth evaluation using Paris' law was performed using the values of J computed from the stress field corresponding to the second cyle, while CASTEM 2000's J values were obtained from the first cycle stress field.

In CASTEM's predictions, we see that, in the unloading zone, for some crack lengths, such as 3mm, 20mm, we lose the path-independence property of the J-integral (see figures 17b, c with J calculated using several layers of elements around the crack tip).

It also clearly appears that in the loading region ($t \leq 90s$), CASTEM 2000 and FINAS give very close results, even regarding the maximum value of J. In the unloading phase, there is a distinct discrepancy between the two codes in the estimation of $J_{\min}$. It can be concluded that :

$$\left| J_{\min}(FINAS) \right| \geq \left| J_{\min}(CASTEM\,2000) \right| \approx 0$$

If, in CASTEM 2000's predictions, the J values had been computed as inFINAS', i.e. using the second cycle stress field, the same conclusion would have been reached, as can be seen on figures 17d,e,f,g. These figures display the evolution, with time, of $J_{FINAS}^{second\ cycle}$, $J_{CASTEM\,2000}^{second\ cycle}$ and $J_{CASTEM\,2000}^{first\ cycle}$. Here too, we see that :

$$\left| J_{\min-FINAS}(Cycle\,2) \right| > \left| J_{\min-CASTEM\,2000}(Cycle\,2) \right|$$

Figures 17h,i represent $\Delta J_{elastic}(FINAS)$ and $\Delta J_{plastic}(FINAS$. It appears that $\Delta J_{elastic}(G-\theta)$ (figure 11) is very close to $\Delta J_{elastic}(FINAS)$, and that $\Delta J_{plastic}(FINAS)$ is greater than

$\Delta J_{plastic}(CASTEM\,2000)$ (figure 15). It can also be seen that $\Delta J_{plastic}(FINAS)$ is almost 1.5 times higher than $\Delta J_{elastic}(FINAS)$.

The definition of ΔJ used in FINAS changes, whether one considers the elastic case or the plastic one.

In elasticity, the definition used is :

$$\Delta J_{elastic}(FINAS) = J_{\max} - J_{\min} = J_{\max}$$

which is the same one as the one used in CASTEM's prediction. That explains the good agreement between $\Delta J_{elastic}$ given by the two codes (figures 11 and 17h).

In plasticity, in the FINAS' prediction, ΔJ is defined differently, using the following equations :

$$K_{\max} \equiv \sqrt{E \times J_{T\max}}$$
$$(T = tension \quad J_{T\max} = J_{\max}\ during\ loading\ )$$

$$K_{\min} \equiv -\sqrt{E \times J_{C\max}}$$
$$(C = compression \quad J_{C\max} = J_{\max}\ during\ unloading\ )$$

As $K_{\min} \leq 0$, ΔK is defined as :

$$\Delta K = K_{\max} - K_{\min}$$
$$= \sqrt{E \times J_{T\max}} + \sqrt{E \times J_{C\max}}$$

ΔJ is then calculated by writing :

$$\Delta J = \frac{\Delta K^2}{E}$$

which leads to

$$\Delta J = J_{T\max} + J_{C\max} + 2\sqrt{J_{T\max} \times J_{C\max}}$$

$J_{T\max}$ occurs during loading and is positive. $J_{C\max}$ occurs during unloading and is negative. As from a physical point of view, J should be positive, the absolute value of $J_{C\max}$ is considered. Therefore :

$$\Delta J_{plastic}(FINAS) = J_{T\max} + J_{C\max} + 2\sqrt{J_{T\max} \times J_{C\max}}$$
$$\geq J_{T\max} = \Delta J_{plastic}(CASTEM\,2000)$$

Thus, if $J_{C\max}$ is assumed negligible compared to $J_{T\max}$, then :

$$\Delta J_{plastic}(FINAS) = \Delta J_{plastic}(CASTEM\,2000)$$

Somehow, the values of $\Delta J_{plastic}(FINAS)$ can be questionned, as they are obtained using $J_{C\min}$ quantities different from 0. These quantities are computed during unloading, i.e. outside the validity domain of J. That could explain the good agreement between $J_{\max}^{plastic}(FINAS)$ and $J_{\max}^{plastic}(CASTEM\,2000)$, and the discrepancy between their minimum values.

Moreover, as seen previously, the definition adopted by FINAS for $\Delta J_{plastic}$ leads to :

$$\Delta J_{plastic}(FINAS) \geq \Delta J_{elastic}(FINAS)$$

which seems in contradiction with the fact that a thermal load, being equivalent to imposed strain, would lead to a decrease of the stresses with plasticity (in comparison with elastic stresses), and therefore to $J_{plastic}$ values smaller than $J_{elastic}$ ones. We should thus have :

$$\Delta J_{plastic}(FINAS) \leq \Delta J_{elastic}(FINAS)$$

That is why in CASTEM 2000's predictions, we prefer not to take the $J_{\min}$ values into account, thus setting them equal to 0.

D / Crack growth results

Having computed ΔJ from elastic and plastic analysis, the crack growth rate is obtained using Paris'law :

$$\frac{da}{dN} = C \times \Delta J^{n}$$
$$C_{\max} = 4.0430E-3$$
$$C_{nom} = 1.2022E-3$$
$$C_{\min} = 3.5753E-4$$
$$n = 1.4435$$

Figure 18 shows the crack growth versus the number of cycles in the elastic case. There is good agreement with the experimental values, using C_{nom}, where as C_{max} and C_{min} lead to larger and lower predictions.

Figure 19 shows the crack growth in the plastic case, computed with CASTEM 2000. In spite of some discrepancy with the measured data, the prediction is good using the maximum and nominal values of C, but too low using its minimum value.

The same phenomenon is observed in the case of the A-16 predictions (see figure 20). The discrepancy can be explained by the assumption that the temperature gradient is linear throughout the wall thickness. Linearized expressions are thus used for the stresses. But at one stage of the computation, the non-linear stresses are accounted for, as $\Delta J_{elastic}$ is computed using the real stress field.

Figures 21, 22, 23 indicate that the A-16 predictions are slightly higher, thus better than G-θ 's.

Figure 24 shows FINAS' predictions. The elastic one is very close to CASTEM 2000's, but the plastic one is higher than CASTEM 2000's, as :

$$\Delta J_{plastic}(FINAS) > \Delta J_{plastic}(CASTEM\,2000)$$

Therefore, FINAS's plastic predictions are closer to the experimental values than CASTEM 2000's.

As seen previously, in plasticity, both the codes would give the same crack growth estimations if the same definition of $\Delta J_{plastic}$ had been adopted.

Figure 25 shows a prediction using PNC's Simplified Method. This method [5-6] uses a database of non-dimensional values of stress intensity factors for a crack on various types of structures, subjected to unit distributed loads of the 0-th order to the 3rd order on its surface, as shown on the figure below. The major portion of the database is built with reference to published results. In addition, a series of FEM analyses were carried out to extend the database. One can therefore evaluate K for an arbitrary crack by using this database and stress

analysis on an uncracked body. The FEM analyses leads to $\sigma_{membrane}$, $\sigma_{bending}$, $\sigma_{parabolic}$. K is then written as :

$$K = K_{1mem} + K_{2ben} + K_{3par}$$

and then converted into J-integral, assuming plane stress :

$$J = \frac{K^2}{E}$$

J is further converted into elasto-plastic J-integral, following the CEGB R6 Method :

$$J_{ep} = f_{ep} \times J$$

with

$$f_{ep} = E\frac{\varepsilon_R}{\sigma_R} + \left\{\frac{\sigma_R^3}{2E\varepsilon_R\sigma_y^2}\right\}$$

where

$\sigma_R, \varepsilon_R, \sigma_y$ are reference stress and strain, and yield stress

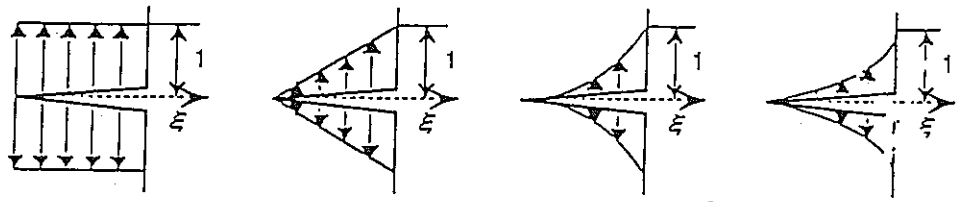

(a) 0th order $\sigma = 1$ (b) 1st order $\sigma = \xi$ (c) 2nd order $\sigma = \xi^2$ (d) 3rd order $\sigma = \xi^3$

Unit distributed load

This simplified method leads to very good agreement using C_{nom}.

V / Conclusion

The aim of this study was to predict crack propagation in a structure subject to cyclic loading. The experimental test simulated was carried out at PNC in the framework of the ATTF program (thermal fatigue applied to 304 stainless steel precracked tubes).

The simulation was to be performed with the Finite Element computer code CASTEM 2000, and with a Simplified Method developped in the A-16 Appendix of the French RCCMR.

Our work included elastic and plastic simulations.

The G-θ procedure of CASTEM 2000 allowed us to compute J for each crack length, from the stress field in the structure. This gave us the ΔJ curve versus the crack length.

Application of the A-16 rules enabled us to get a similar curve, using the J_S method.

Crack growth versus the number of cycles was then determined from Paris' law.

Results were then compared to experimental data and to predictions performed with PNC's Finite Element code FINAS.

It appears that elastic predictions using both the codes are very similar, and in good agreement with the measured values. In the plastic case, the results predicted with the G-θ procedure and the A-16 rules are close to one another. Though the A-16 results are not as good as the elastic evaluation because of simplifying assumptions on the shape of the thermal gradients, they still remain satisfactory. FINAS's predictions are better, but a different definition of ΔJ is used. It is shown that the use of a standard definition of ΔJ would lead to the two codes giving the same results.

This study shows that the G-θ procedure of CASTEM 2000 and the J_S method of the A-16 Appendix of the French RCCMR can predict crack growth values close to measured ones in the case of thermal fatigue, and close to those predicted by FINAS.

The next step will be the extension of the simulation to the case of creep fatigue loading.

REFERENCES

[1] J. Brochard - X.Z. Suo :" Le taux de restitution de l'energie G en mecanique de la rupture non lineaire - Formulation de la methode G-θ et description de la programmation dans Castem 2000" CEA internal report DMT/94-640

[2] B. Drubay :" Annexe A-16 du RCCMR - Analyse de la nocivite des defauts - 2eme version preliminaire" CEA internal report DMT/94-043

[3] T. Wakai :" ATTF - Crack Propagation Analysis under Thermal Fatigue " - PNC/OEC - PNC ZN9410 93-145

[4] B. Drubay : CEA internal report DMT/94-381 - to be published

[5] P.M. Besuner " Mechanics of crack growth" ASTM STP, 590, (1976), 403

[6] I. Milne et al. :" Assesment of the integrity of structures containing defects" Inte. J. of PVP, Vol.32, pp.3-104 (1985)

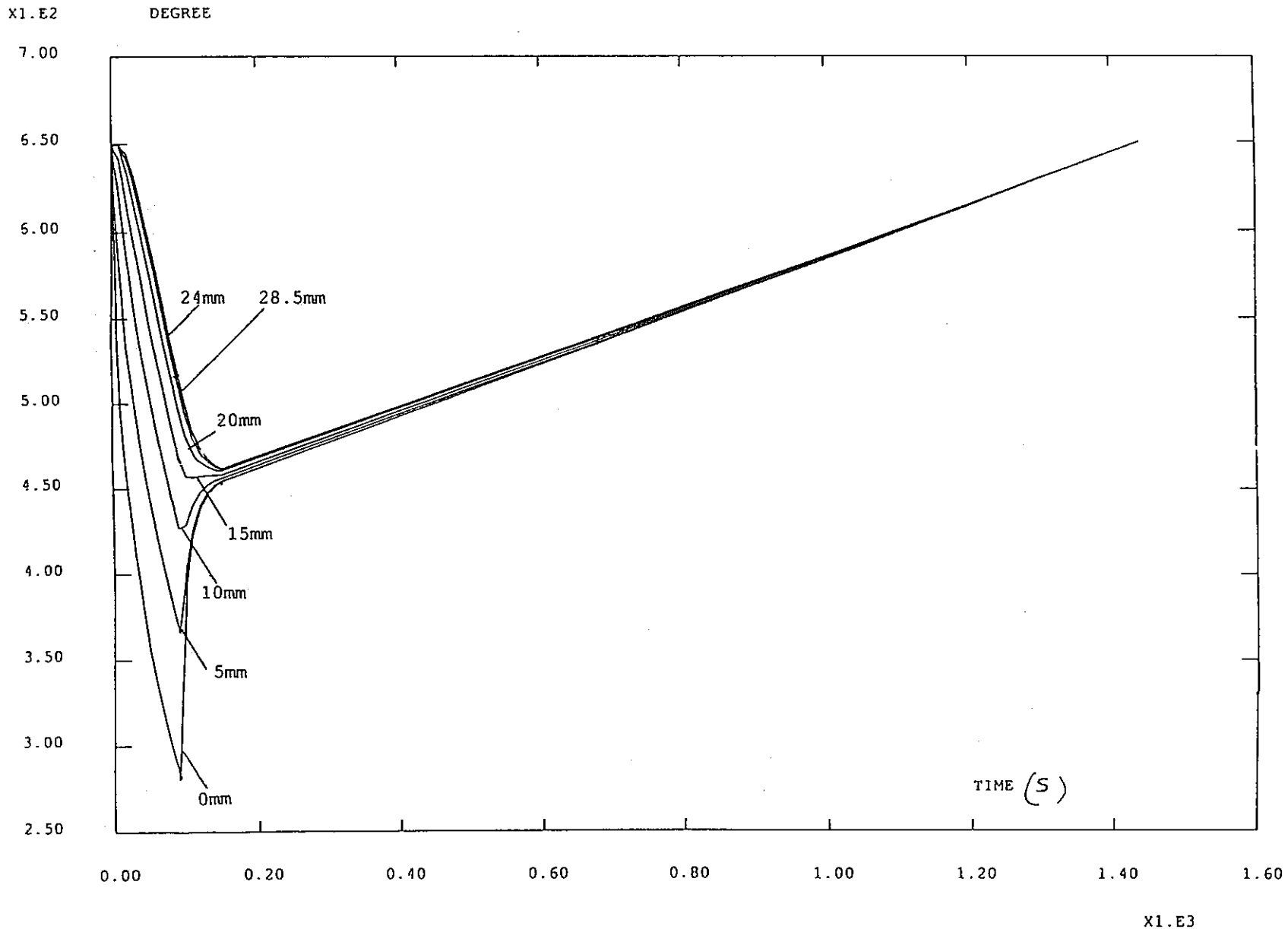

- Figure 1 - Temperature profiles in the radial direction at various points measured from the inner surface of the tube (Temperatures in Degree C - Time in seconds)

- Table 1 - Mechanical characteristics used in the computation

Material properties of type 304 stainless steel

温　度 (℃)	縦弾性係数 (kg/mm^2)	ポアソン比	熱膨張係数 ($\times 10^{-6}$ 1/℃)
50	19600	0.268	15.65
100	19400	0.272	16.48
150	19100	0.275	17.22
200	18800	0.279	17.85
250	18400	0.283	18.36
300	18000	0.287	18.79
350	17600	0.291	19.19
400	17200	0.295	19.57
450	16700	0.298	19.93
500	16200	0.302	20.28
550	15700	0.306	20.60
600	15200	0.310	20.87
650	14700	0.314	21.09
	E	nu	alpha

Yield stress and work hardening coefficient of type 304 stainless steel

(kg/mm^2)

材料パラメータ	温　度（℃）						
	400	450	500	550	600	650	
降伏応力	22.75	22.75	22.75	21.76	20.13	18.59	SIGy
加工硬化係数	2240.8	2240.8	2240.8	1844.0	1381.2	1045.7	H

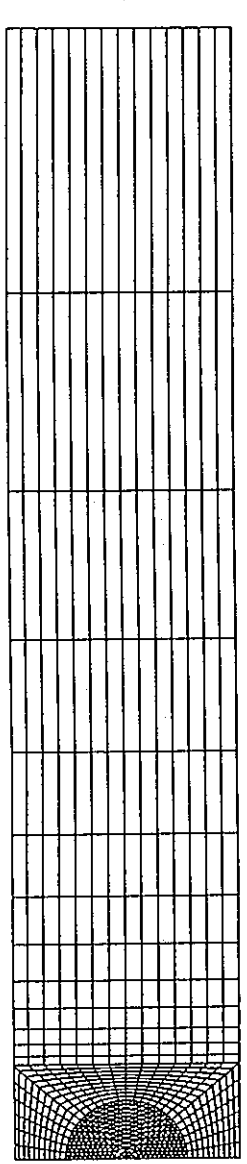

- Figure 2a -
CASTEM 2000's Finite Element mesh

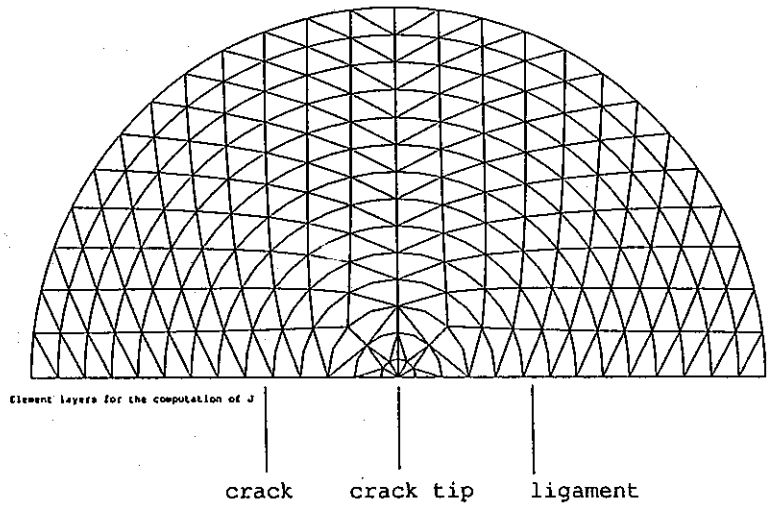

- Figure 2b -
Domain around the crack tip for
the computation of J

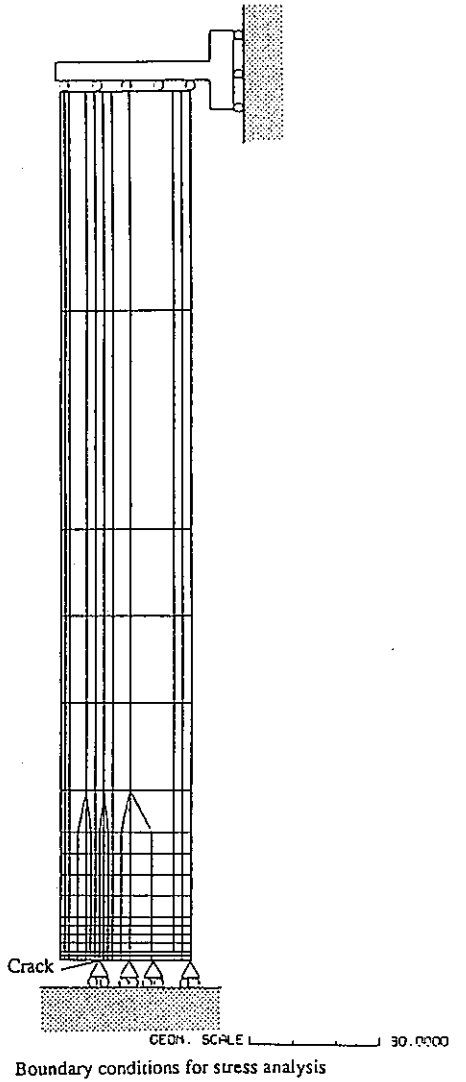

Boundary conditions for stress analysis

- Figure 3 -
FINAS' Finite Element mesh

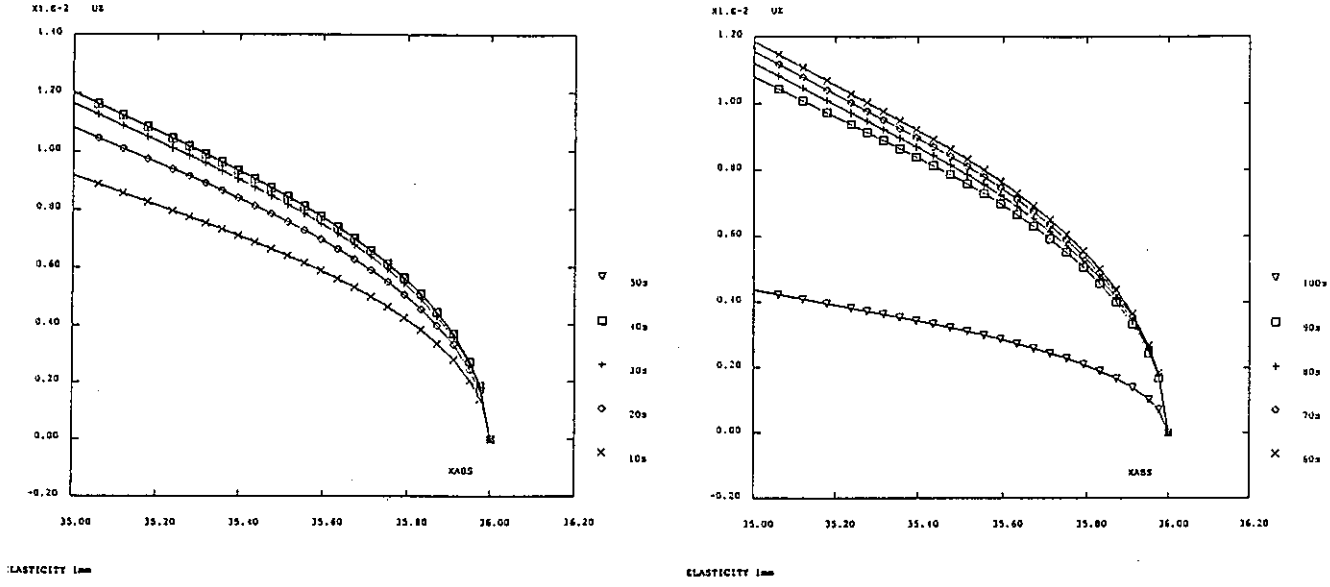

- Figure 4.a.1 (CASTEM 2000) -

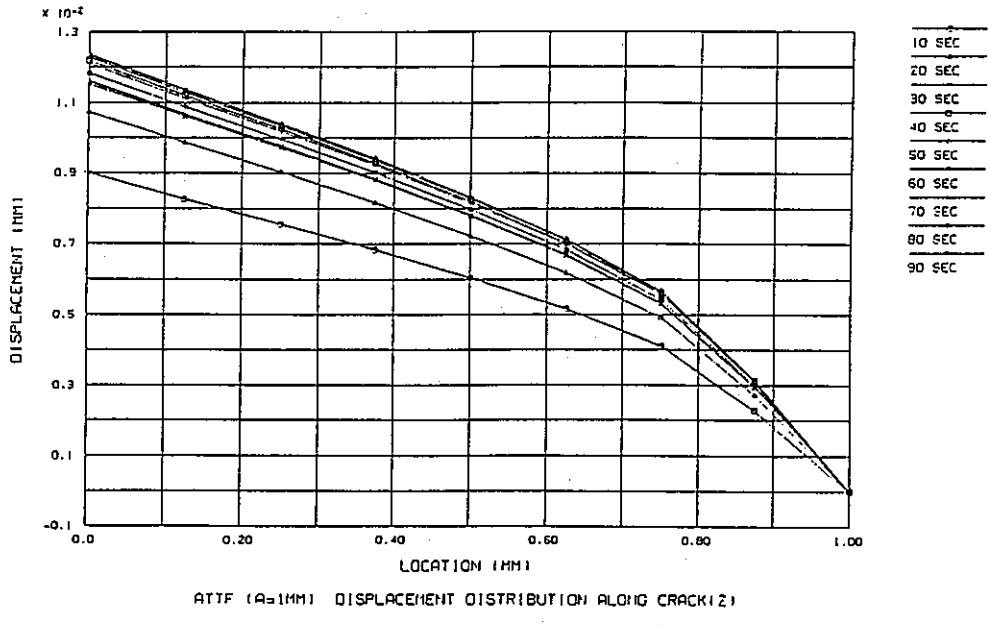

Crack opening shape with elastic analysis (a=1mm)

- Figure 4.a.2 (FINAS) -

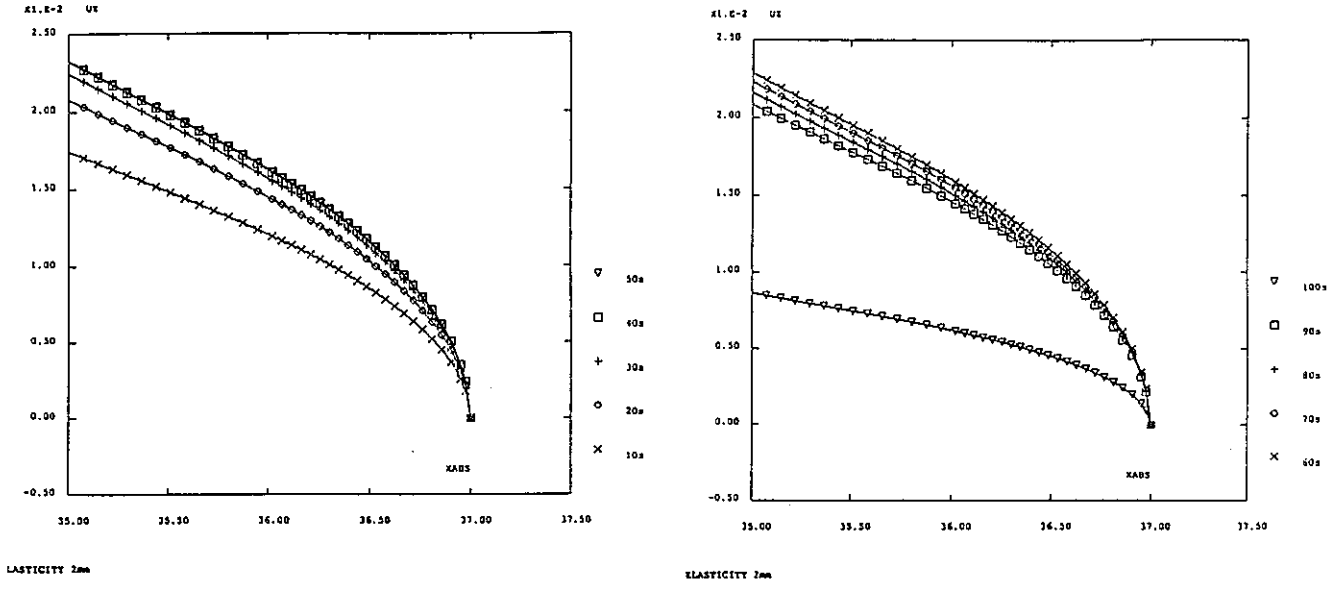

- Figure 4.b.1 (CASTEM 2000) -

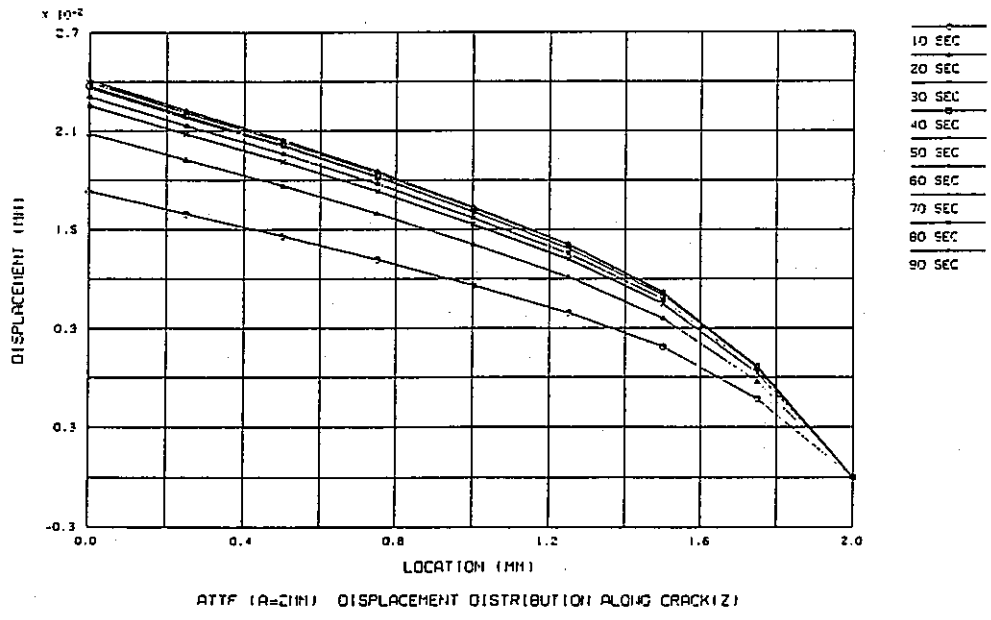

Crack opening shape with elastic analysis (a=2mm)

- Figure 4.b.2 (FINAS) -

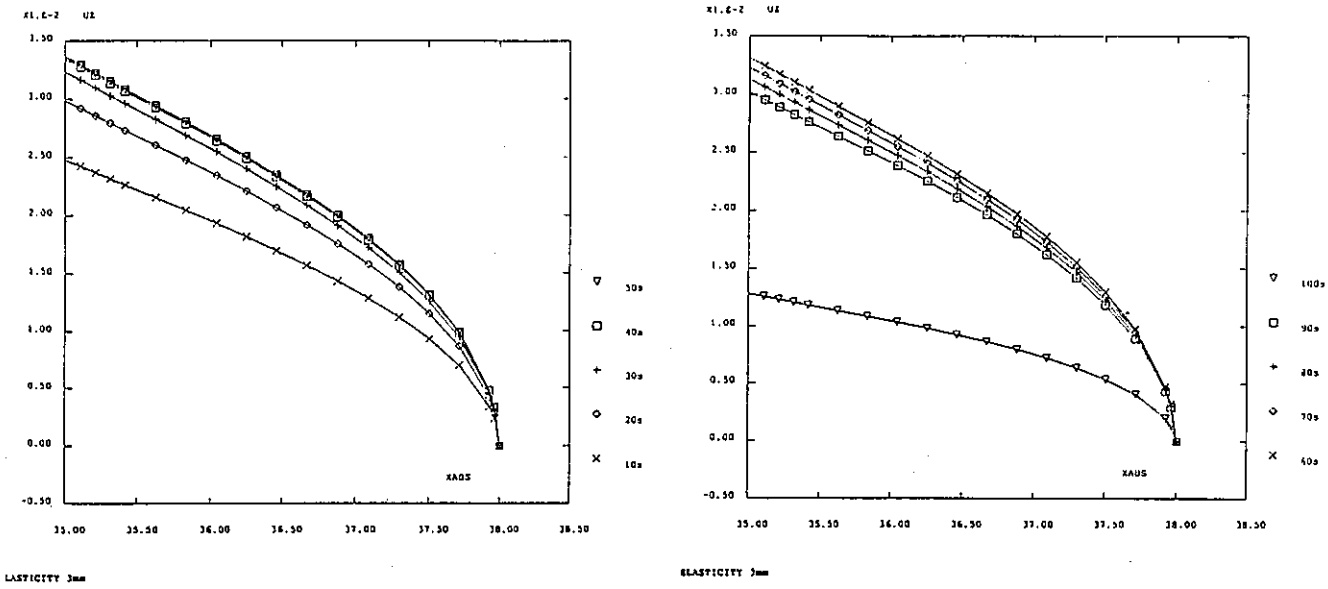

- Figure 4.c.1 (CASTEM 2000) -

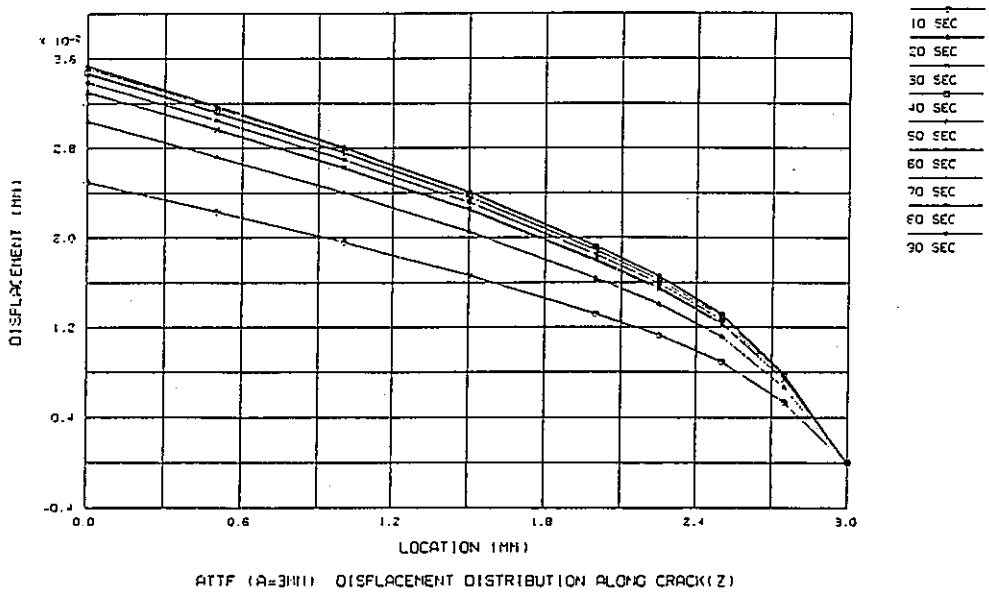

Crack opening shape with elastic analysis (a=3mm)

- Figure 4.c.2 (FINAS) -

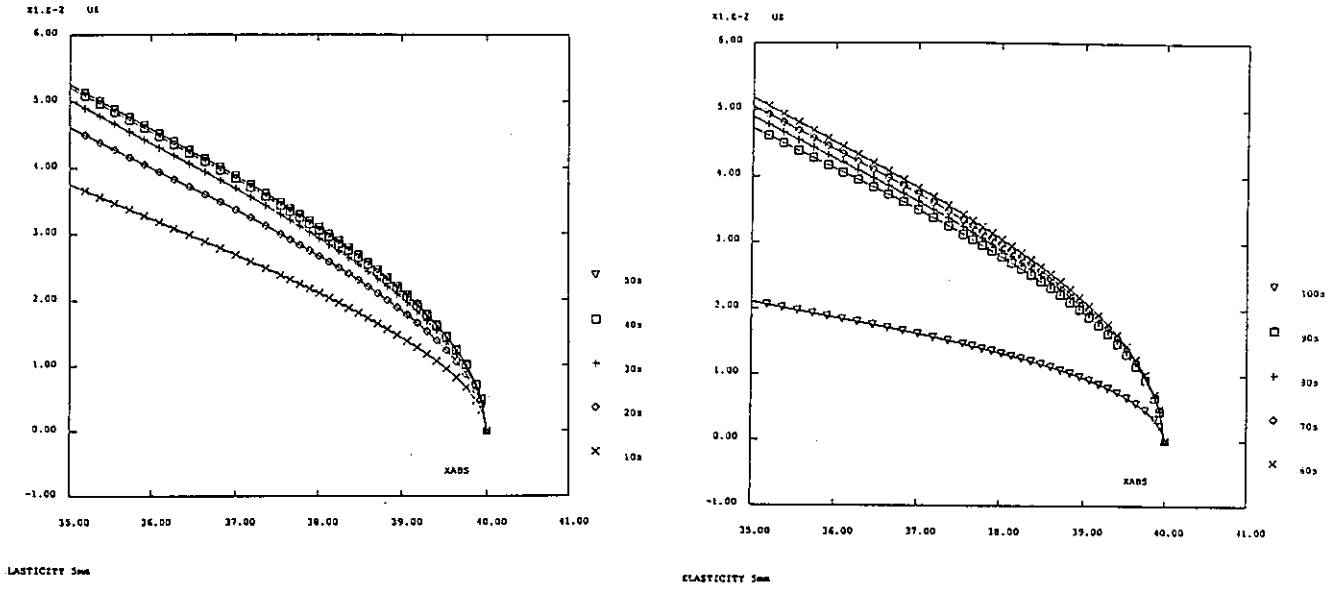

- Figure 4.d.1 (CASTEM 2000) -

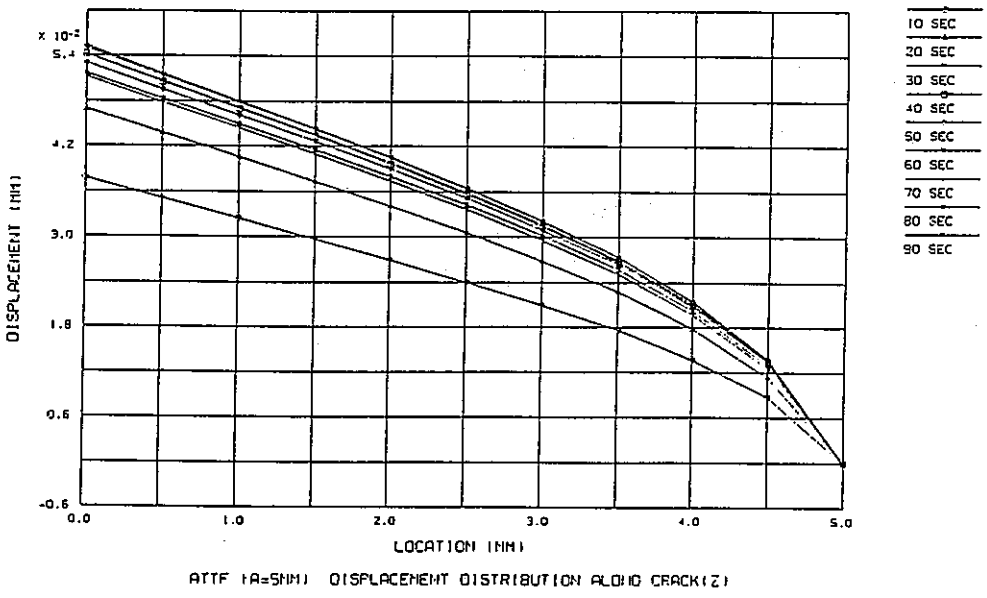

Crack opening shape with elastic analysis (a=5mm)

- Figure 4.d.2 (FINAS) -

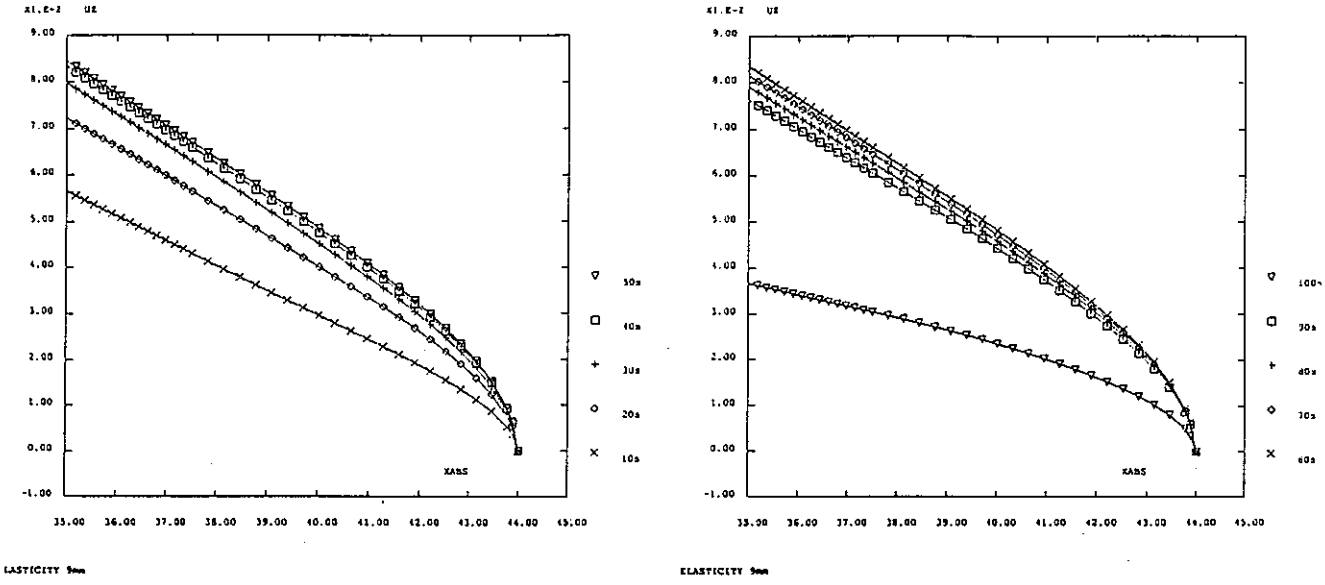

- Figure 4.e.1 (CASTEM 2000) -

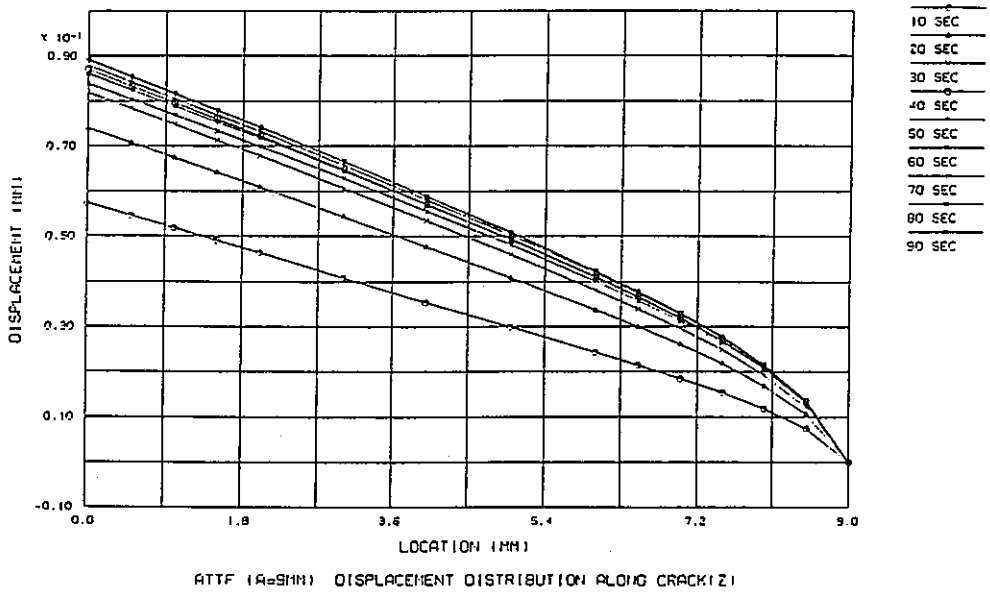

Crack opening shape with elastic analysis (a=9mm)

- Figure 4.e.2 (FINAS) -

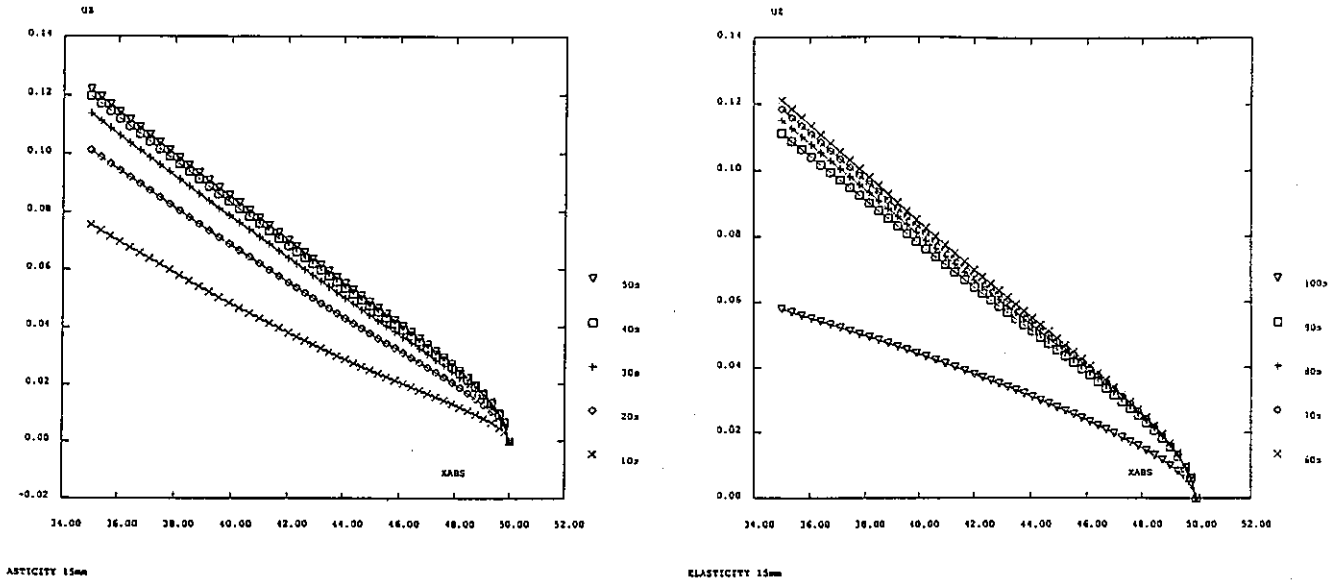

- Figure 4.f.1 (CASTEM 2000) -

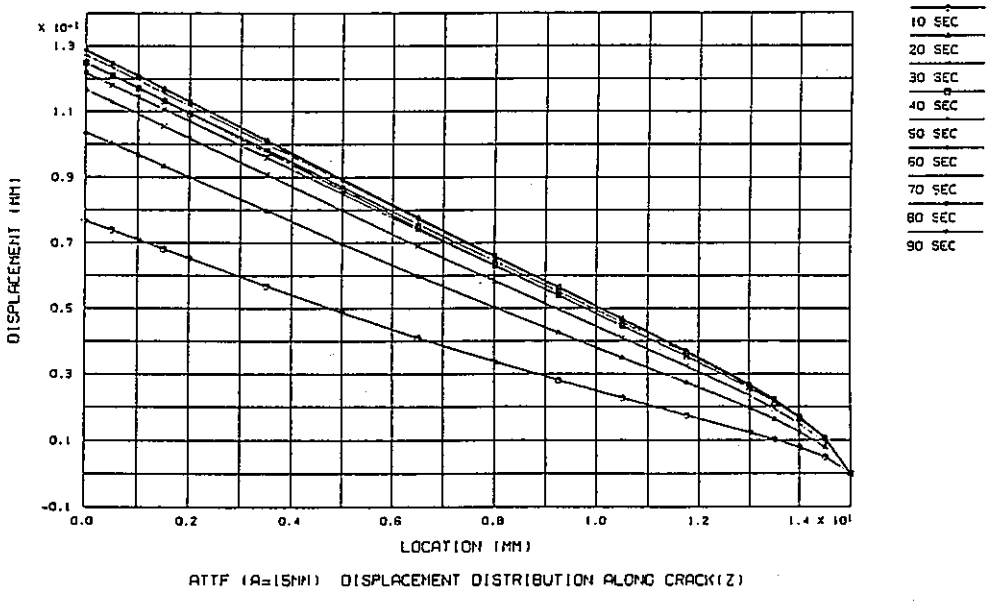

Crack opening shape with elastic analysis (a=15mm)

- Figure 4.f.2 (FINAS) -

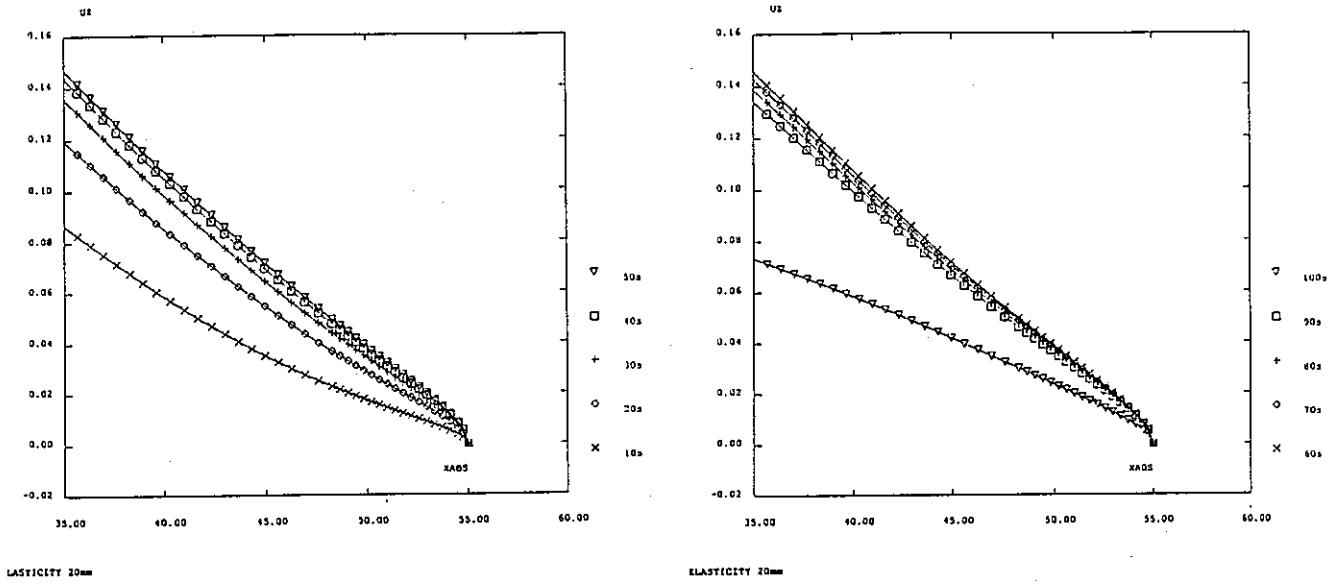

- Figure 4.g.1 (CASTEM 2000) -

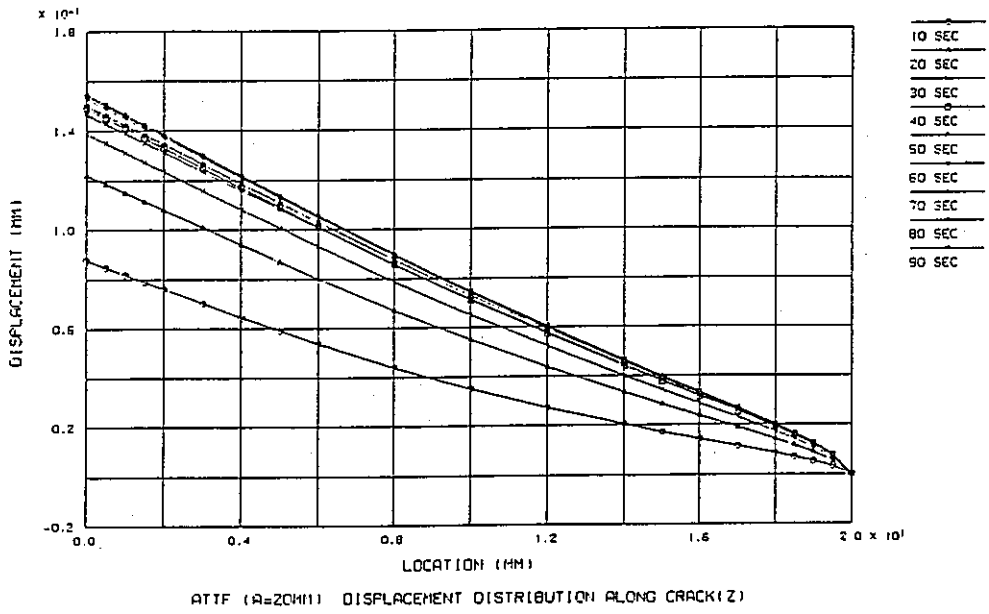

Crack opening shape with elastic analysis (a=20mm)

- Figure 4.g.2 (FINAS) -

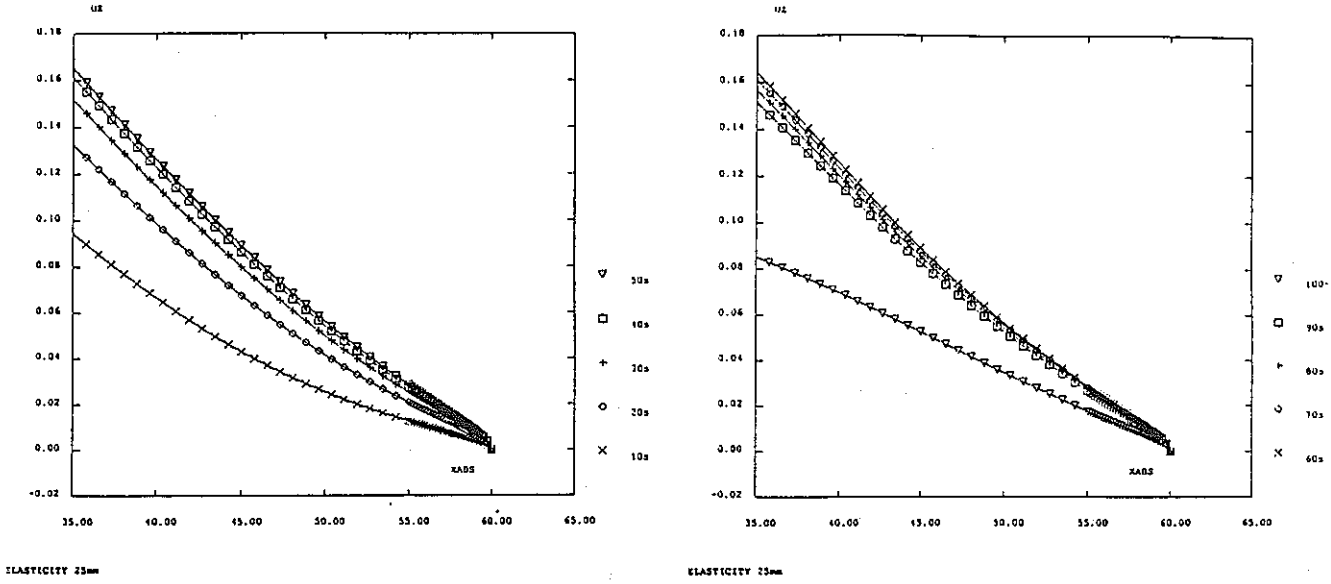

- Figure 4.h.1 (CASTEM 2000) -

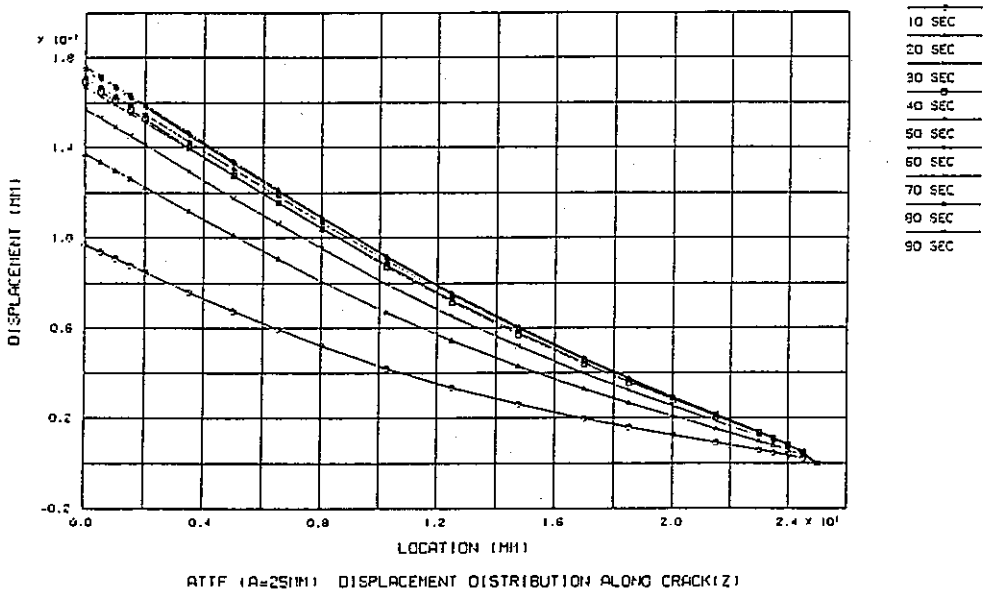

Crack opening shape with elastic analysis (a=25mm)

- Figure 4.h.2 (FINAS) -

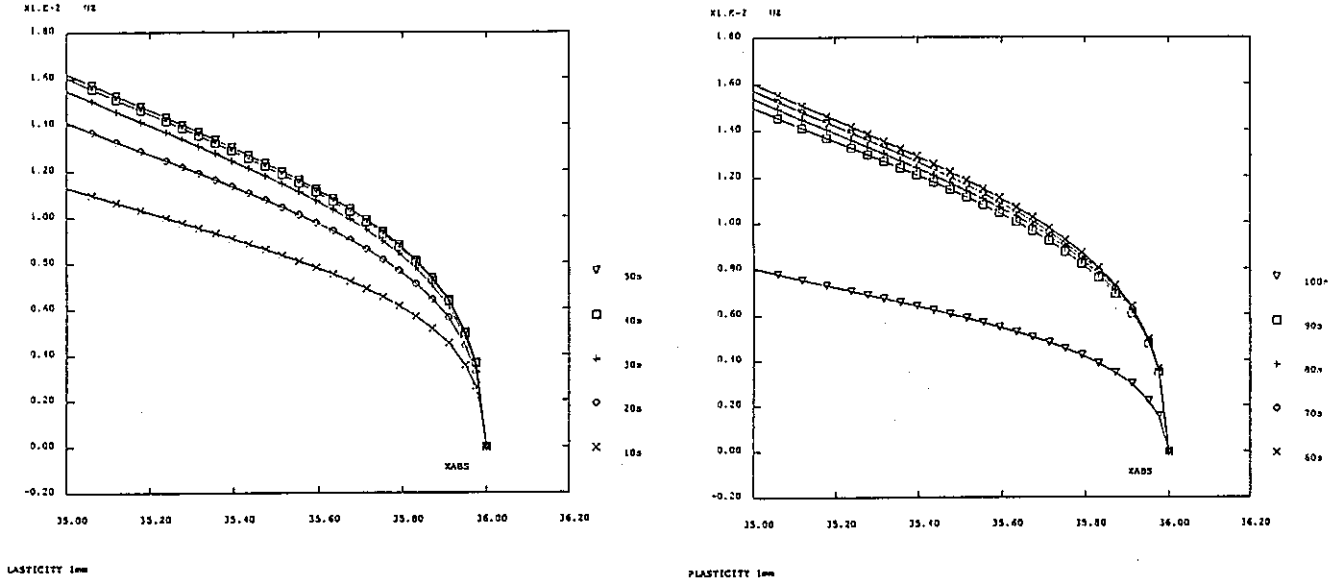

- Figure 5.a.1 (CASTEM 2000) -

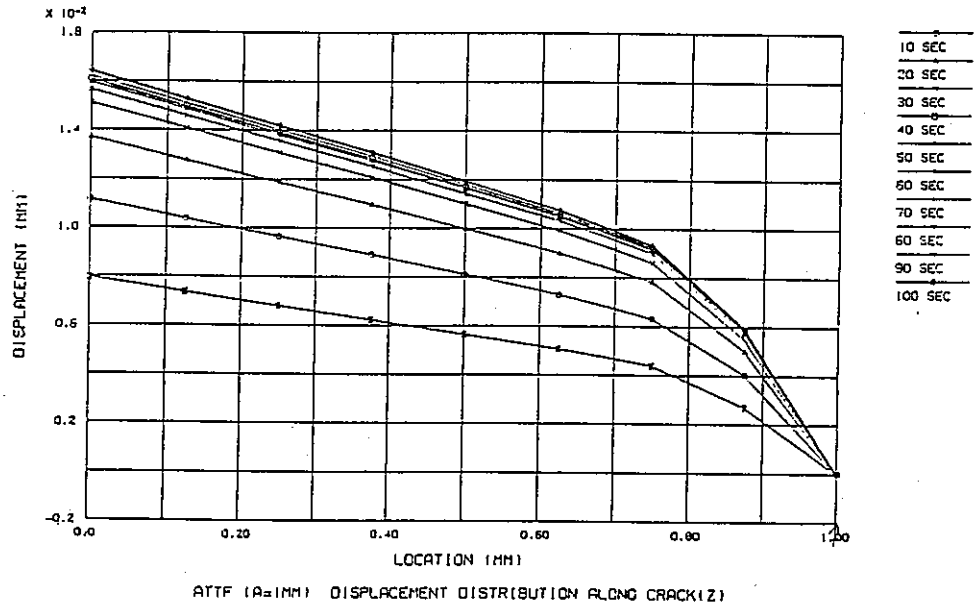

Crack opening shape with elast-plastic analysis (a=1mm)

- Figure 5.a.2 (FINAS) -

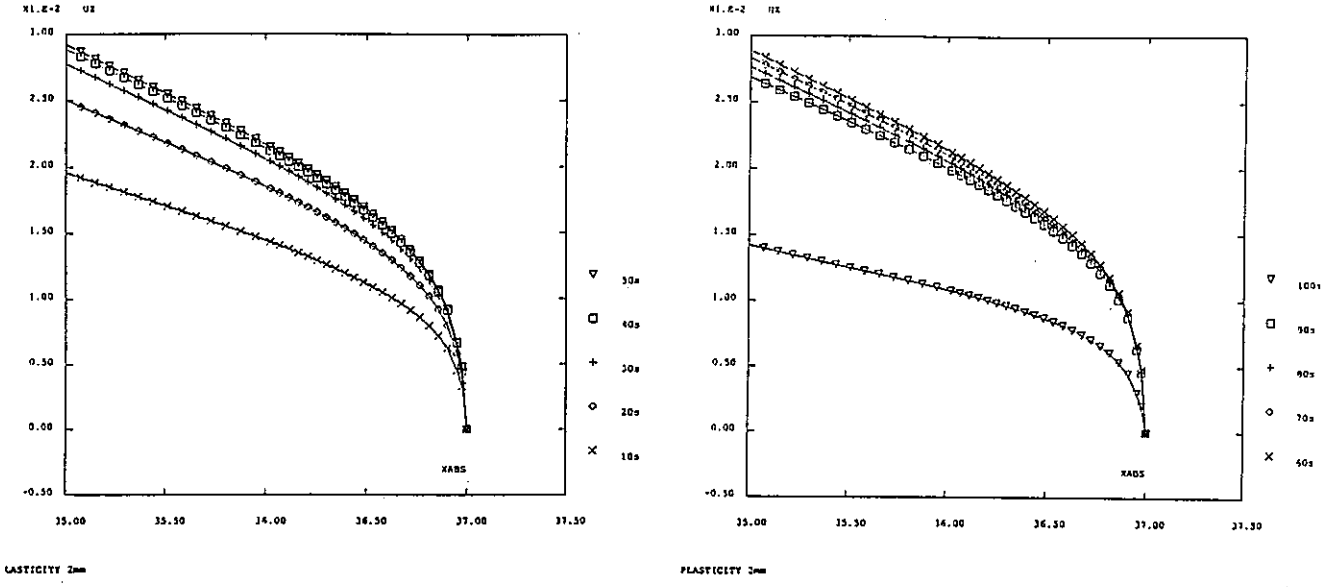

- Figure 5.b.1 (CASTEM 2000) -

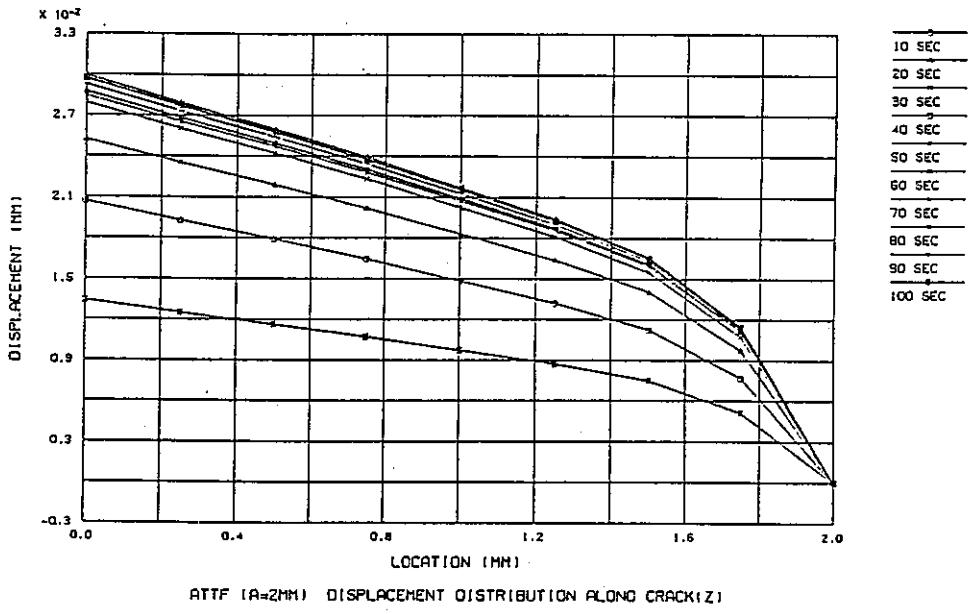

Crack opening shape with elast-plastic analysis (a=2mm)

- Figure 5.b.2 (FINAS) -

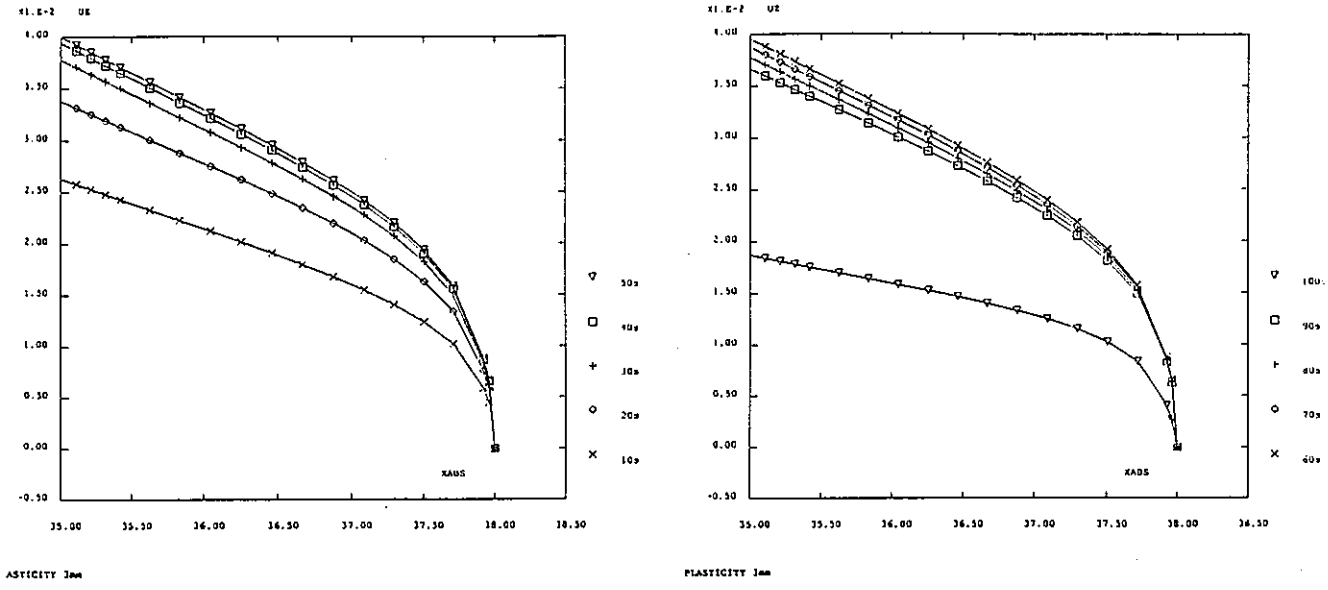

- Figure 5.c.1 (CASTEM 2000) -

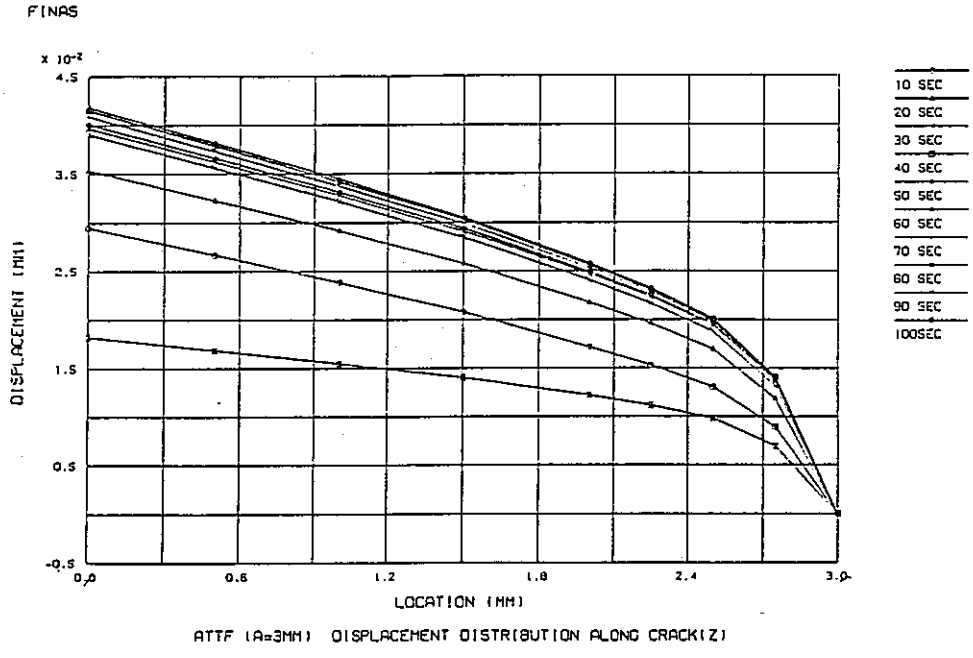

Crack opening shape with elast-plastic analysis (a=3mm)

- Figure 5.c.2 (FINAS) -

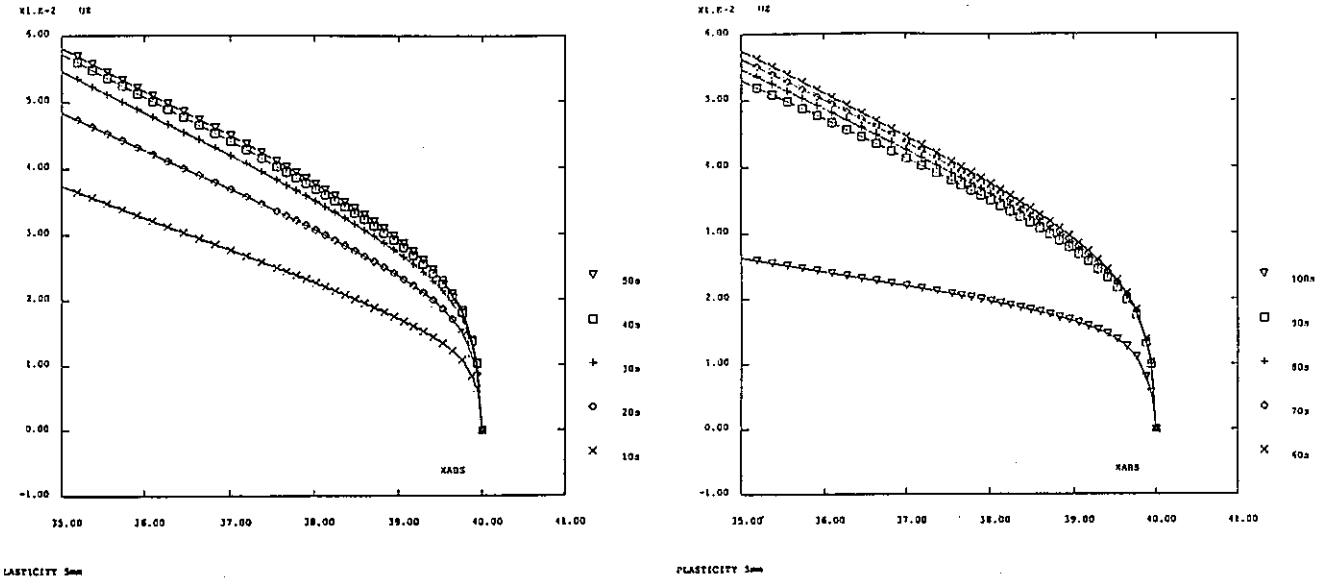

- Figure 5.d.1 (CASTEM 2000) -

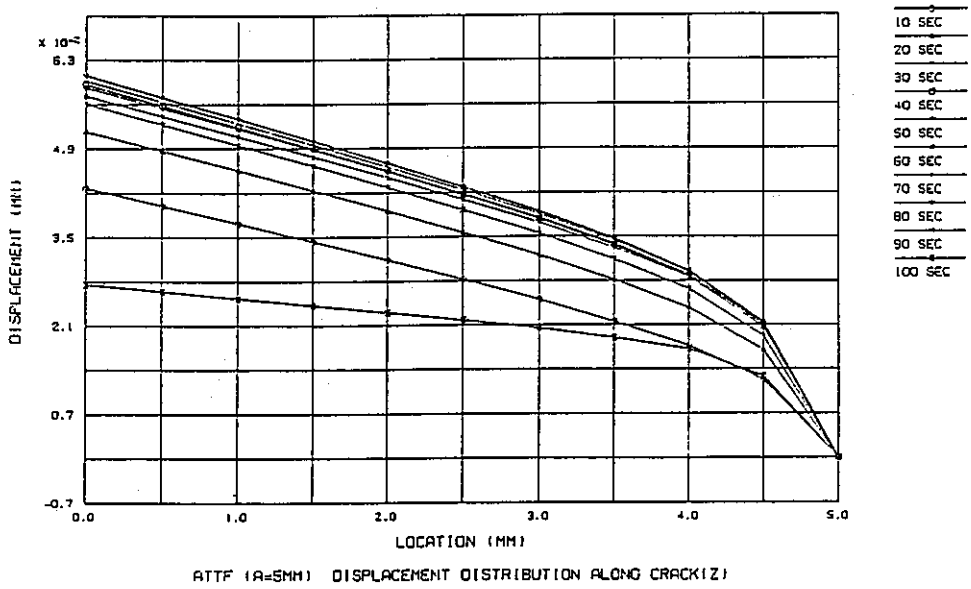

Crack opening shape with elast-plastic analysis (a=5mm)

- Figure 5.d.2 (FINAS) -

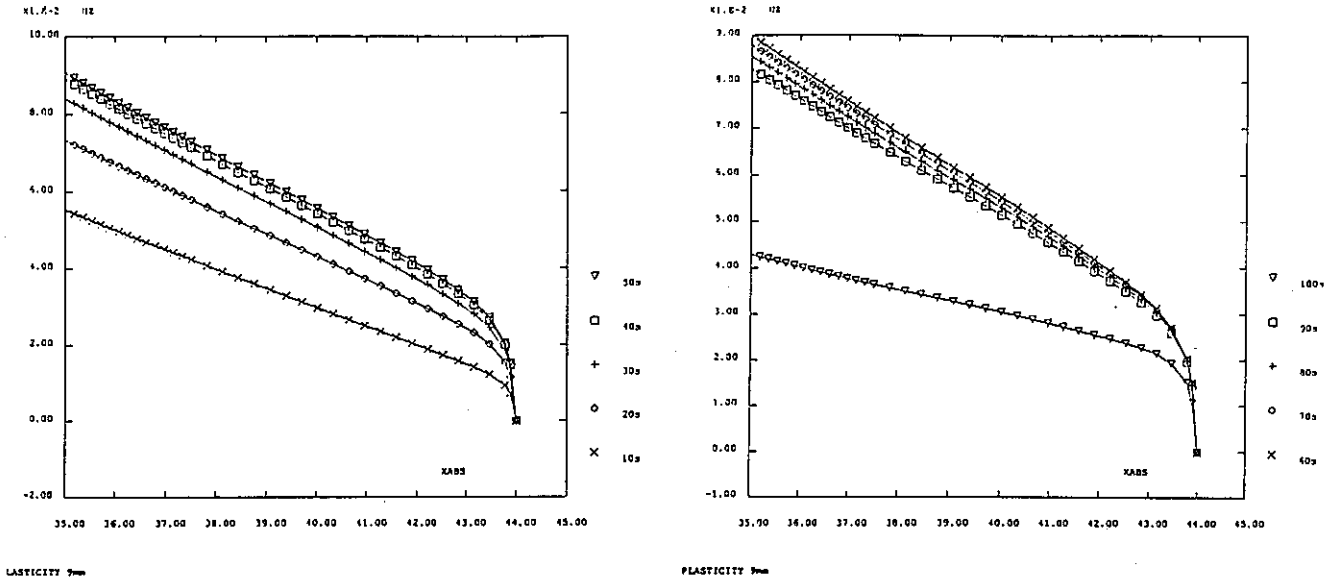

- Figure 5.e.1 (CASTEM 2000) -

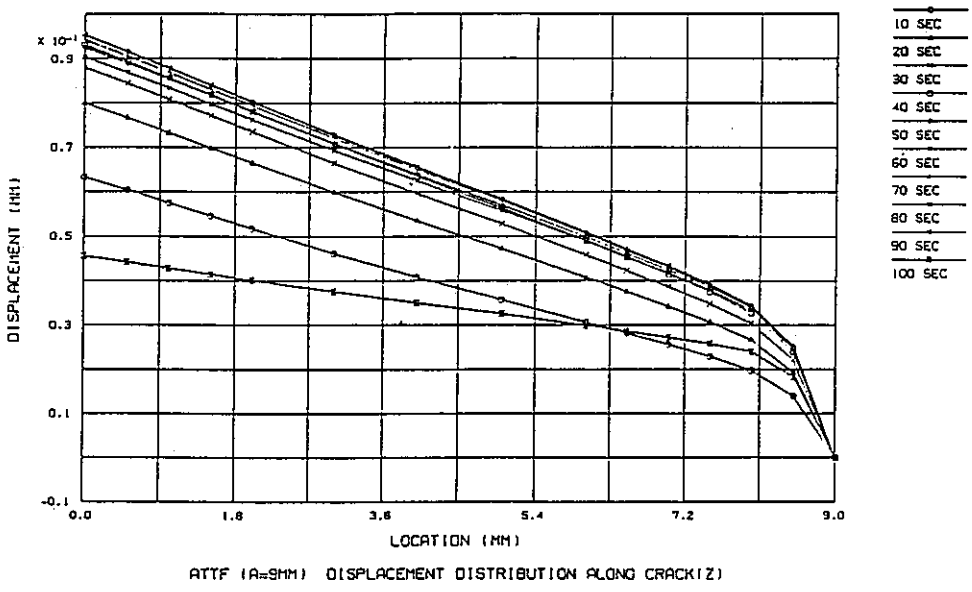

Crack opening shape with elast-plastic analysis (a=9mm)

- Figure 5.e.2 (FINAS) -

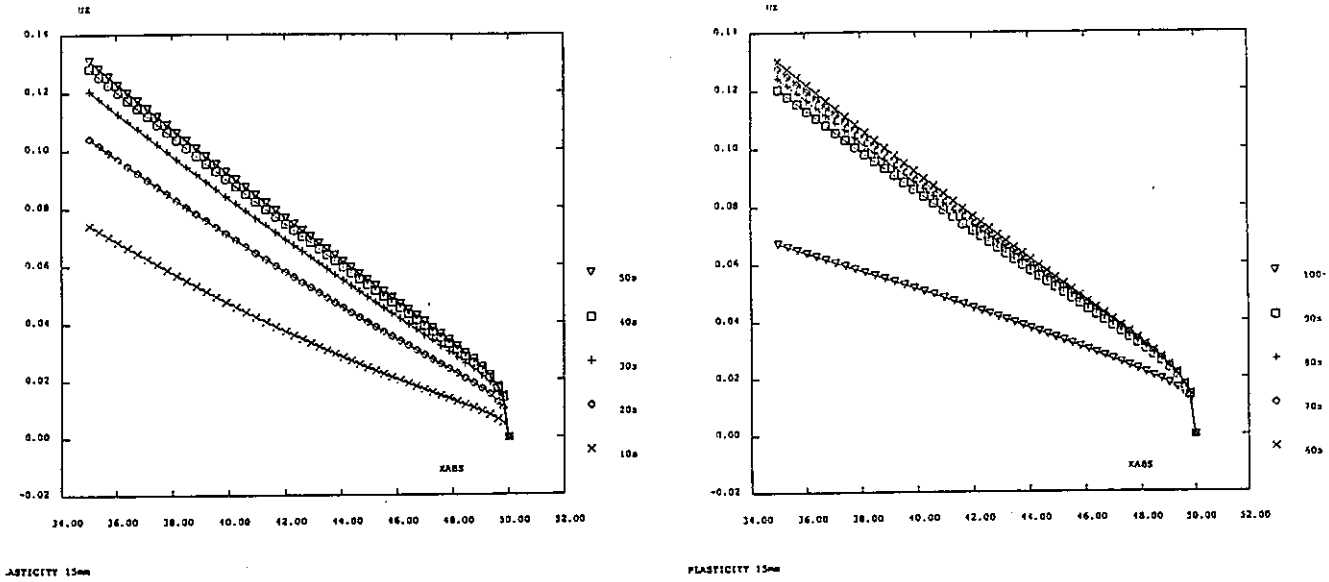

- Figure 5.f.1 (CASTEM 2000) -

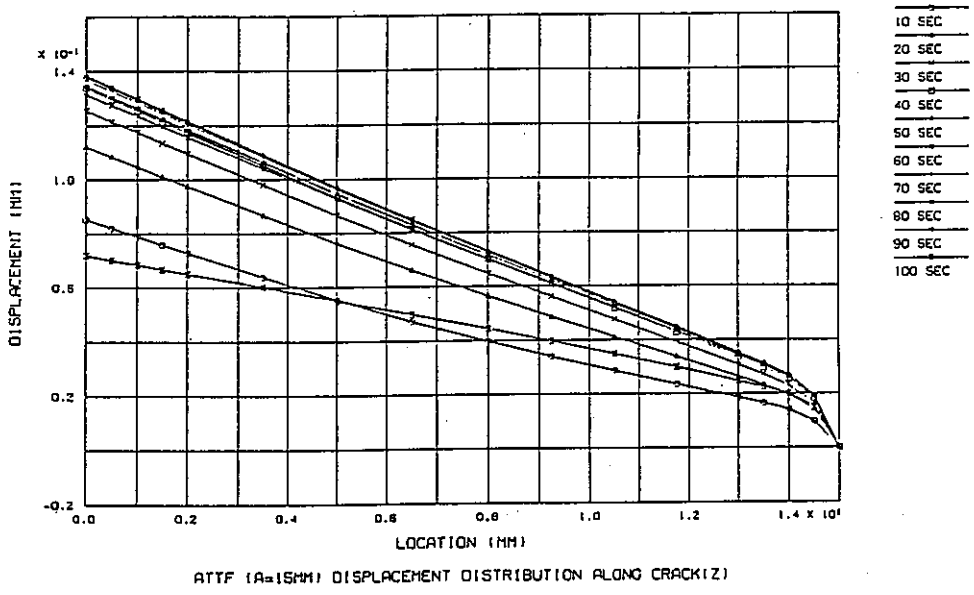

Crack opening shape with elast-plastic analysis (a=15mm)

- Figure 5.f.2 (FINAS) -

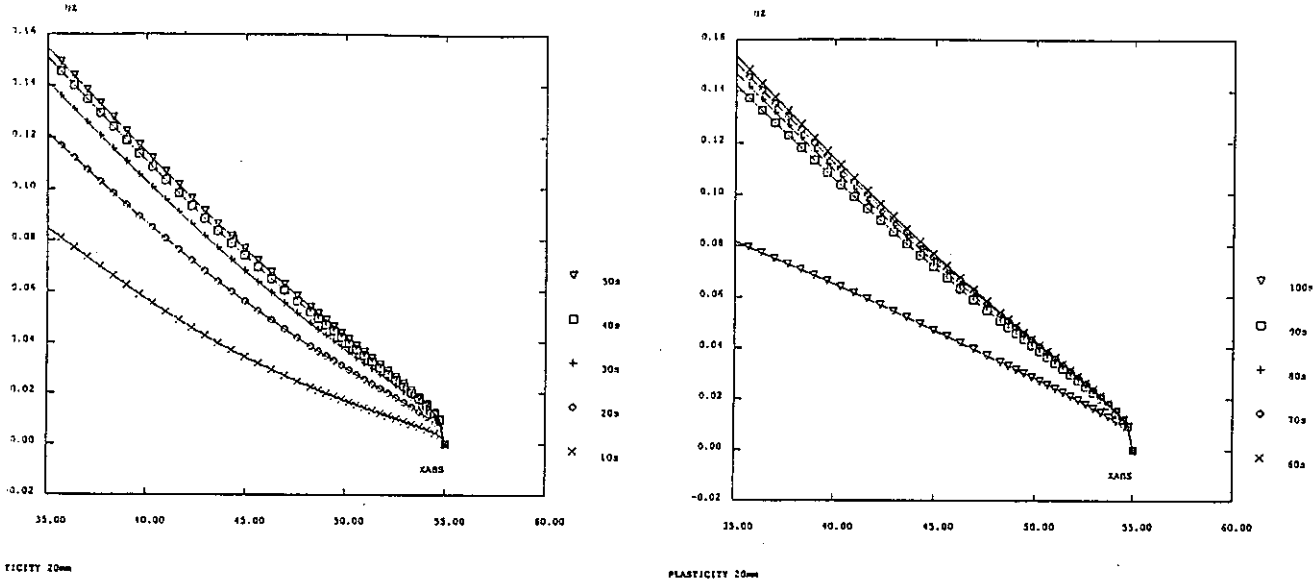

- Figure 5.g.1 (CASTEM 2000) -

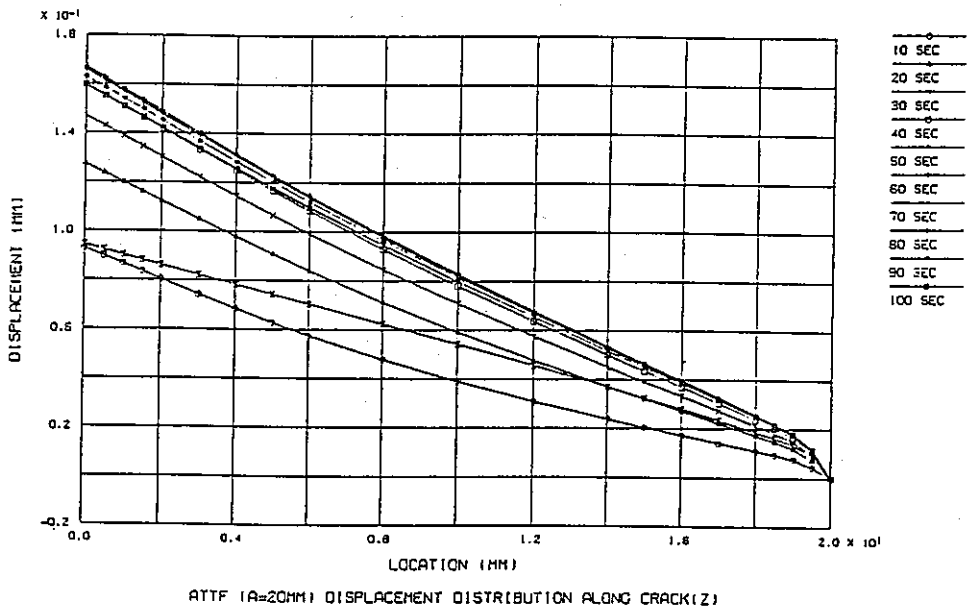

Crack opening shape with elast-plastic analysis (a=20mm)

- Figure 5.g.2 (FINAS) -

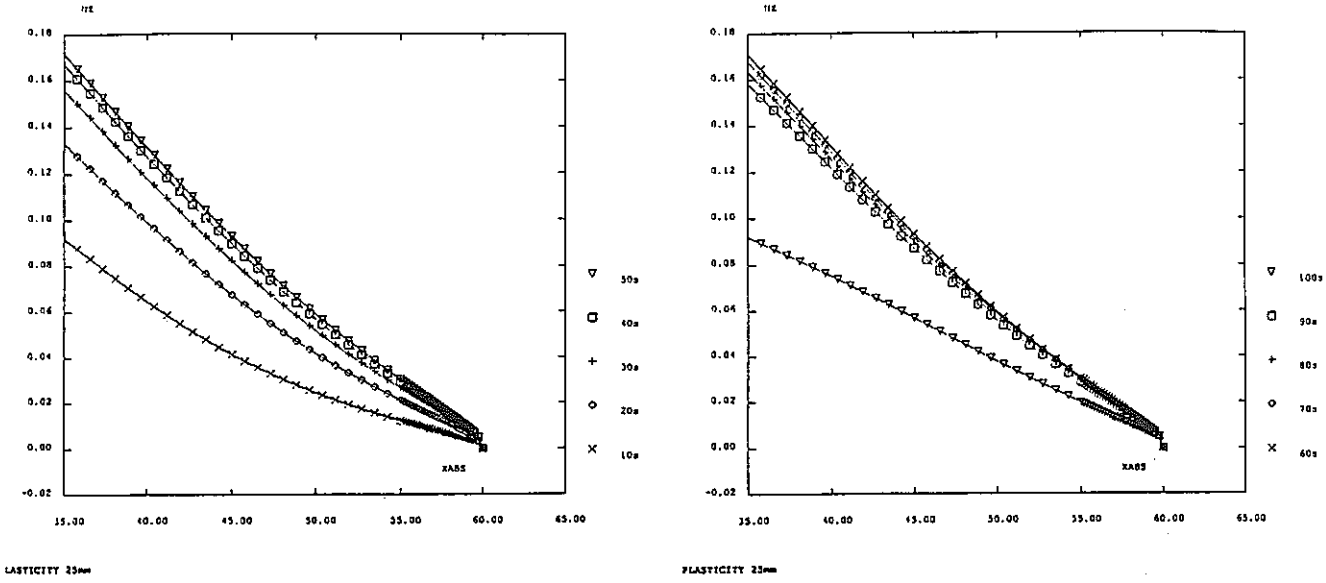

- Figure 5.h.1 (CASTEM 2000) -

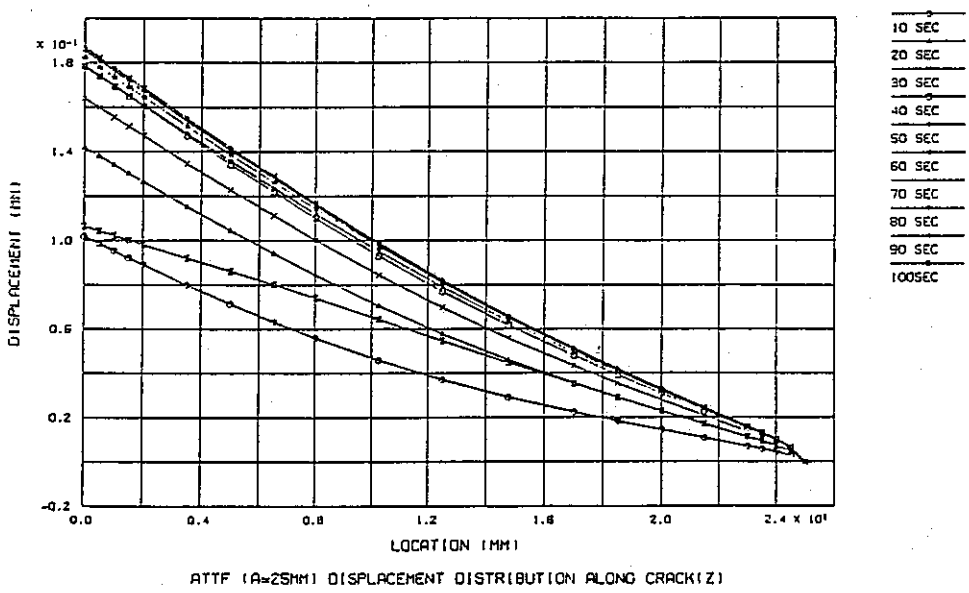

Crack opening shape with elast-plastic analysis (a=25mm)

- Figure 5.h.2 (FINAS) -

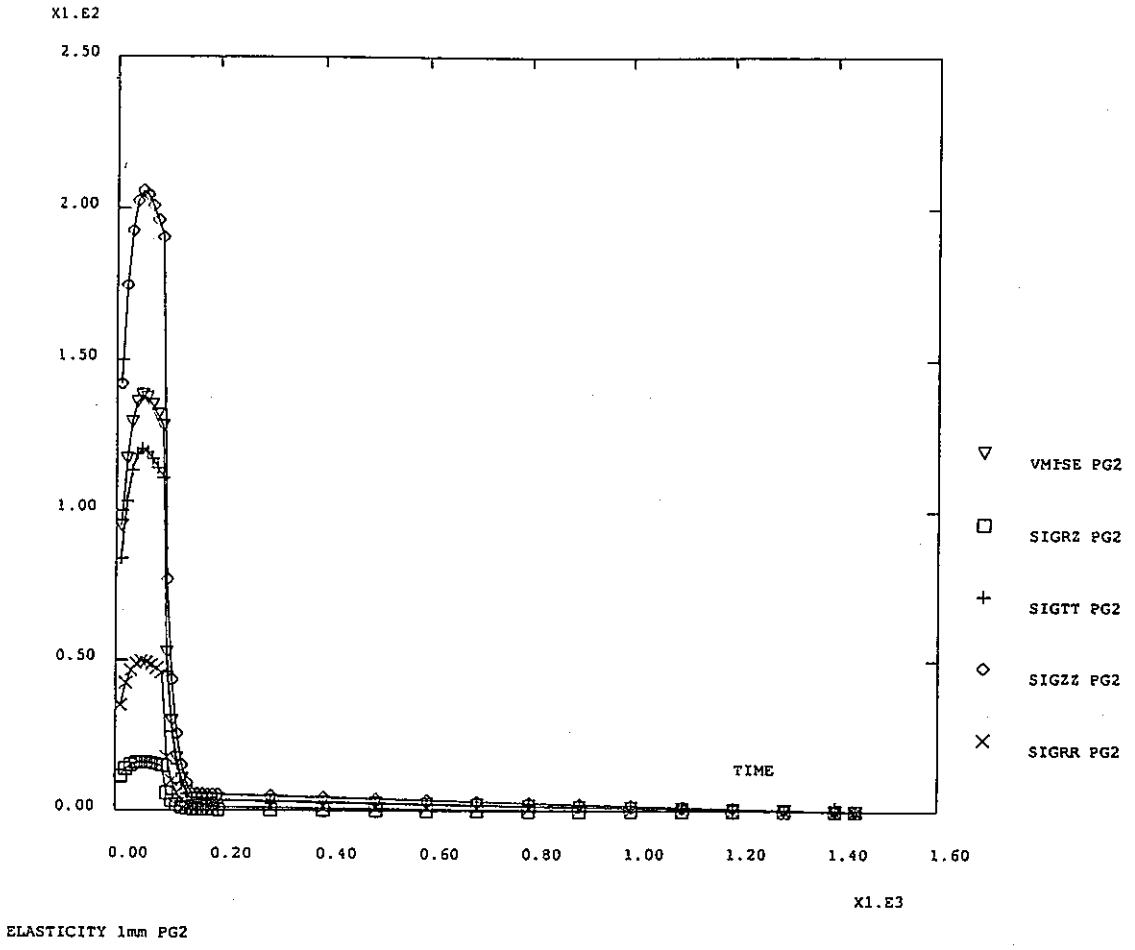

- Figure 6.a.1 (CASTEM 2000) - (36.14mm , 0.1071mm)

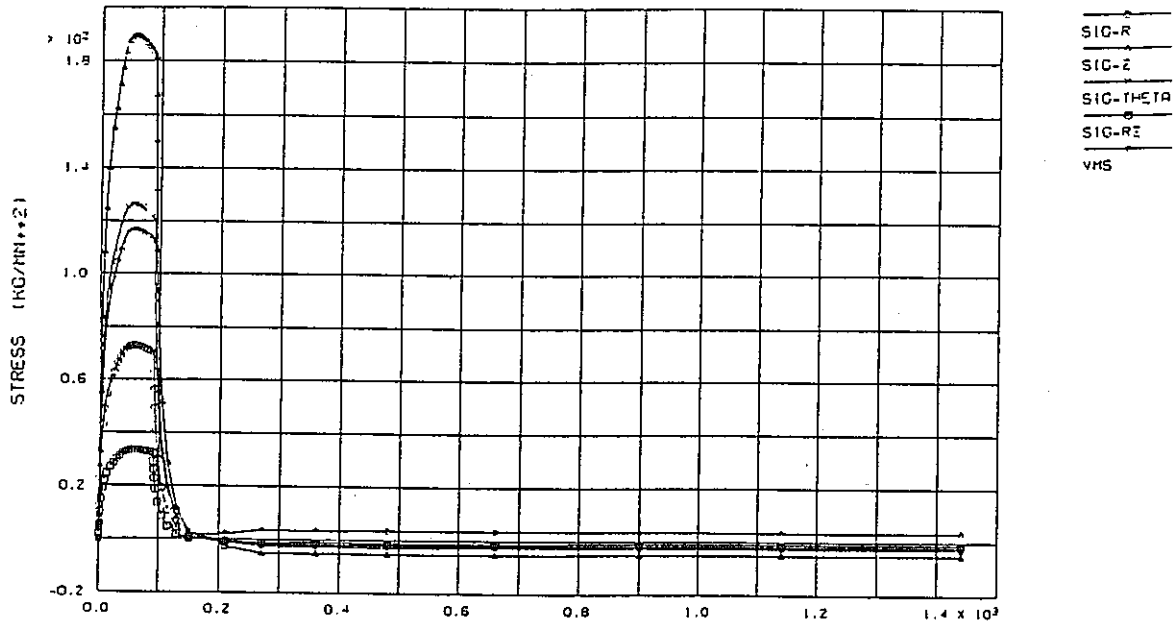

Time (sec)

Stress transition at crack tip with elastic analysis (a=1mm)

- Figure 6.a.2 (FINAS) - (36.05625mm , 0.1125mm)

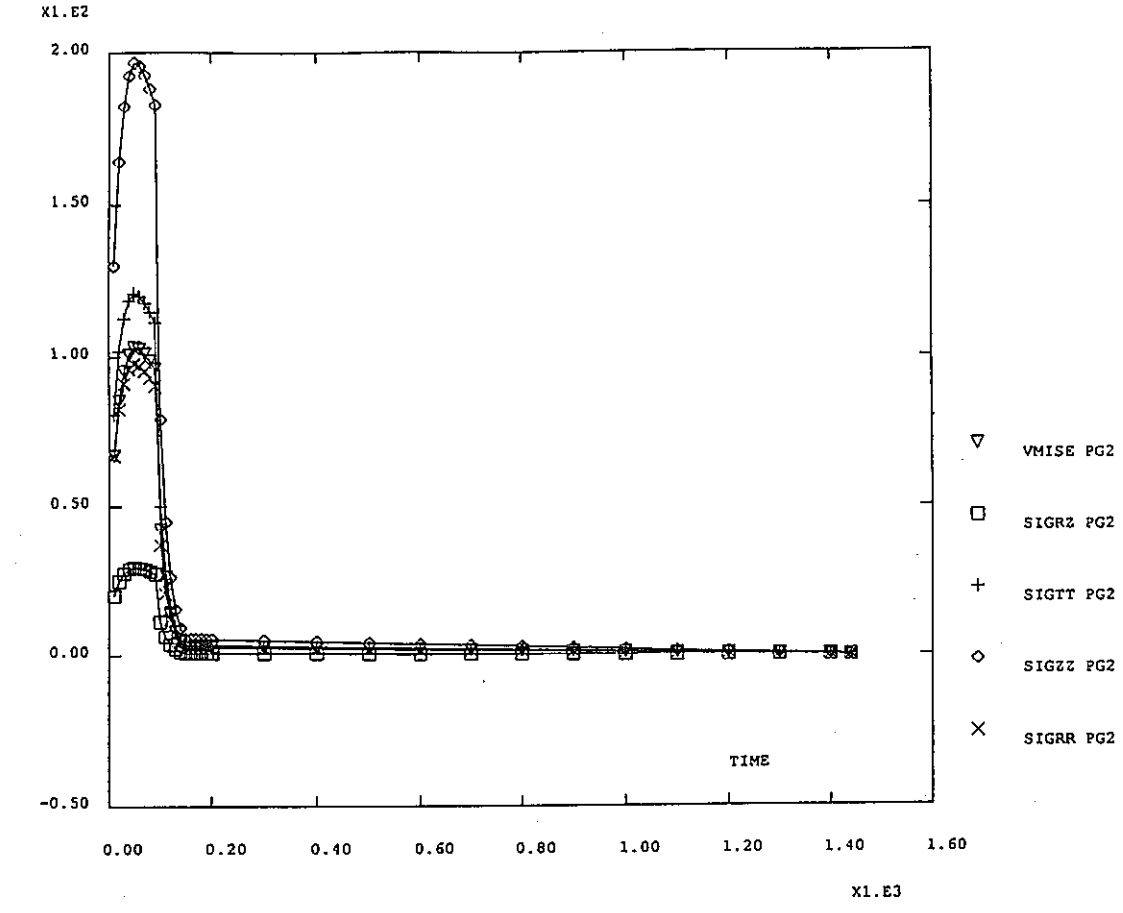

ELASTICITY 2mm PG2 20

- Figure 6.b.1 (CASTEM 2000) - (37.19mm , 0.1267mm)

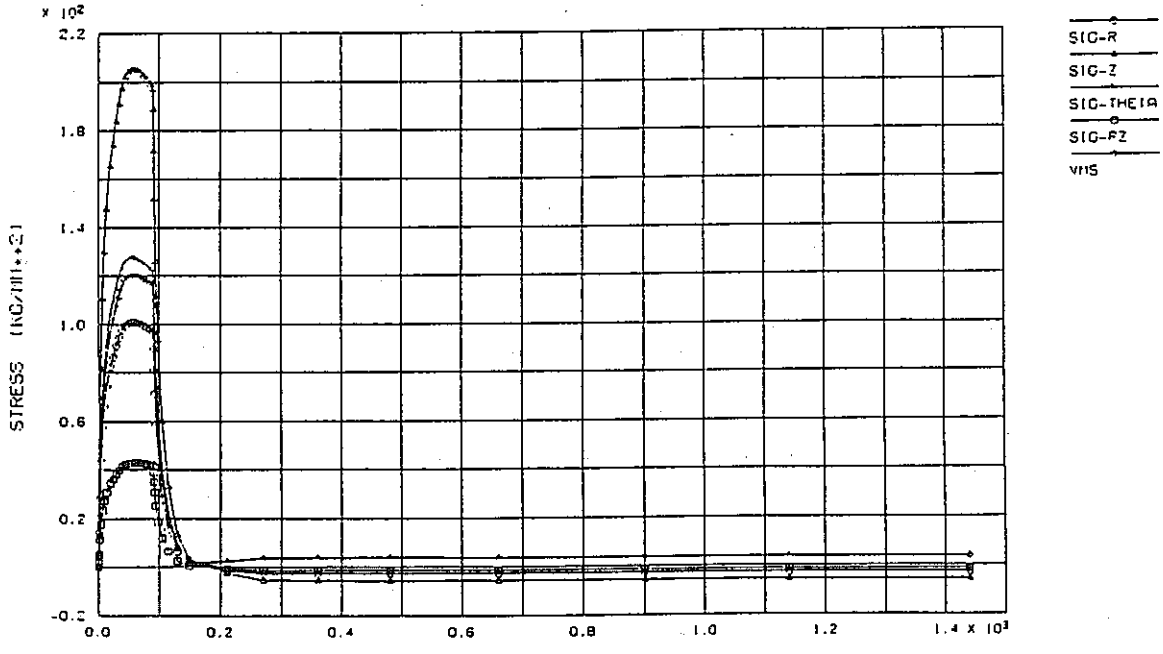

Time (sec)

Stress transition at crack tip with elastic analysis (a=2mm)

- Figure 6.b.2 (FINAS) - (37.1125mm , 0.1125mm)

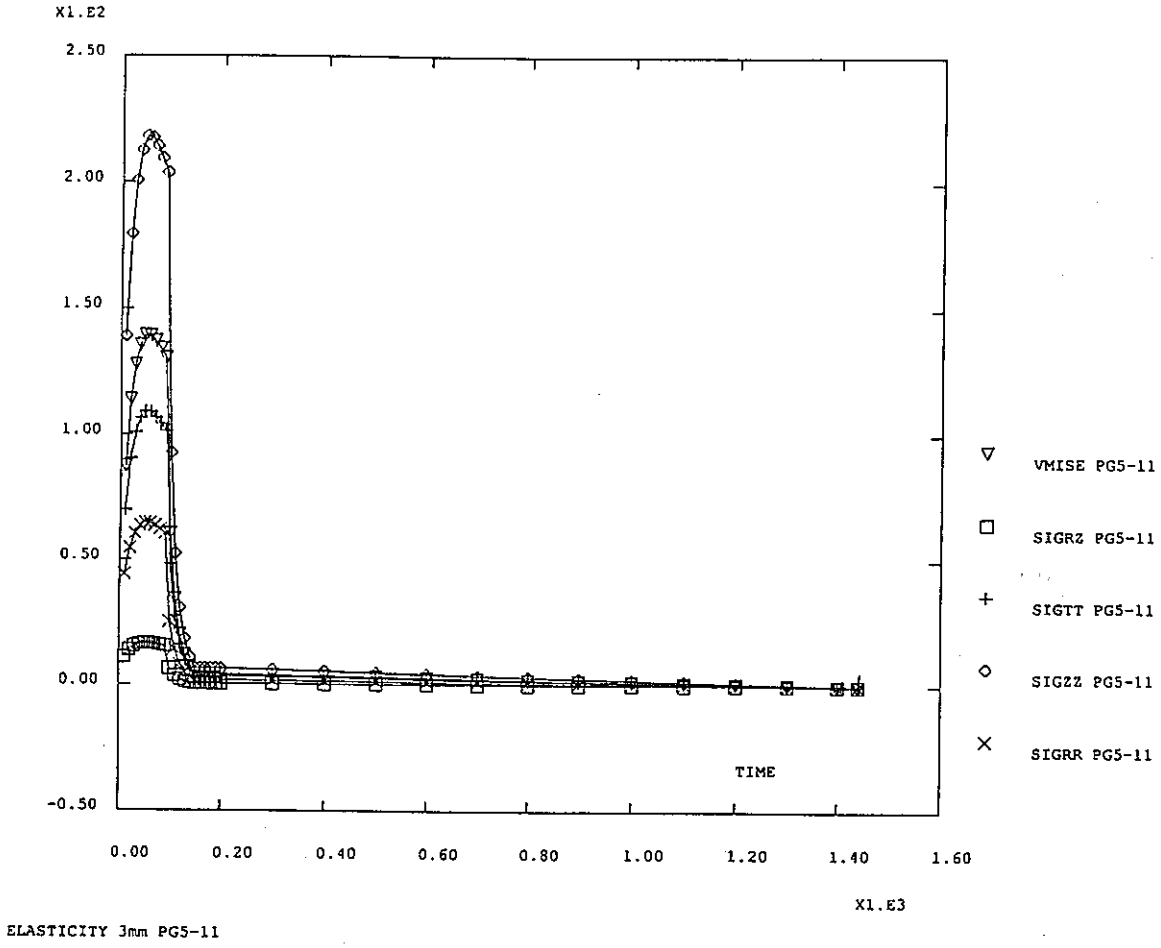

- Figure 6.c.1 (CASTEM 2000) - (38.14mm , 0.2307mm)

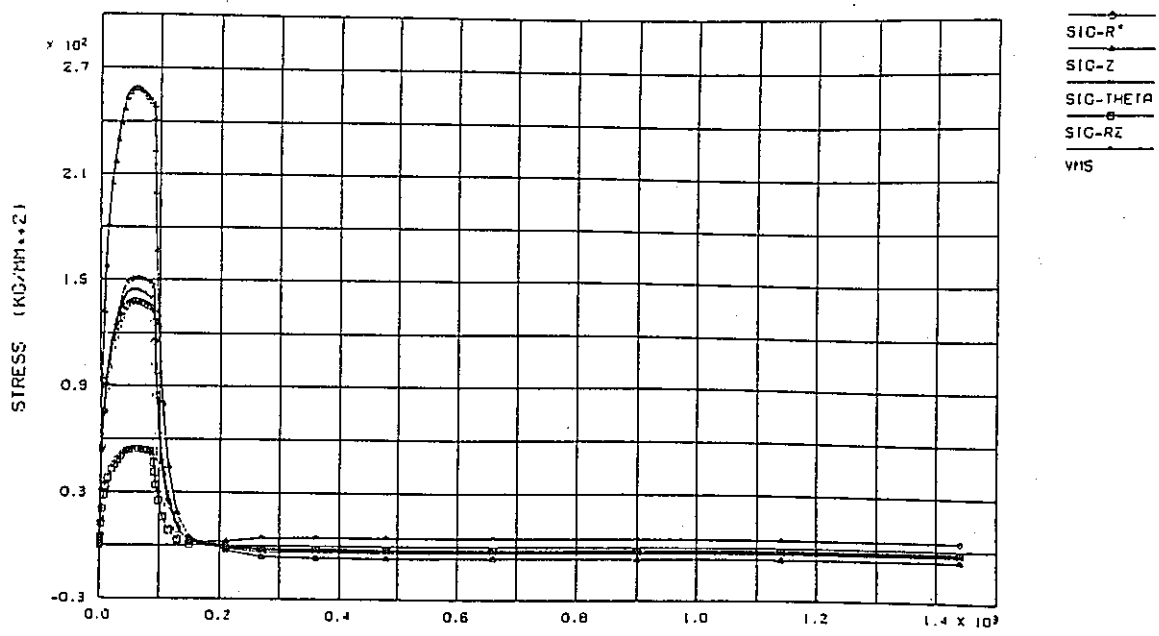

Time (sec)

Stress transition at crack tip with elastic analysis (a=3mm)

- Figure 6.c.2 (FINAS) - (38.05625mm , 0.1125mm)

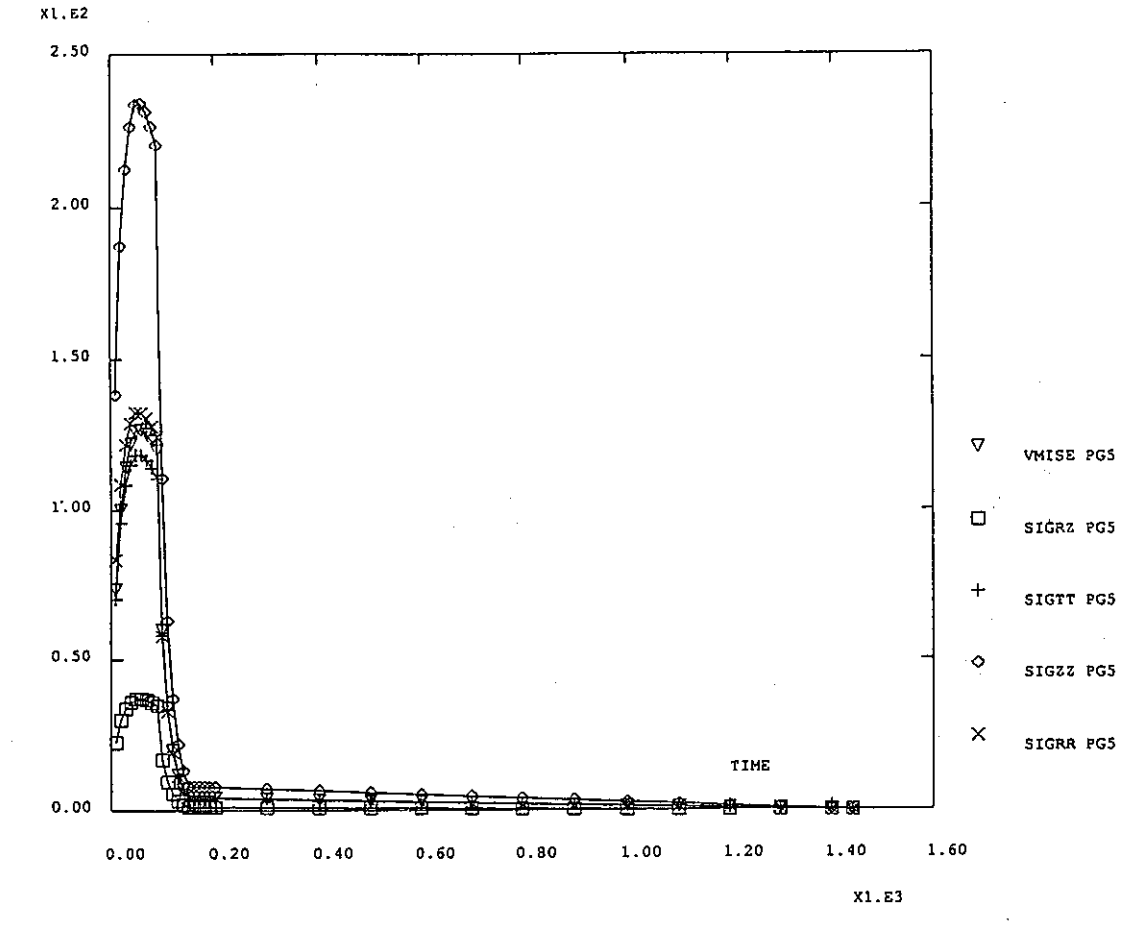

- Figure 6.d.1 (CASTEM 2000) - (40.17mm , 0.1549mm)

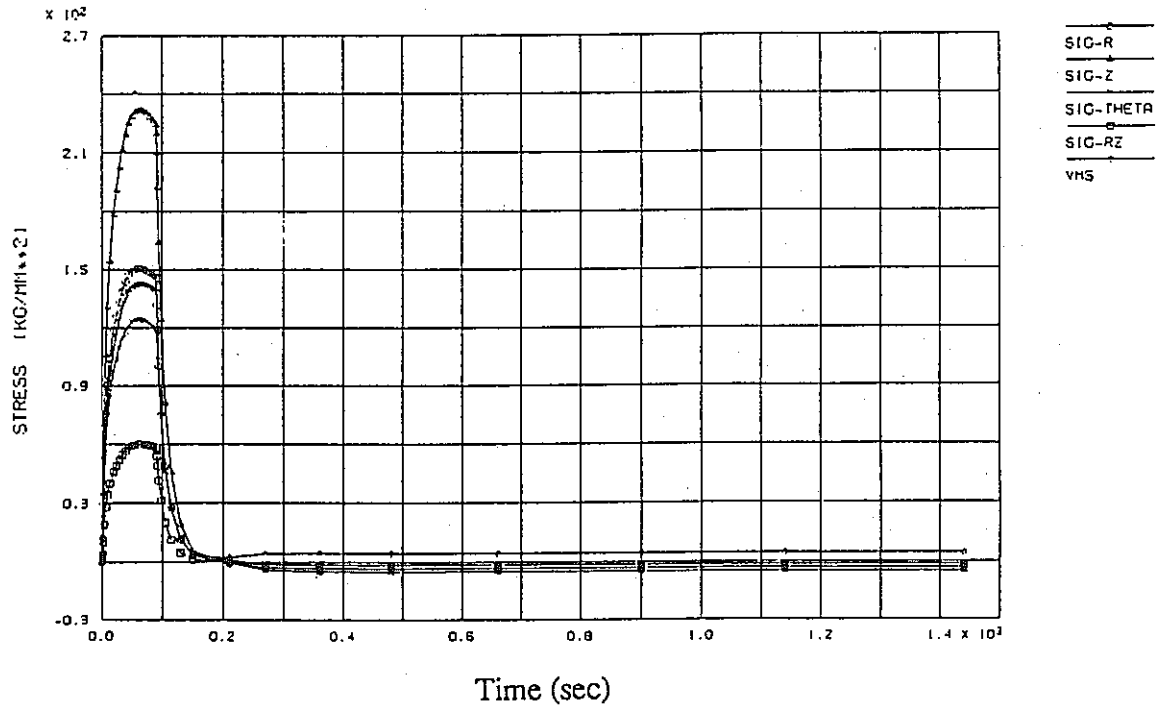

Time (sec)

Stress transition at crack tip with elastic analysis (a=5mm)

- Figure 6.d.2 (FINAS) - (40.1125mm , 0.1125mm)

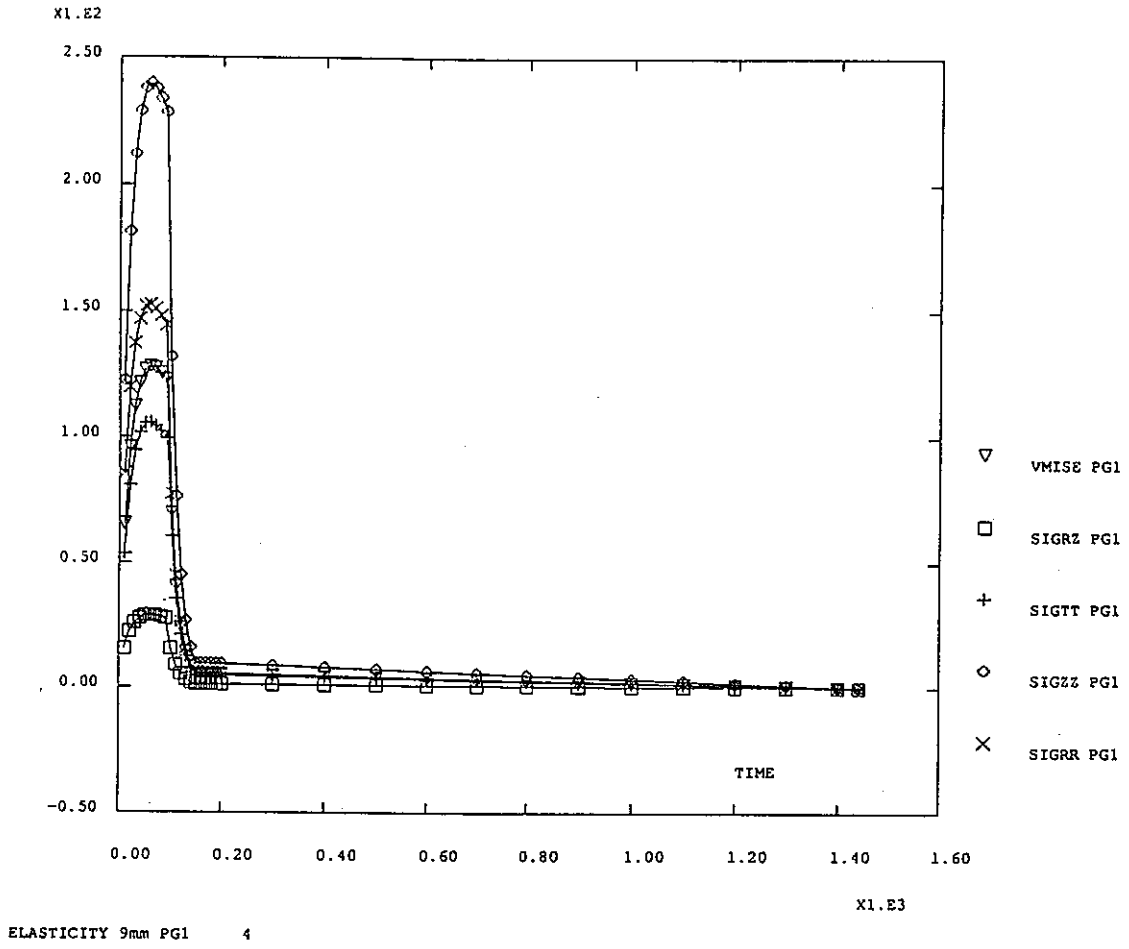

- Figure 6.e.1 (CASTEM 2000) - (44.15mm , 0.1290mm)

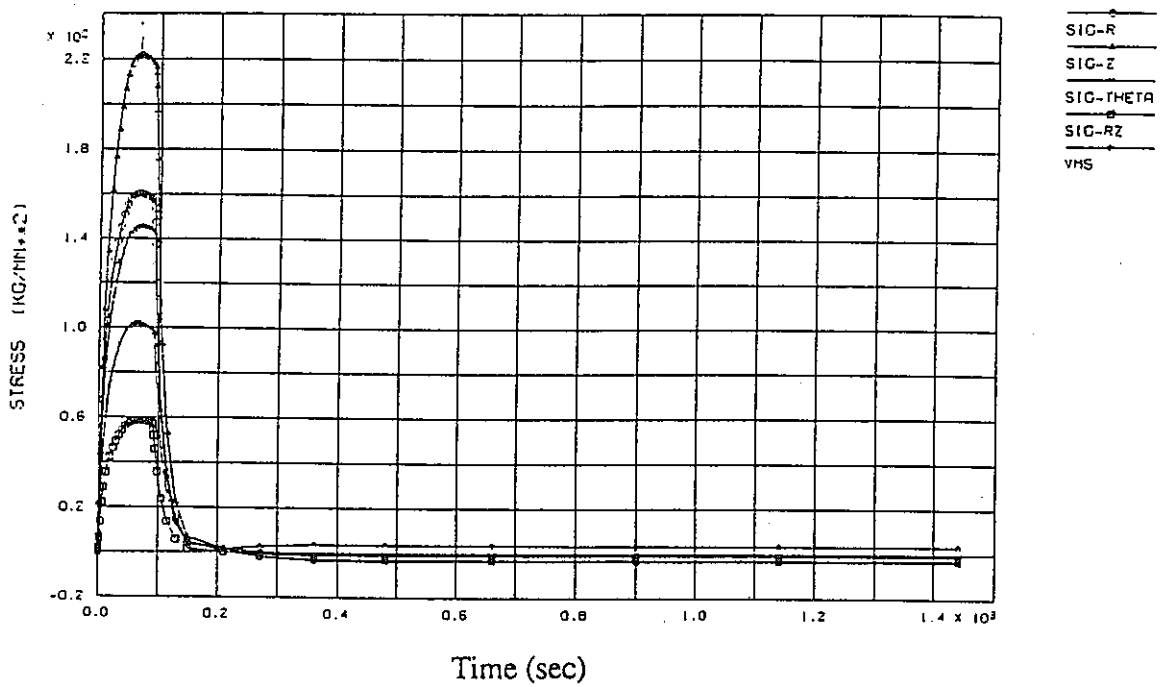

Time (sec)

Stress transition at crack tip with elastic analysis (a=9mm)

- Figure 6.e.2 (FINAS) - (44.1125mm , 0.1125mm)

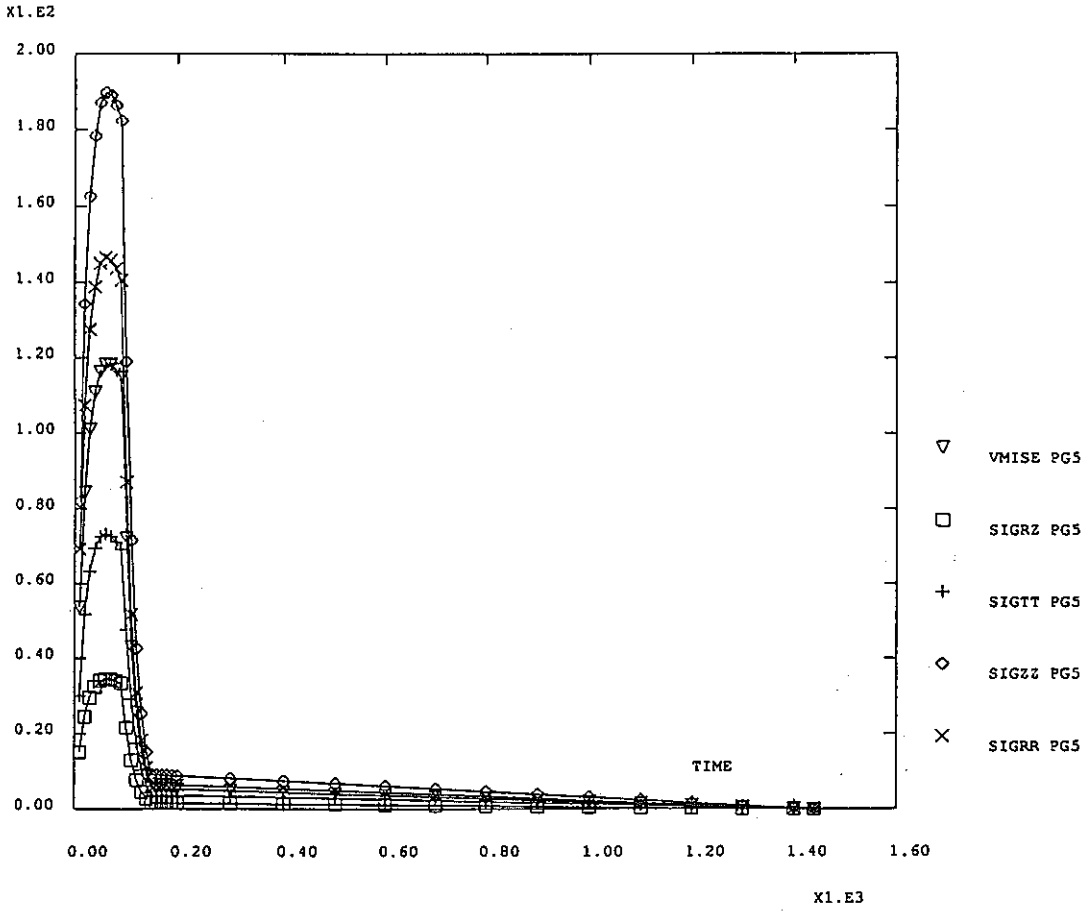

- Figure 6.f.1 (CASTEM 2000) - (50.16mm , 0.1086mm)

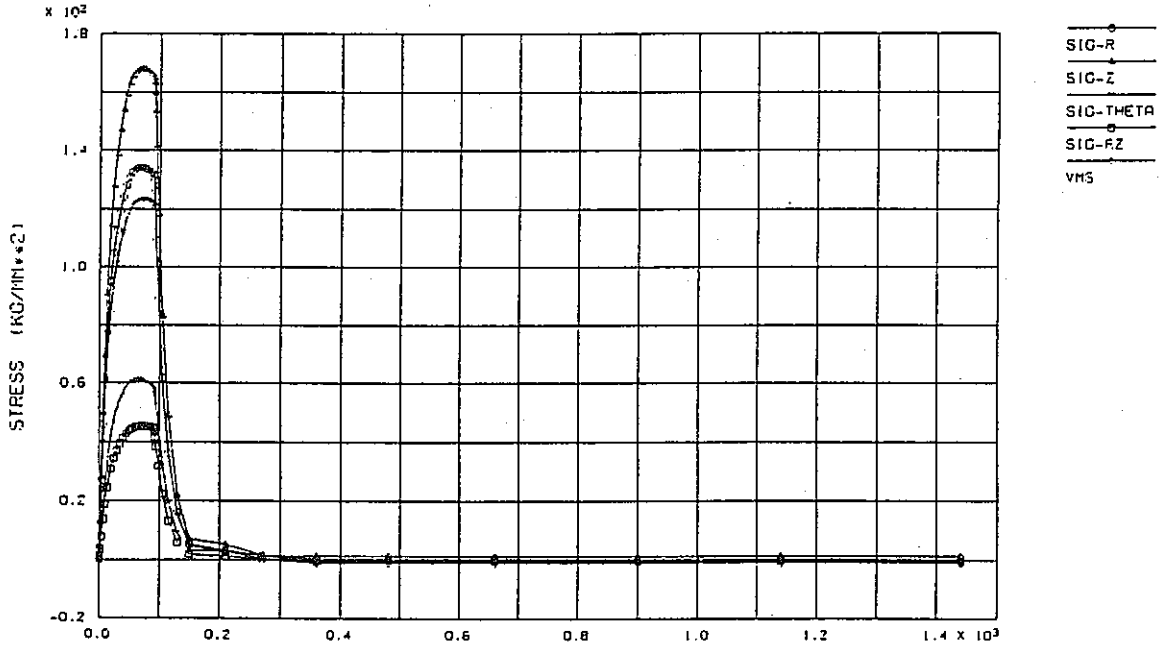

Stress transition at crack tip with elastic analysis (a=15mm)

- Figure 6.f.2 (FINAS) - (50.1125mm , 0.1125mm)

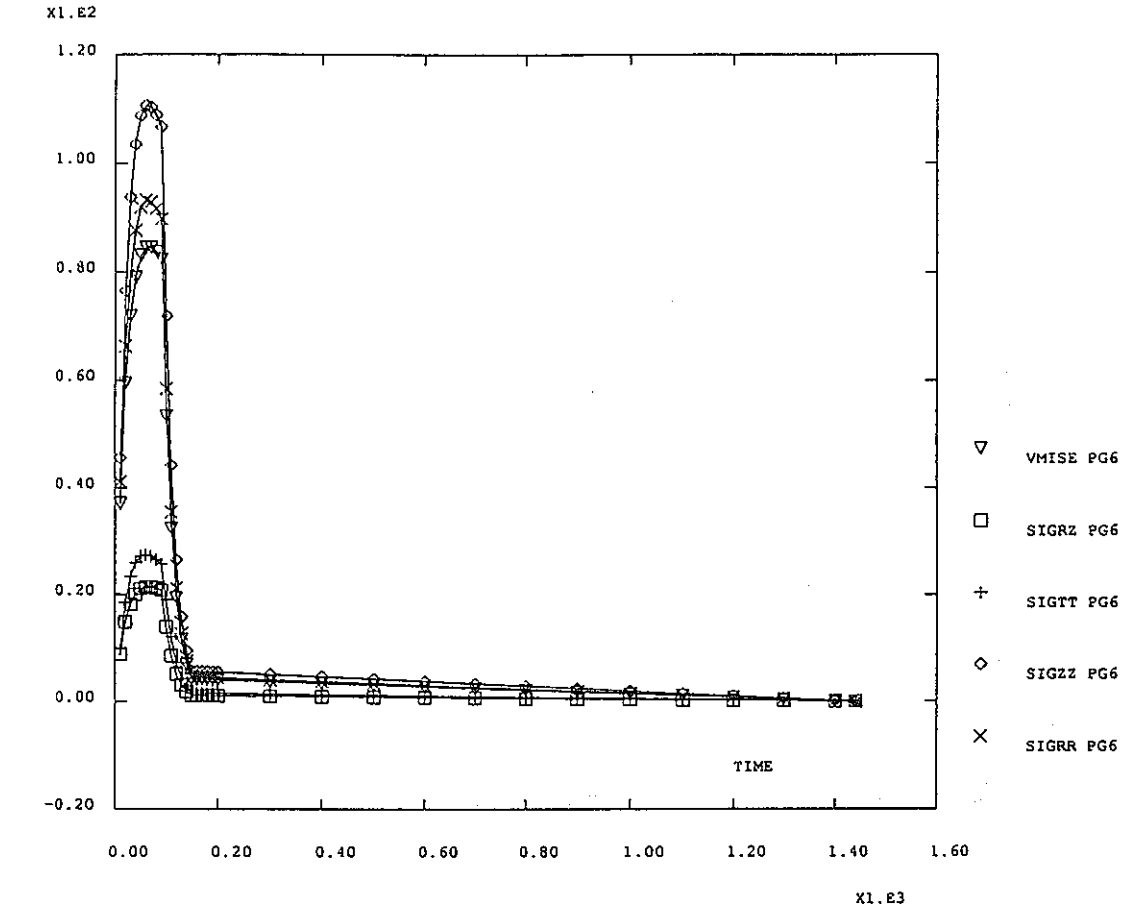

- Figure 6.g.1 (CASTEM 2000) - (55.19mm , 0.1782mm)

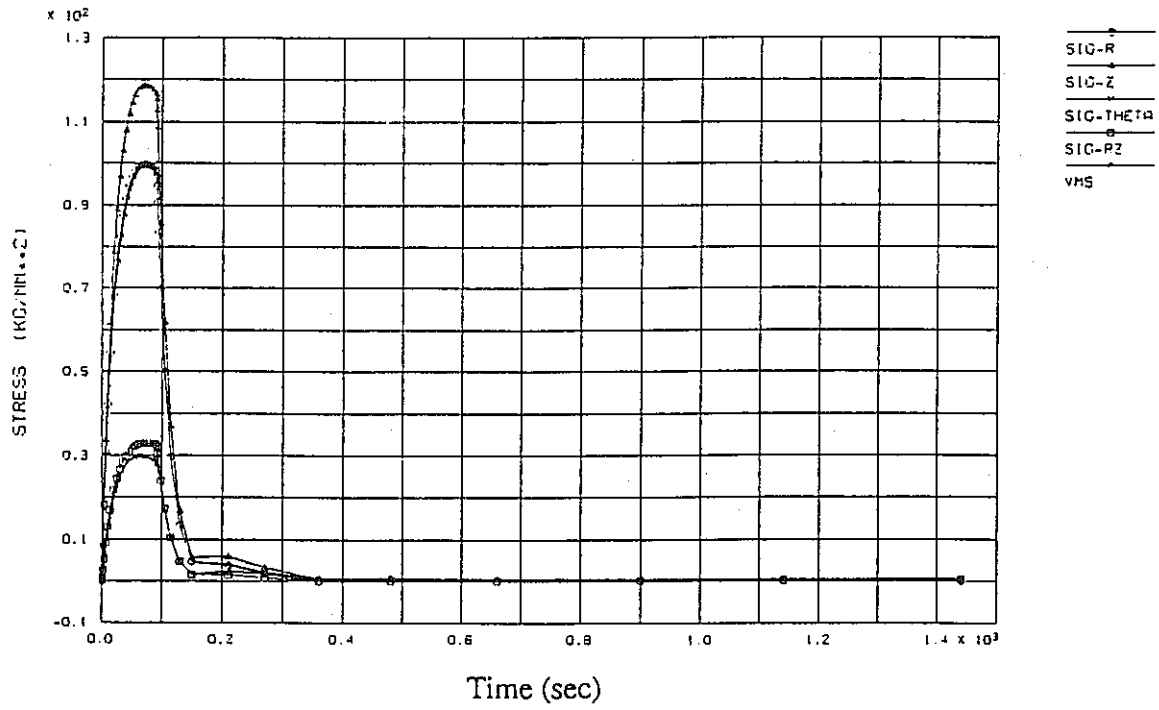

Time (sec)

Stress transition at crack tip with elastic analysis (a=20mm)

- Figure 6.g.2 (FINAS) - (55.1125mm , 0.1125mm)

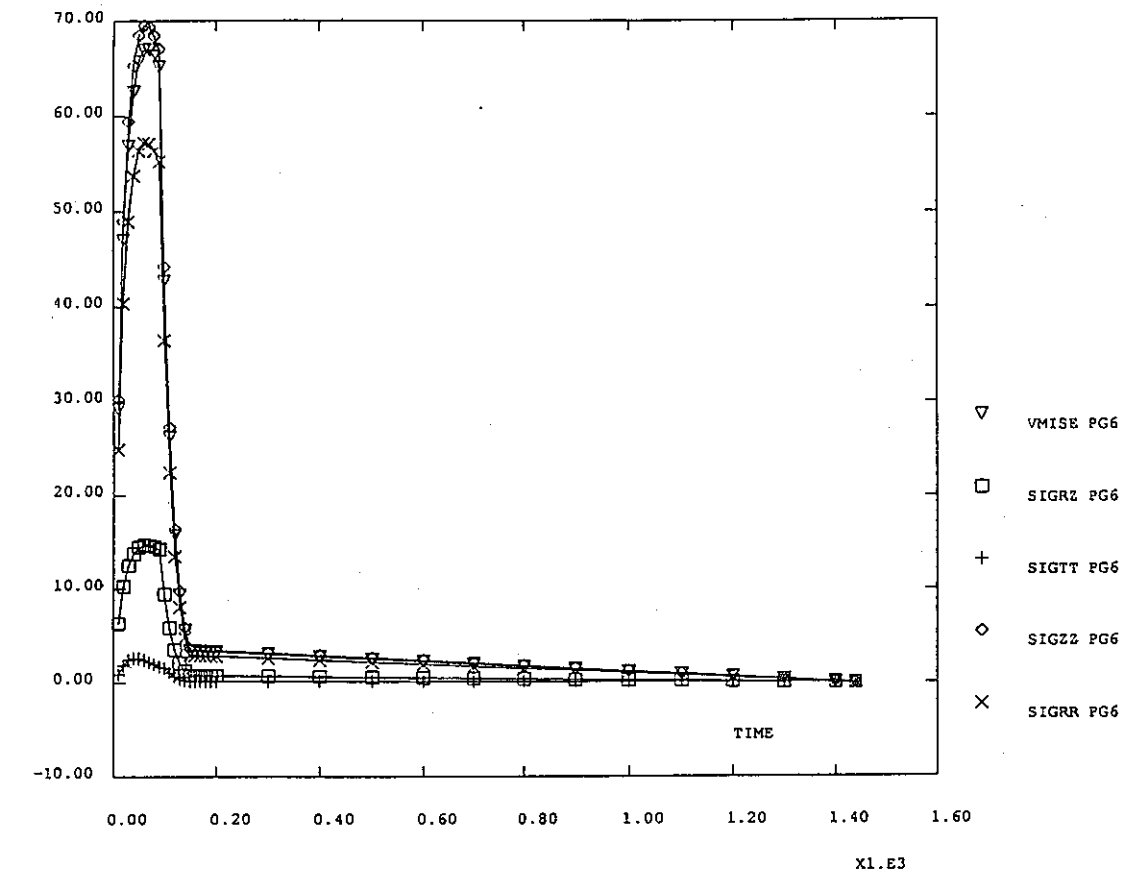

- Figure 6.h.1 (CASTEM 2000) - (60.19mm , 0.1782mm)

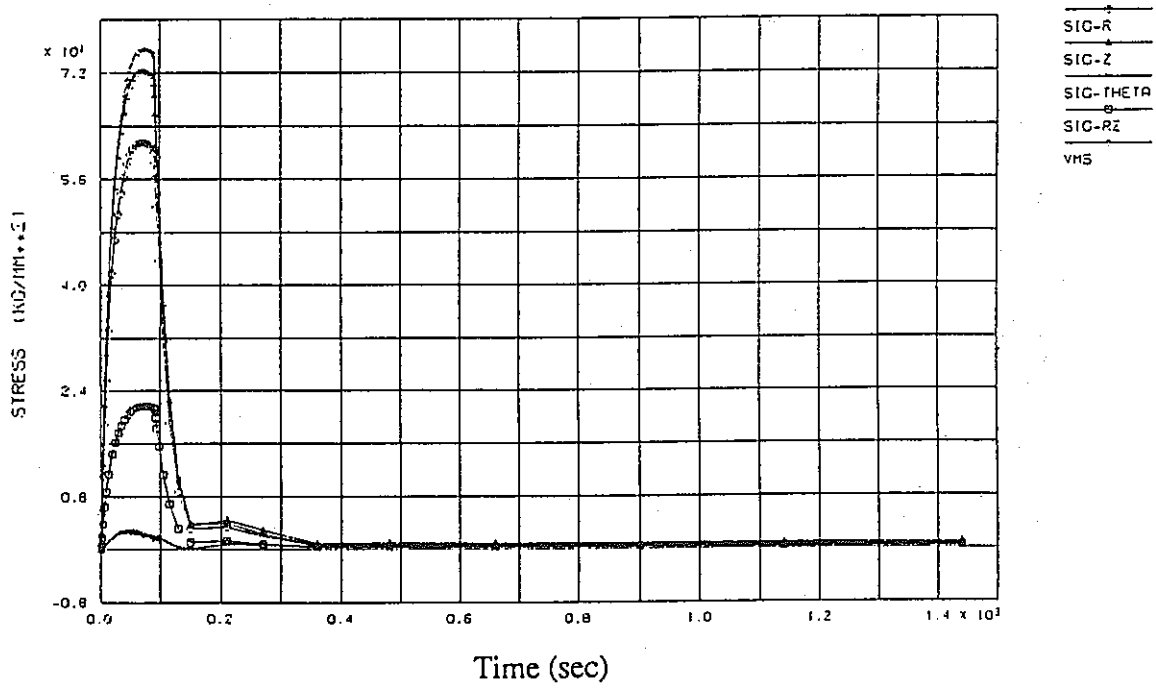

Stress transition at crack tip with elastic analysis (a=25mm)

- Figure 6.h.2 (FINAS) - (60.1125mm , 0.1125mm)

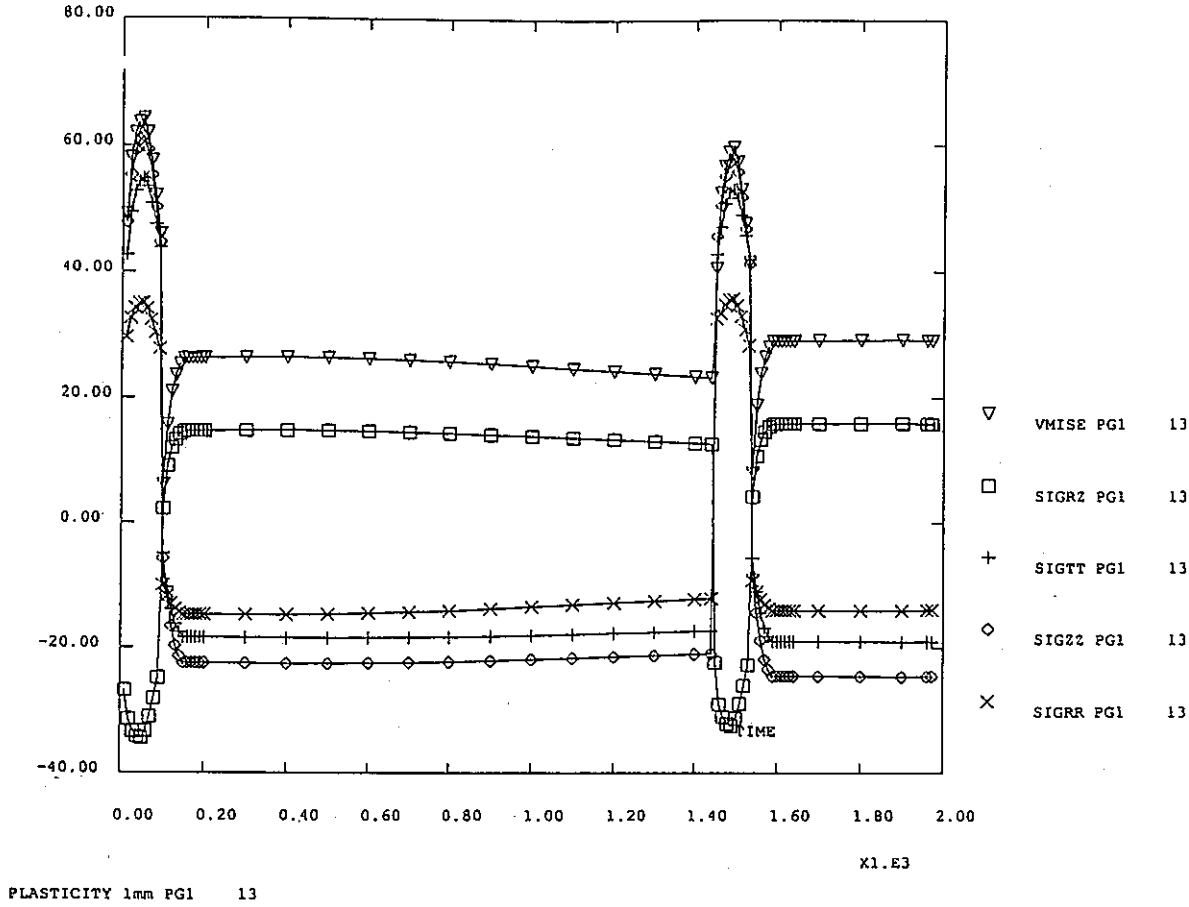

- Figure 7.a.1 (CASTEM 2000) - (35.98mm , 0.05954mm)

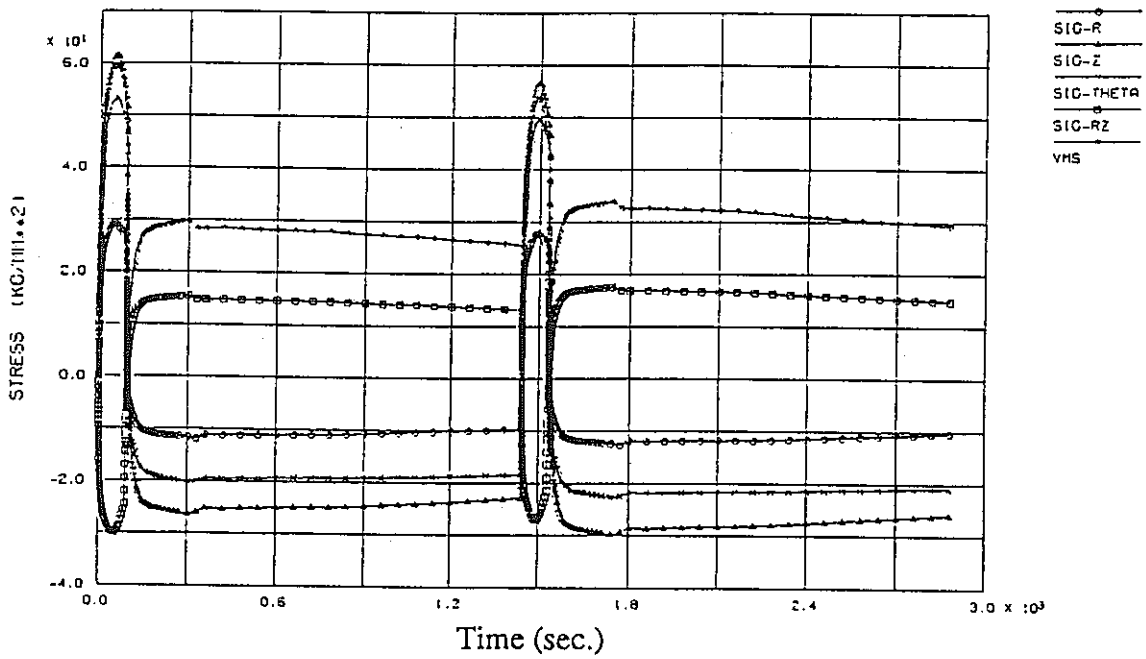

Stress transition at crack tip with elasto-plastic analysis (a=1mm)

- Figure 7.a.2 (FINAS) - (35.971875mm , 0.1125mm)

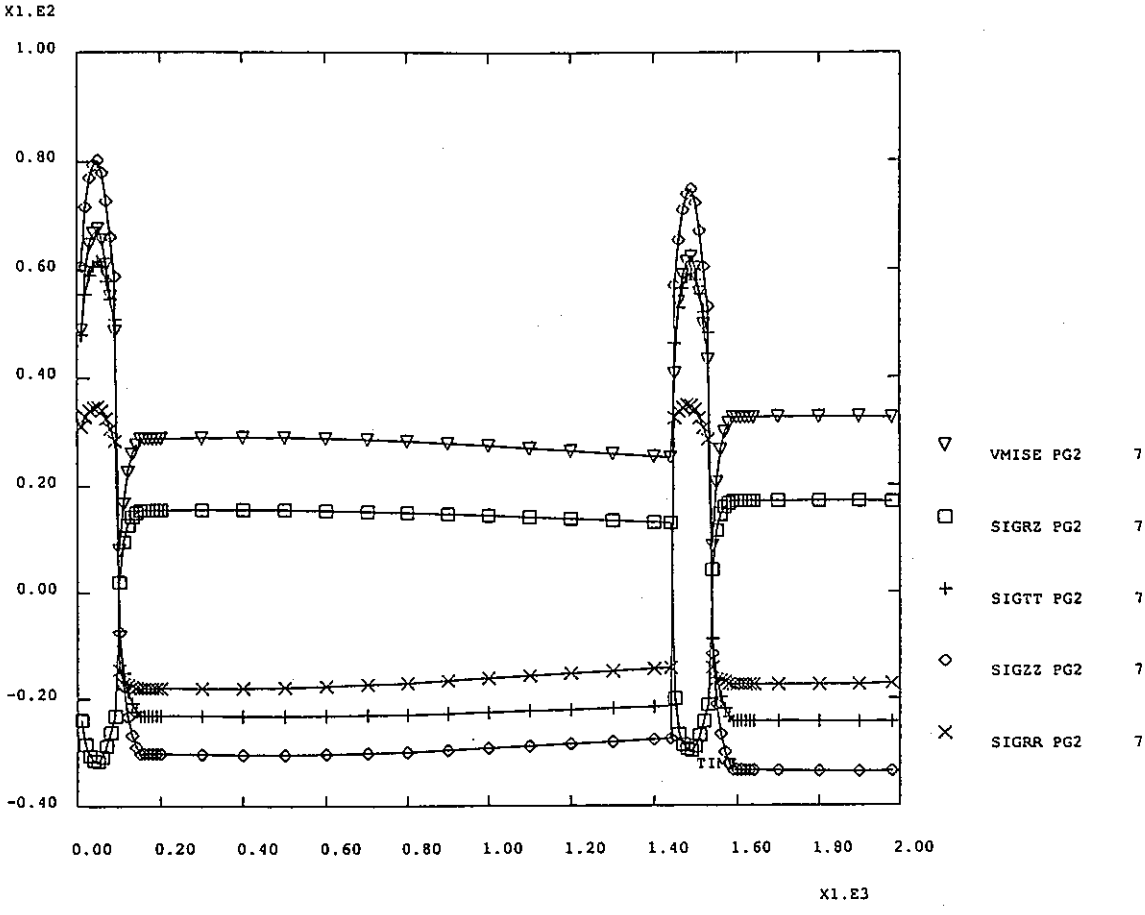

- Figure 7.b.1 (CASTEM 2000) - (36.98mm , 0.1310mm)

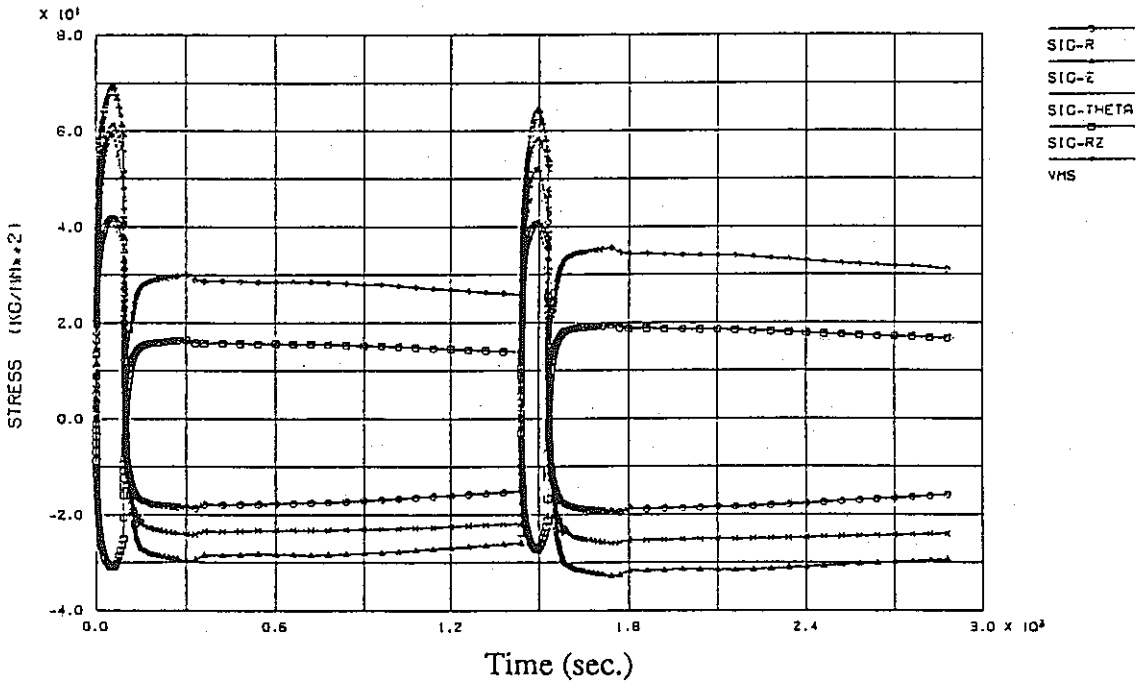

Stress transition at crack tip with elasto-plastic analysis (a=2mm)

- Figure 7.b.2 (FINAS) - (36.94375mm , 0.1125mm)

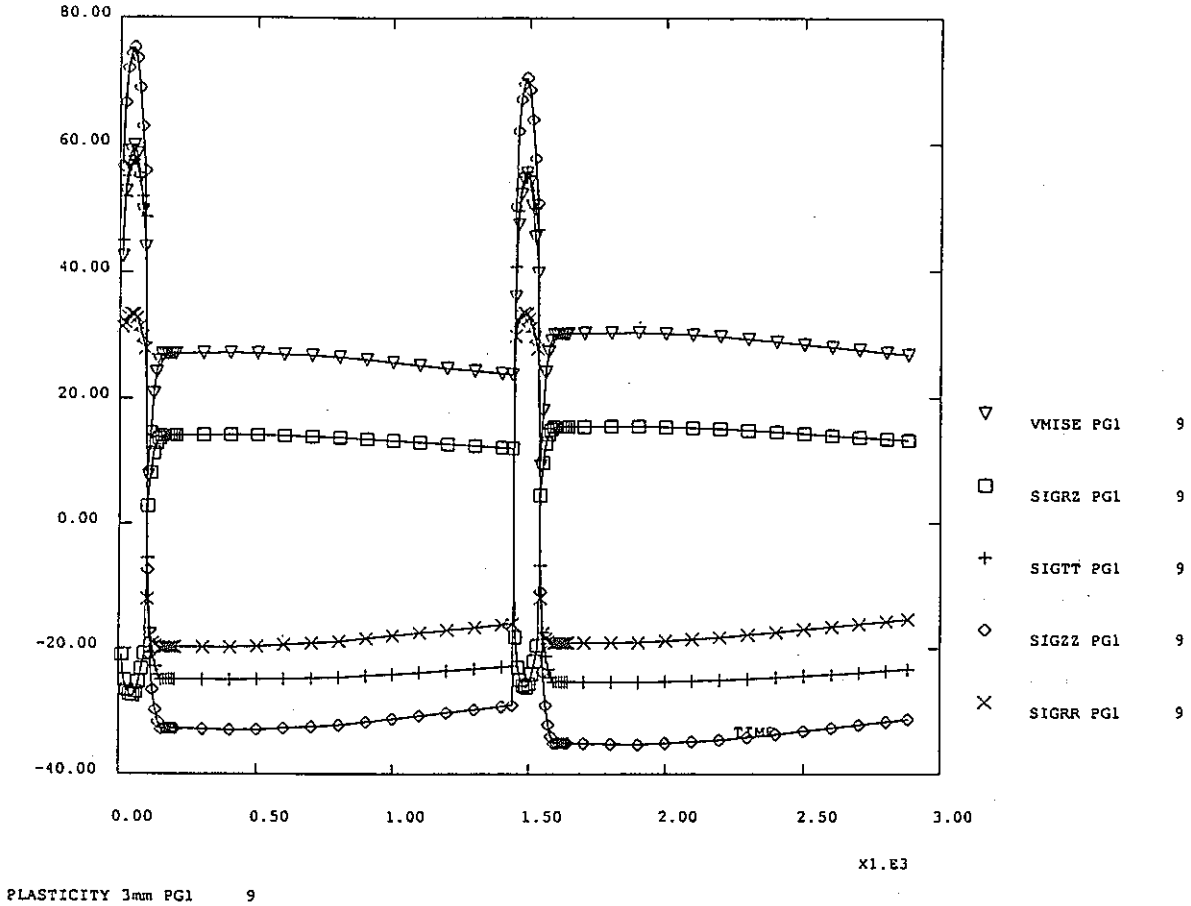

- Figure 7.c.1 (CASTEM 2000) - (37.97mm , 0.1536mm)

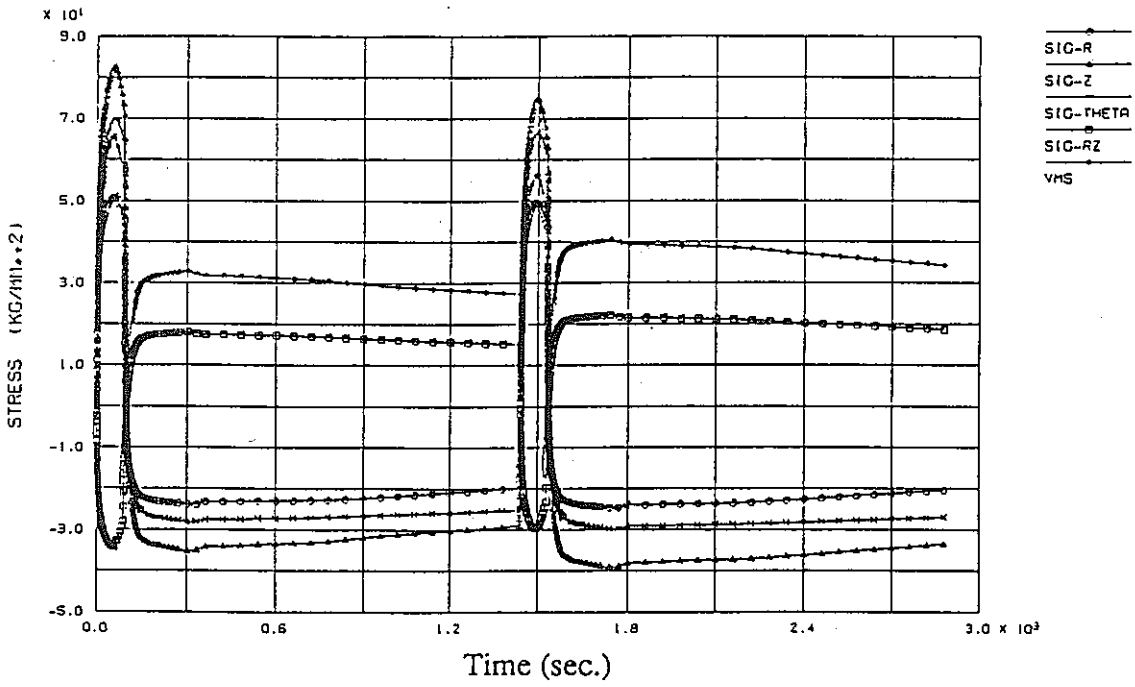

Stress transition at crack tip with elasto-plastic analysis (a=3mm)

- Figure.7.c.2 (FINAS) - (37.94375mm , 0.1125mm)

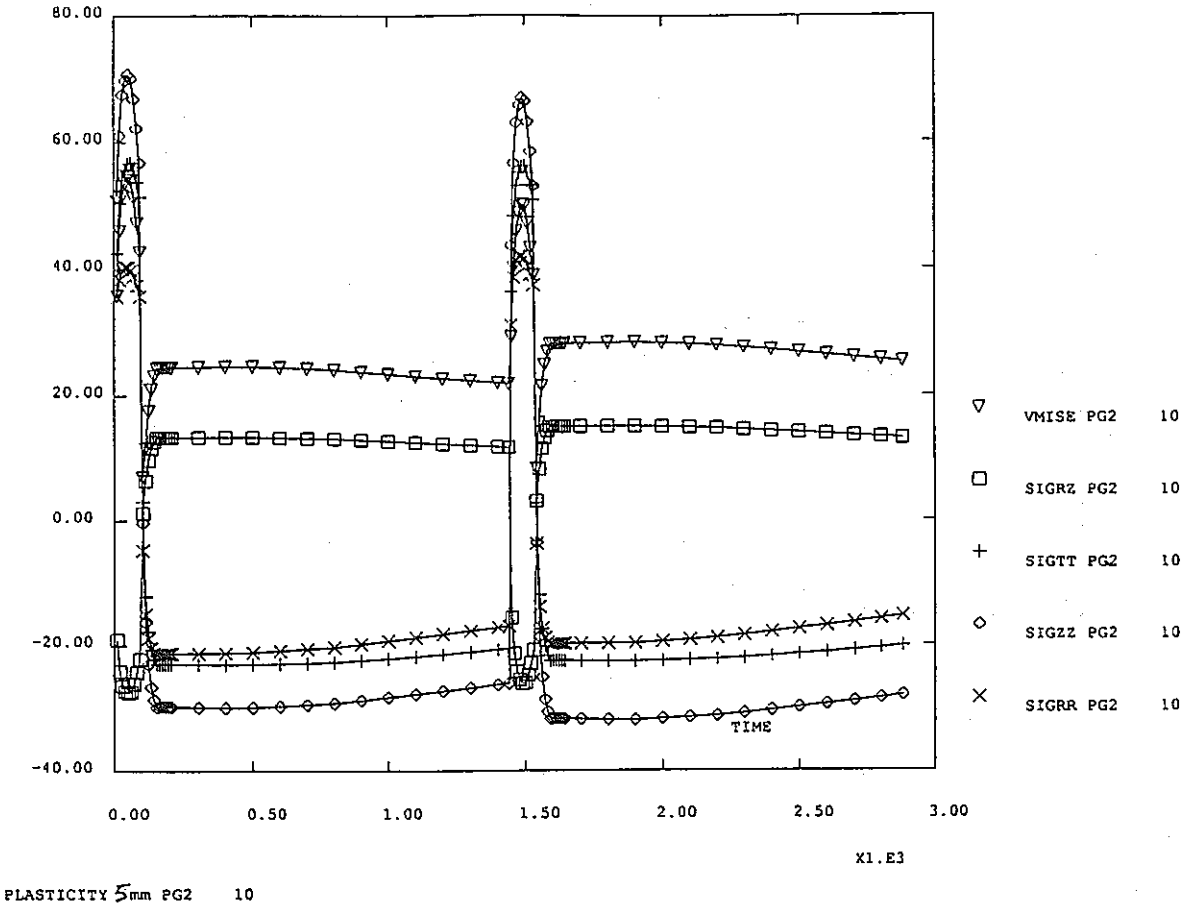

- Figure 7.d.1 (CASTEM 2000) - (39.96mm , 0.3295mm)

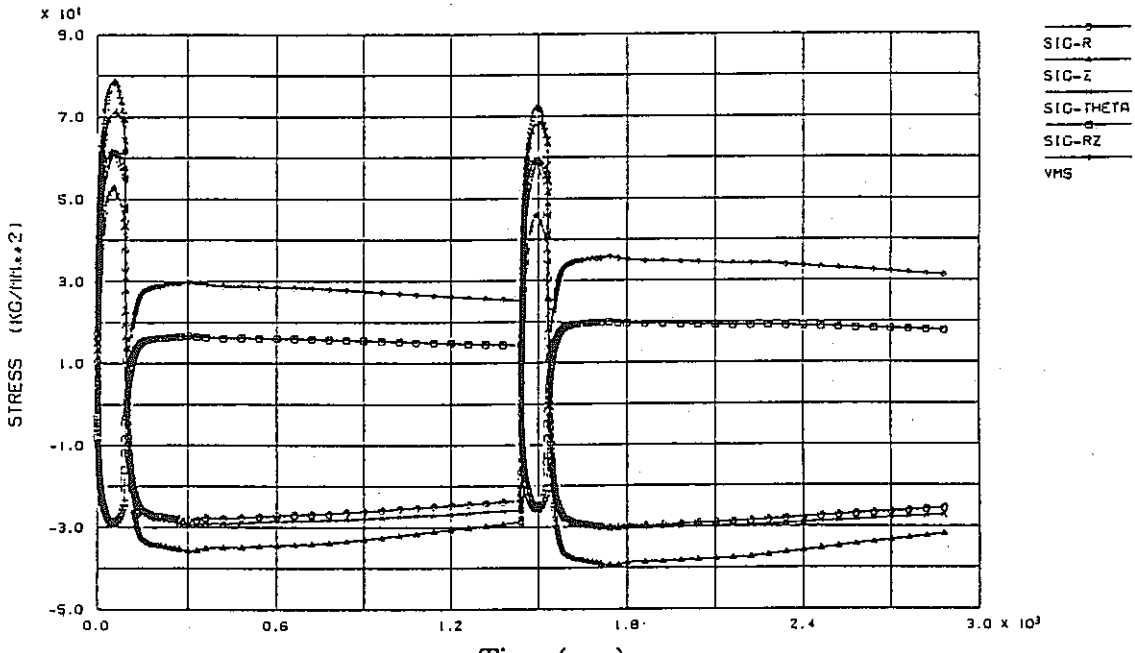

Time (sec.)

Stress transition at crack tip with elasto-plastic analysis (a=5mm)

- Figure 7.d.2 (FINAS) - (39.8875mm , 0.1125mm)

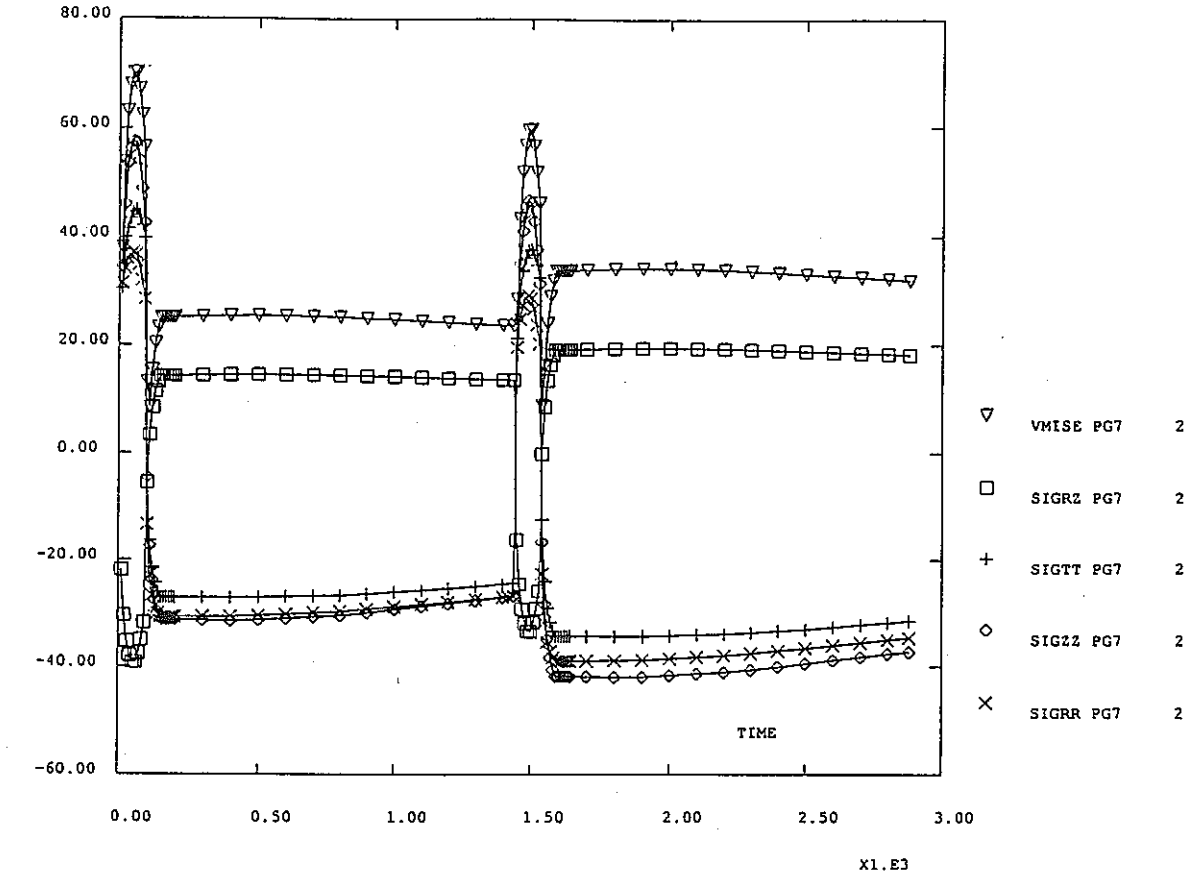

- Figure 7.e.1 (CASTEM 2000) - (43.97mm , 0.2135mm)

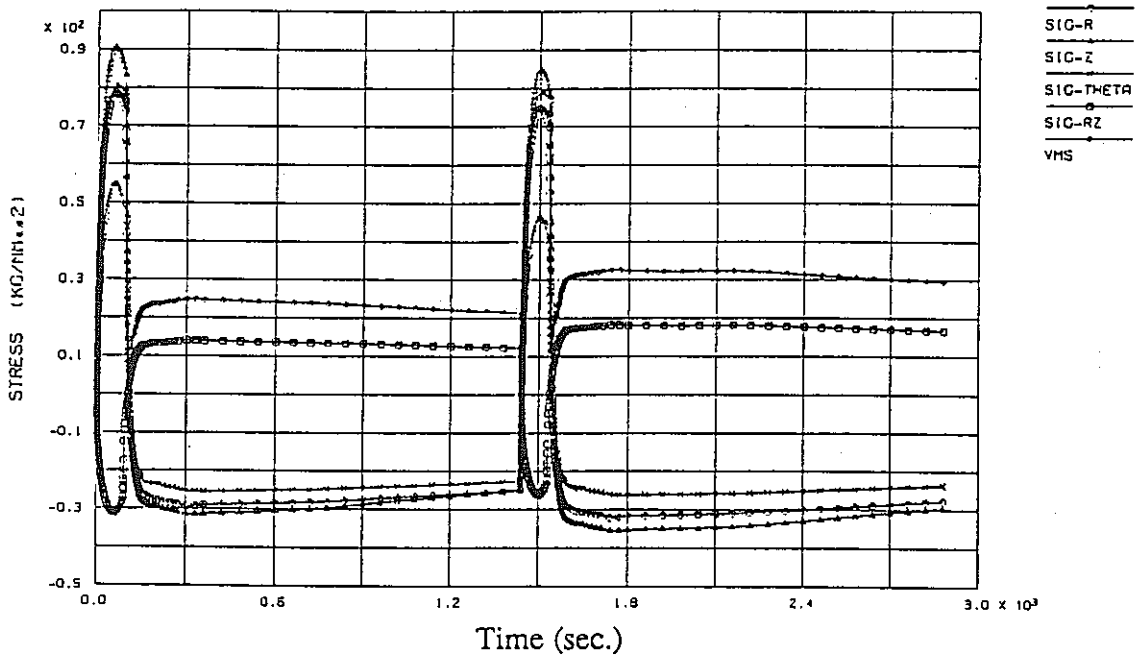

Time (sec.)

Stress transition at crack tip with elasto-plastic analysis (a=9mm)

- Figure 7.e.2 (FINAS) - (43.8875mm , 0.1125mm)

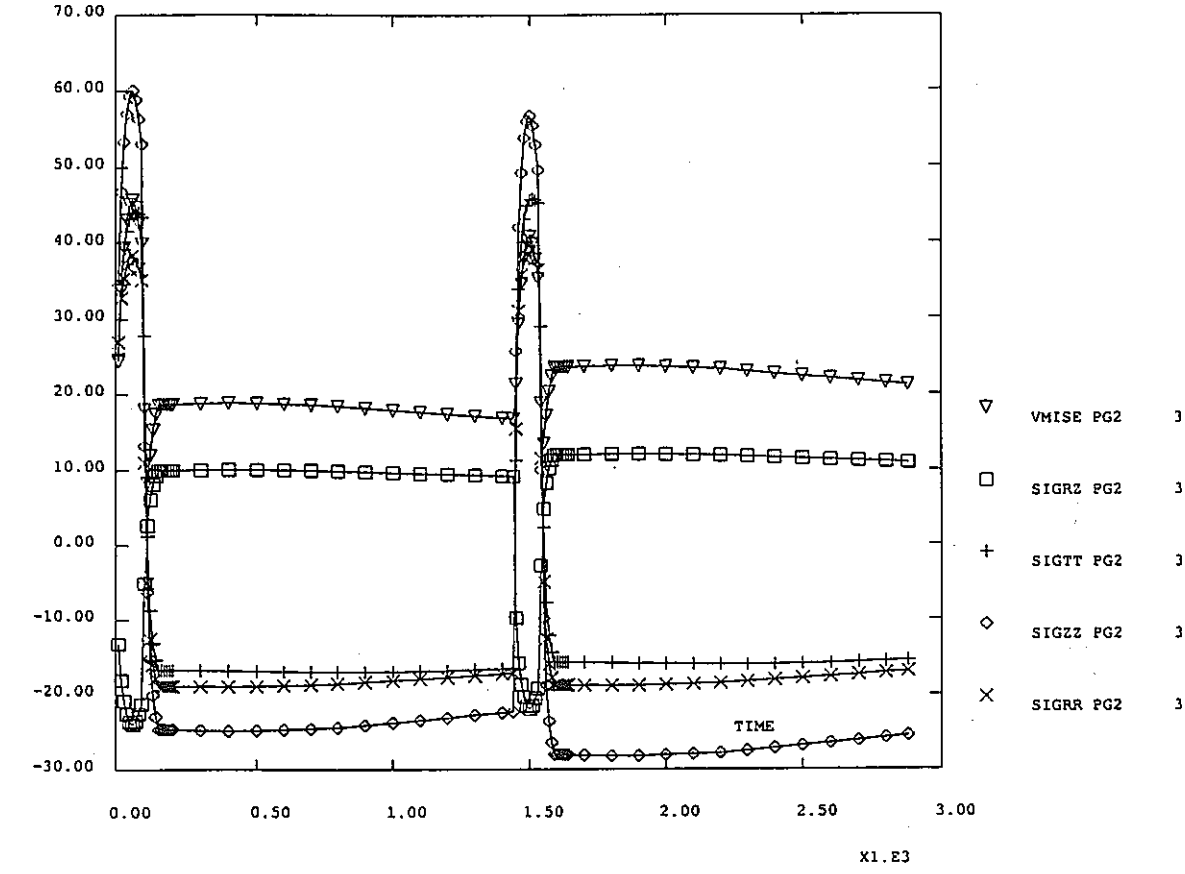

- Figure 7.f.1 (CASTEM 2000) - (49.98mm , 0.3359mm)

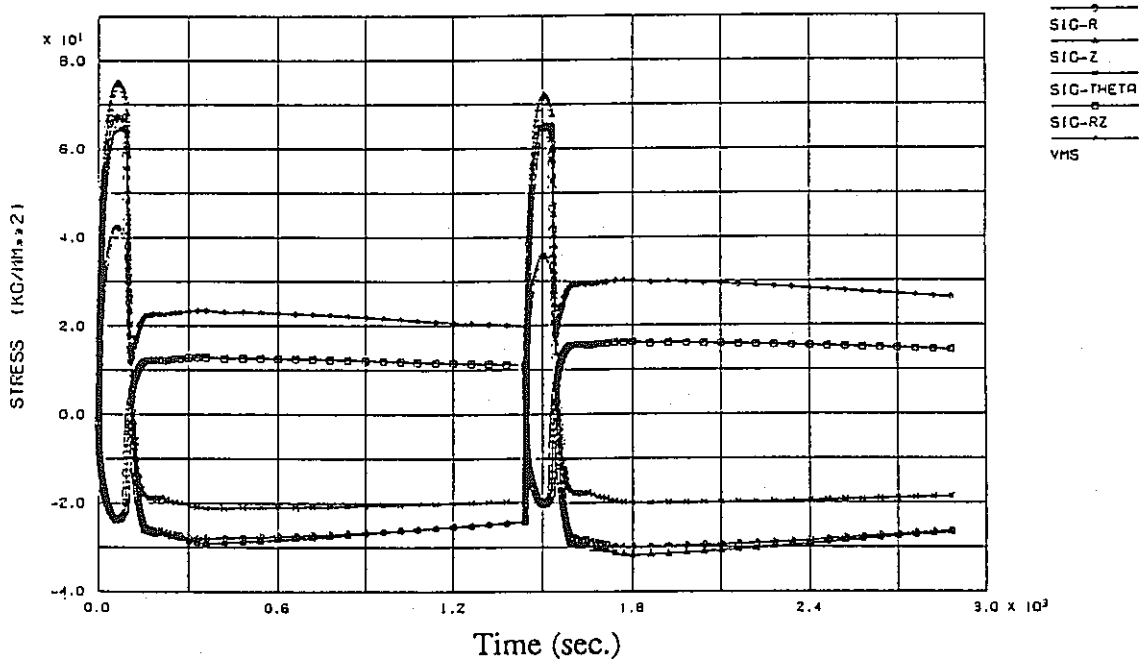

Stress transition at crack tip with elasto-plastic analysis (a=15mm)

- Figure 7.f.2 (FINAS) - (49.8875mm , 0.1125mm)

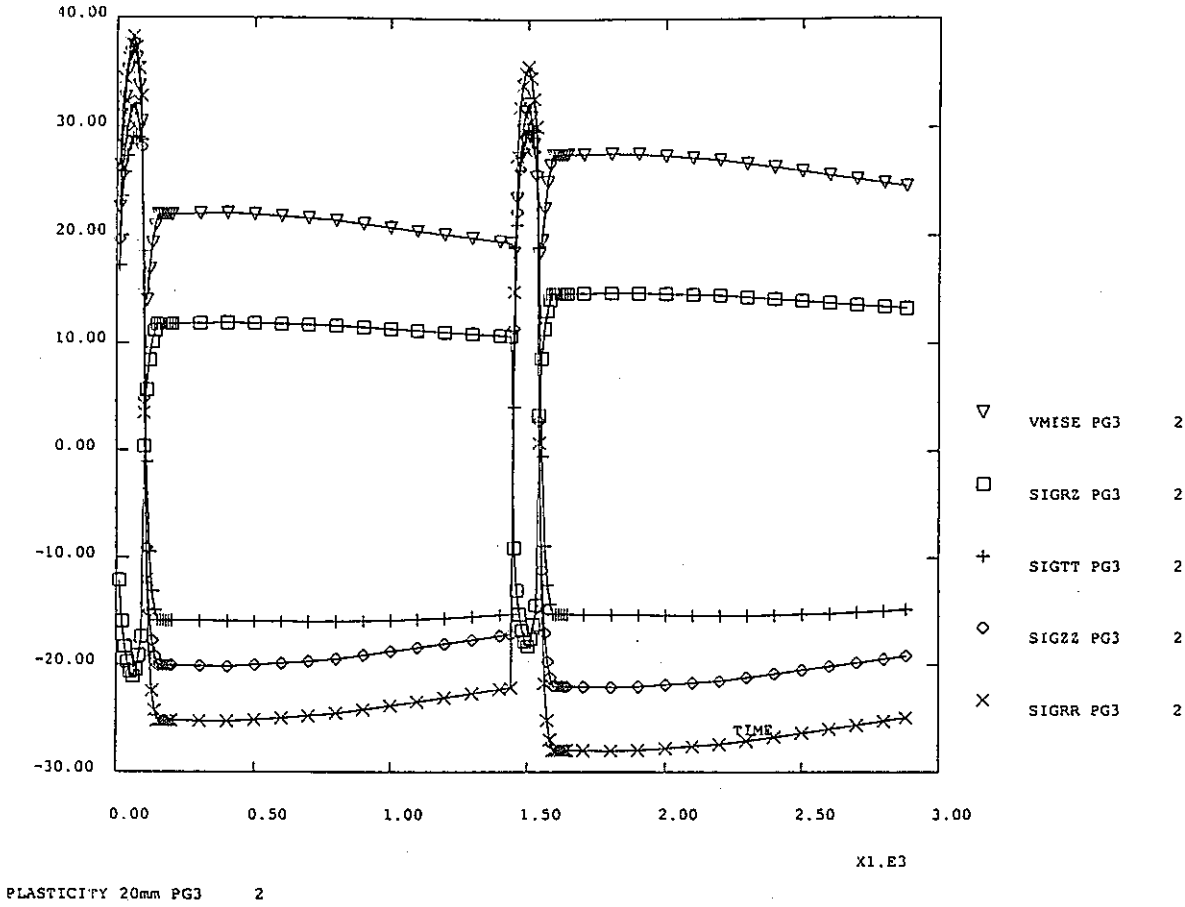

- Figure 7.g.1 (CASTEM 2000) - (54.92mm , 0.0541mm)

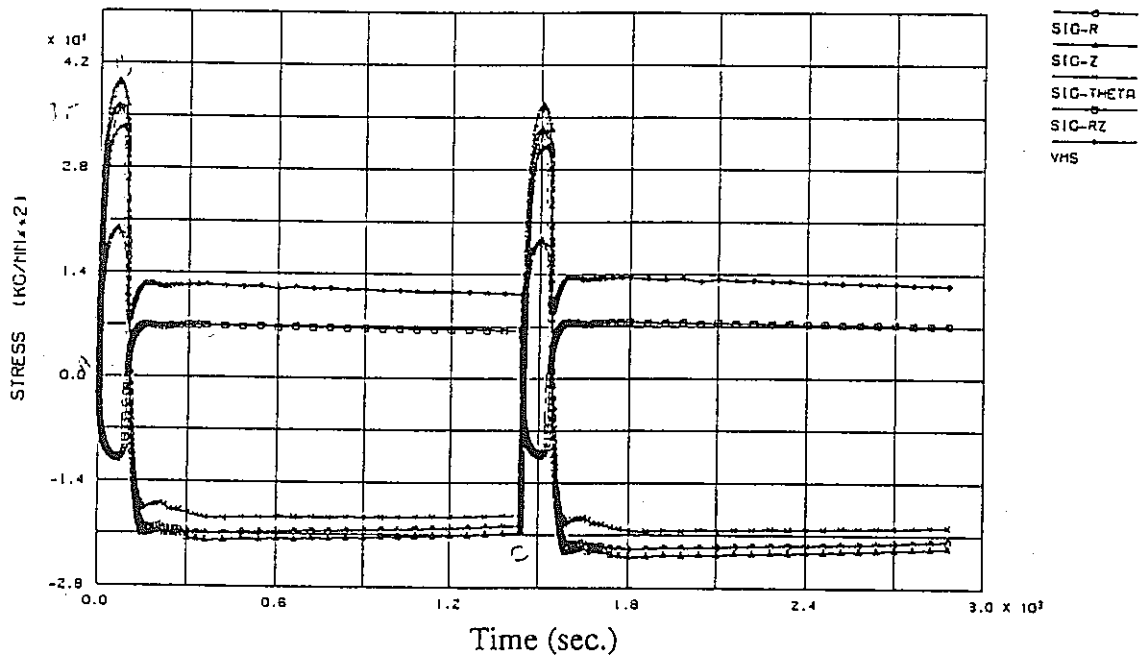

Stress transition at crack tip with elasto-plastic analysis (a=20mm)

- Figure 7.g.2 (FINAS) - (54.8875mm , 0.1125mm)

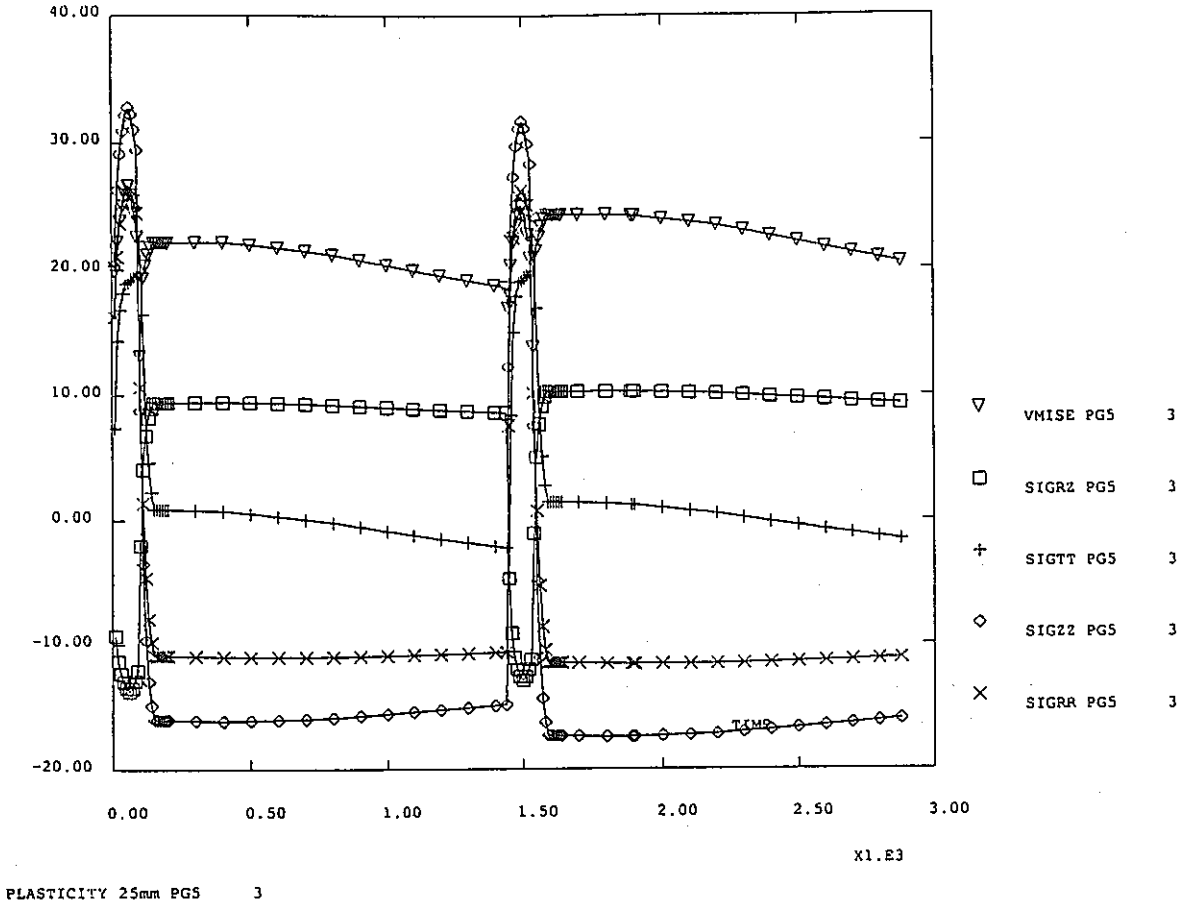

- Figure 7.h.1 (CASTEM 2000) - (58.89mm , 0.2392mm)

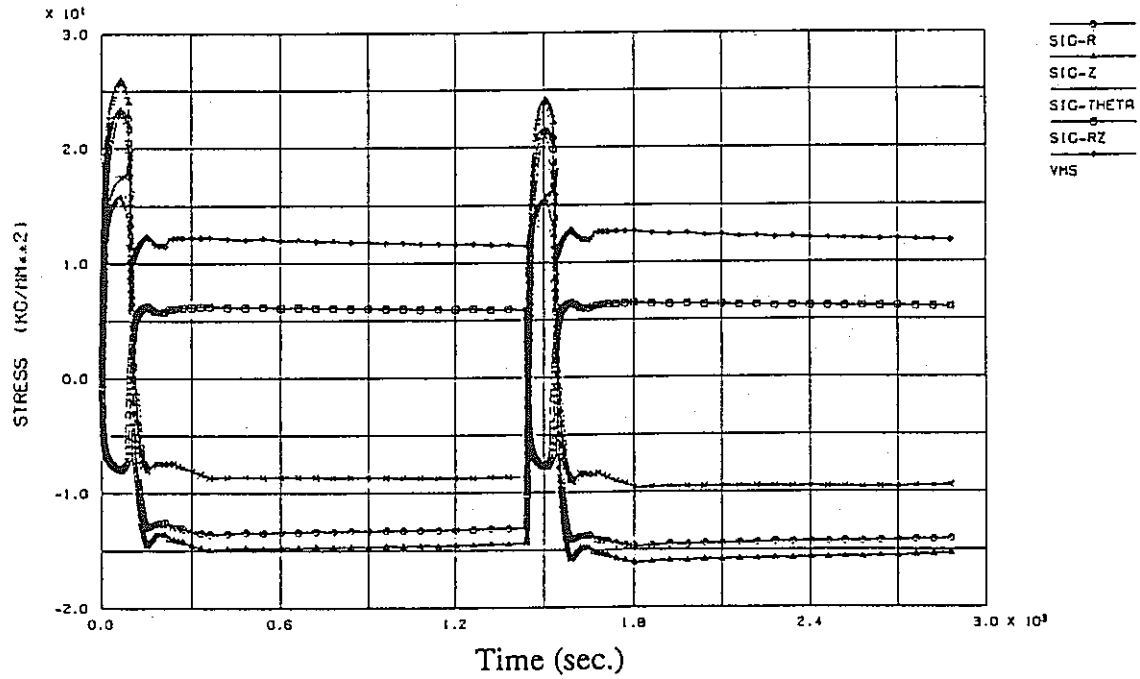

Stress transition at crack tip with elasto-plastic analysis (a=25mm)

- Figure 7.h.2 (FINAS) - (59.8875mm , 0.1125mm)

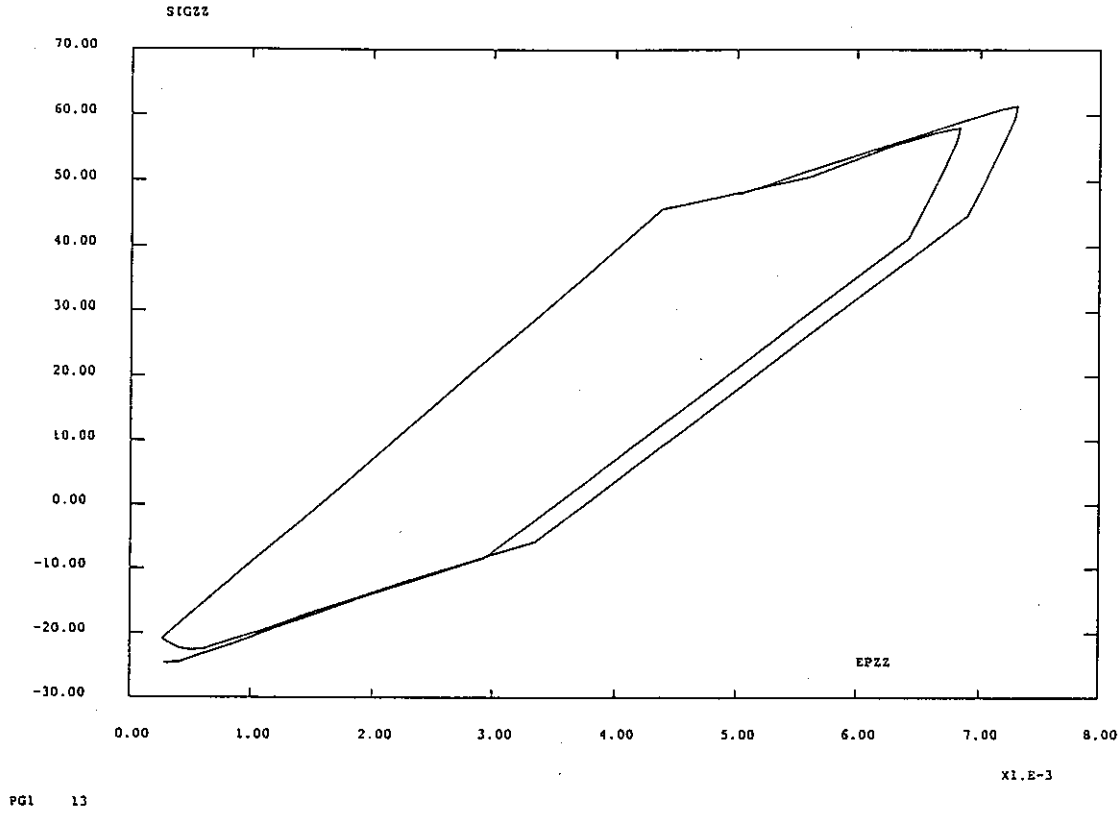

- Figure 8.a.1 (CASTEM 2000) -

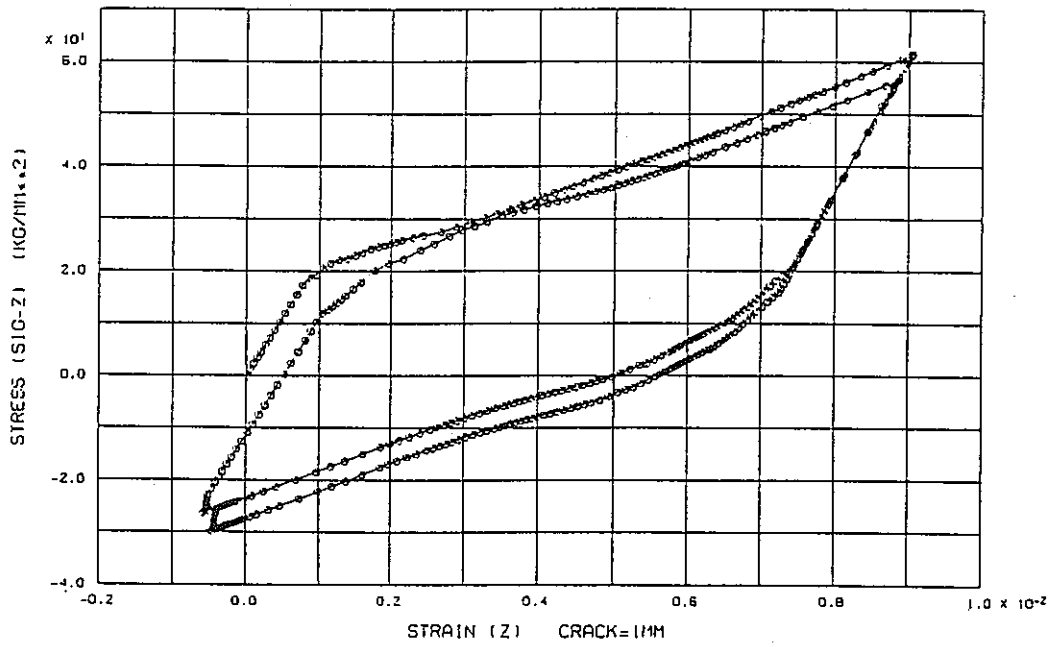

Axial stress and strain histeresis curve (a=1mm)

PLASTICITY (stresses and strains at the same points as in Figure 7)

- Figure 8.a.2 (FINAS) -

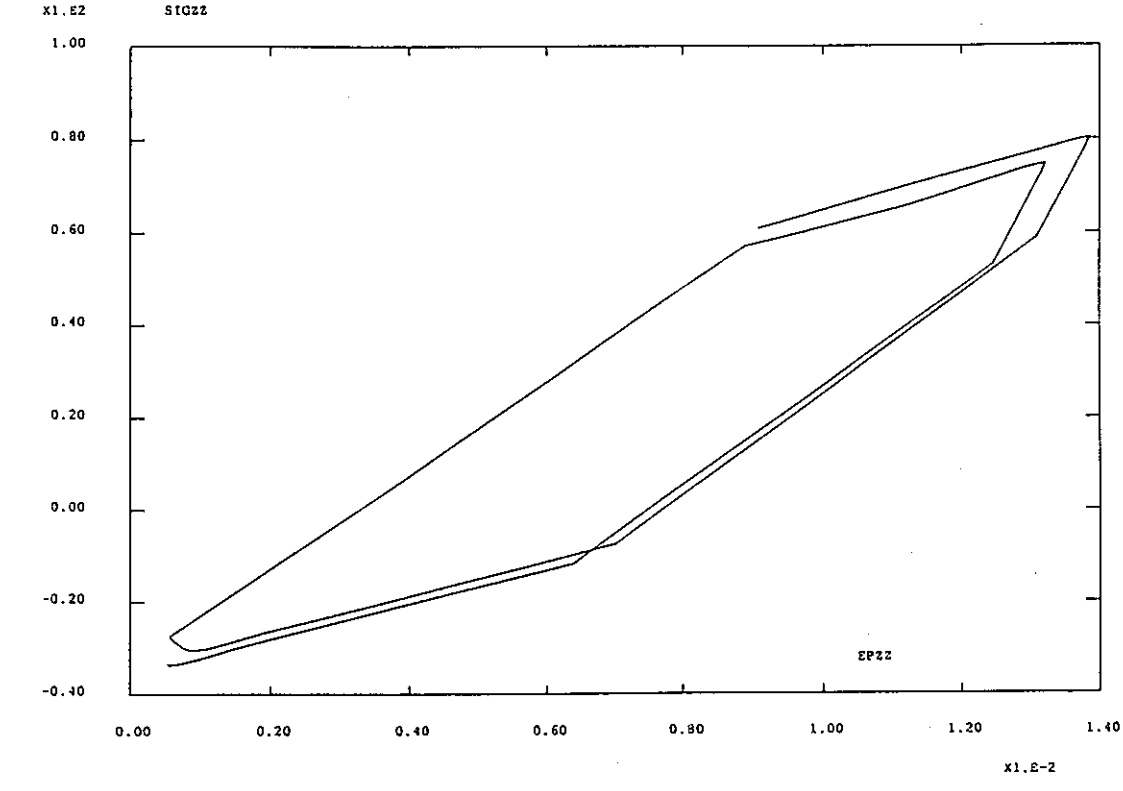

- Figure 8.b.1 (CASTEM 2000) -

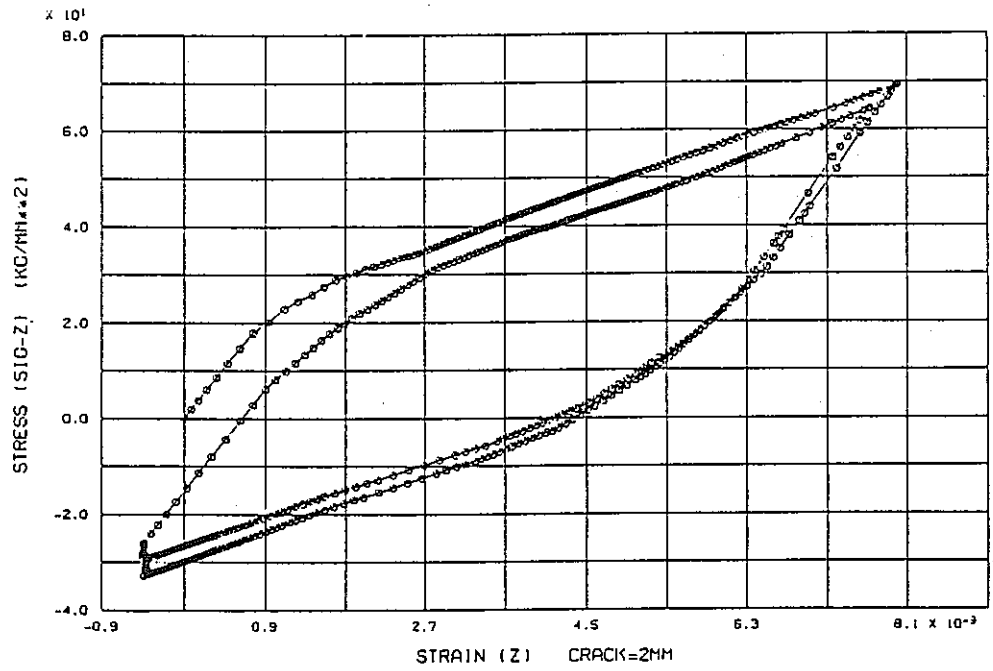

Axial stress and strain histeresis curve (a=2mm)

- Figure 8.b.2 (FINAS) -

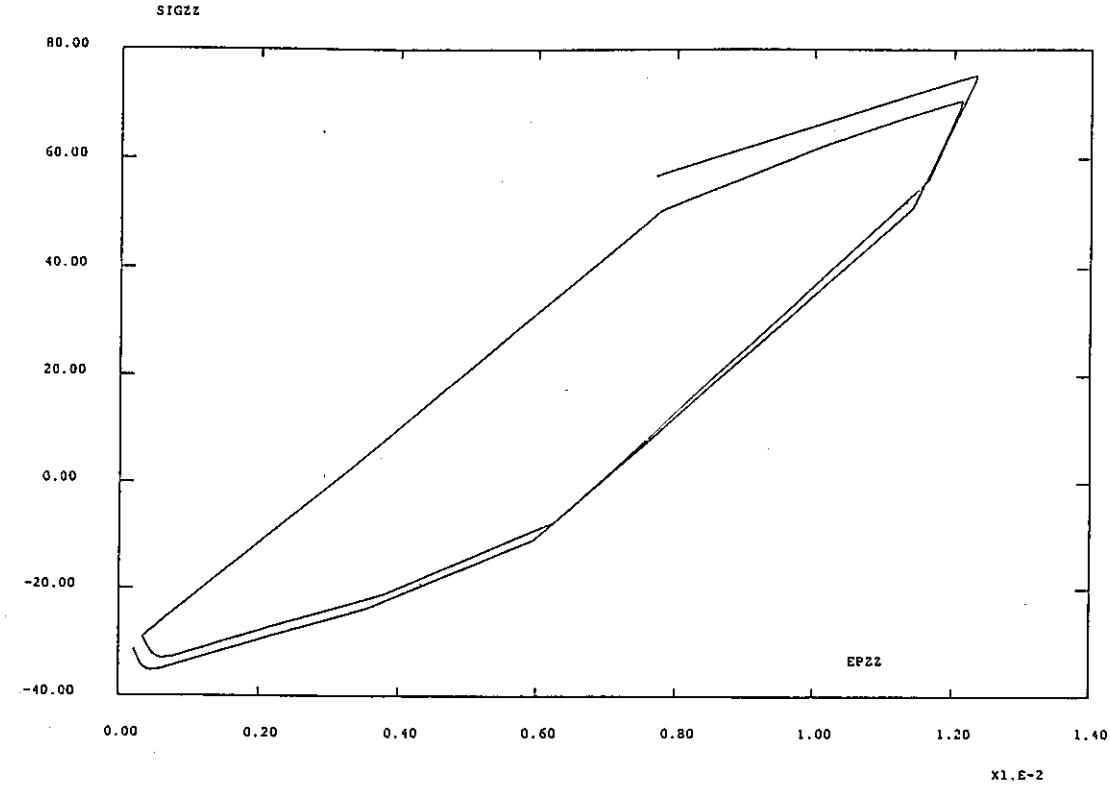

- Figure 8.c.1 (CASTEM 2000) -

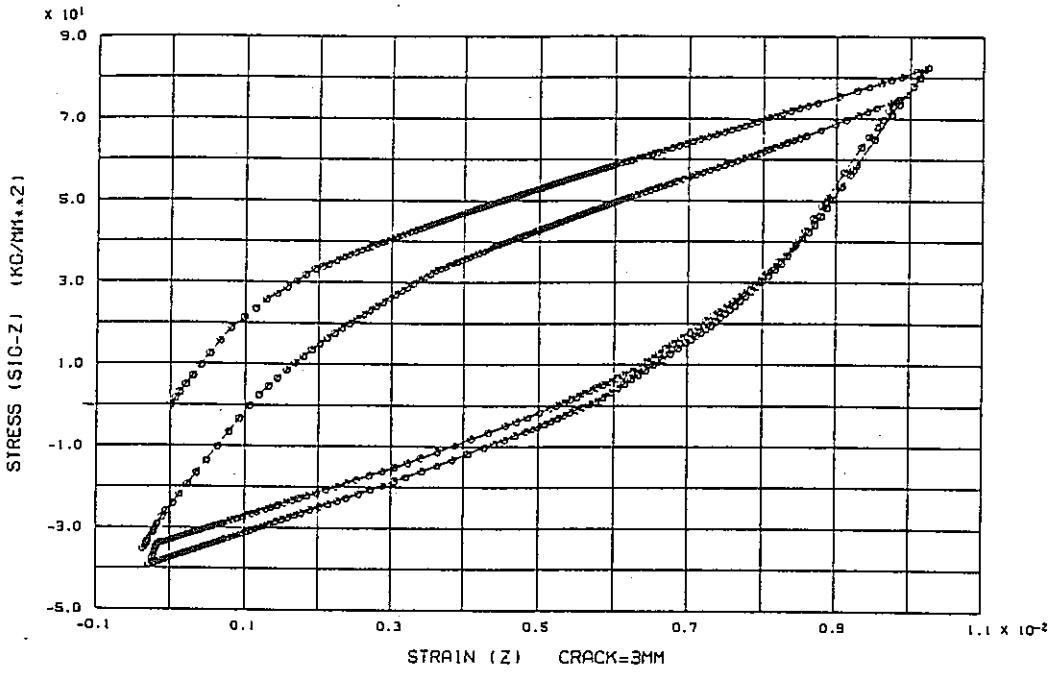

Axial stress and strain histeresis curve (a=3mm)

- Figure 8.c.2 (FINAS) -

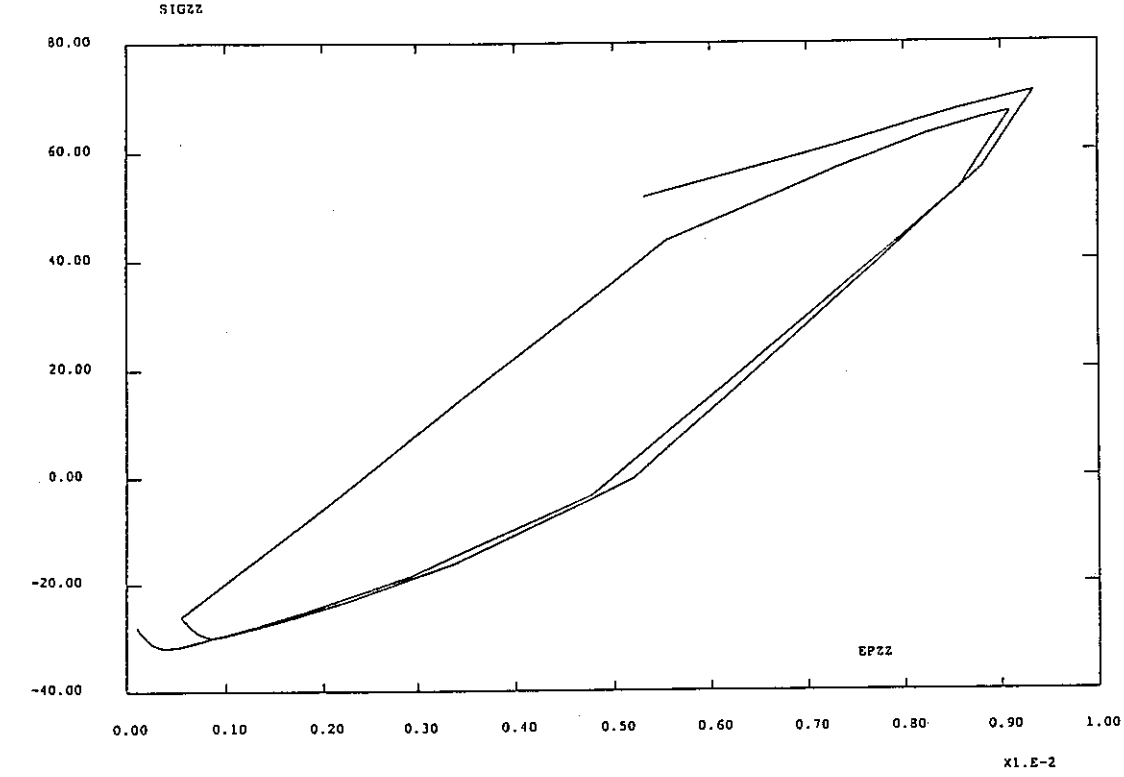

- Figure 8.d.1 (CASTEM 2000) -

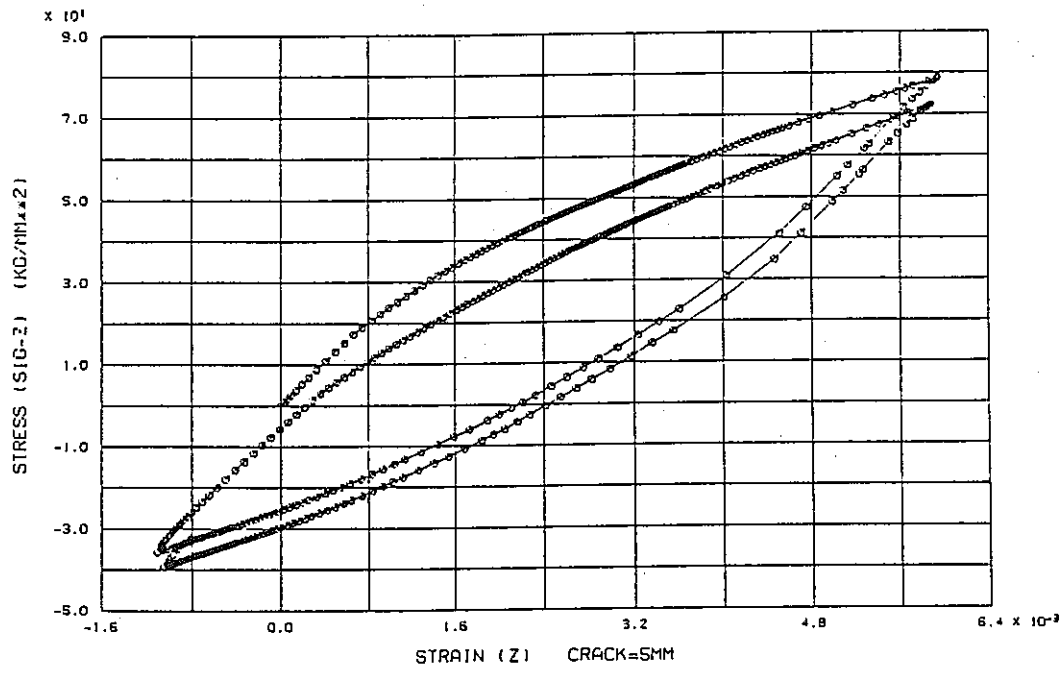

Axial stress and strain histeresis curve (a=5mm)

- Figure 8.d.2 (FINAS) -

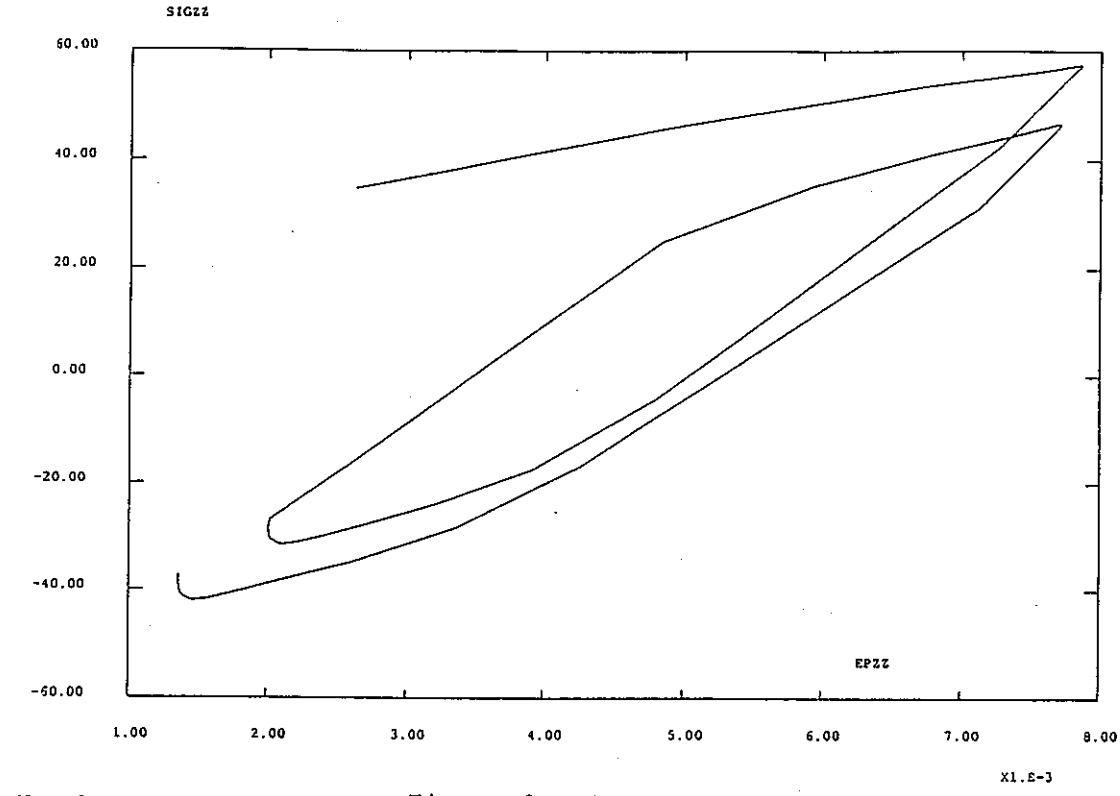

- Figure 8.e.1 (CASTEM 2000) -

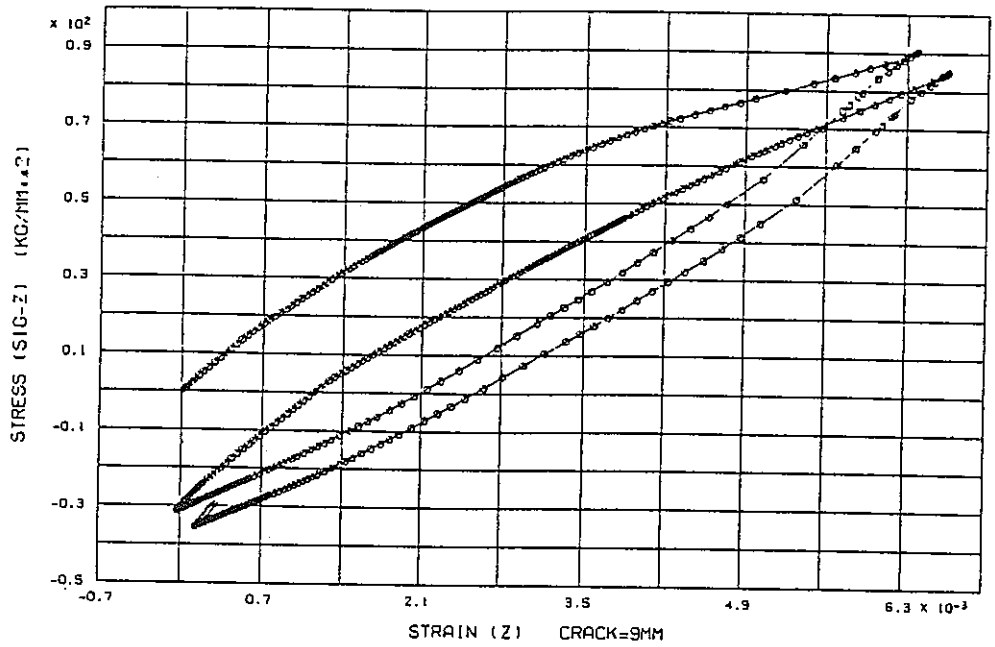

Axial stress and strain histeresis curve (a=9mm)

- Figure 8.e.2 (FINAS) -

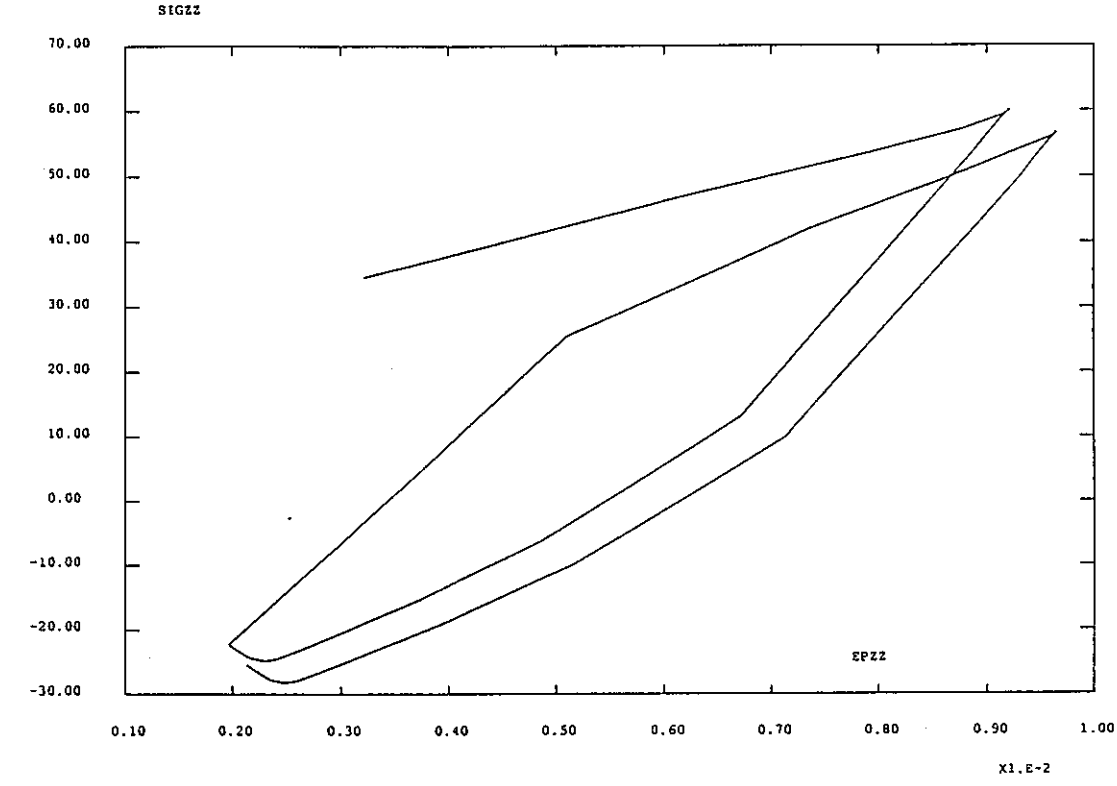

- Figure 8.f.1 (CASTEM 2000) -

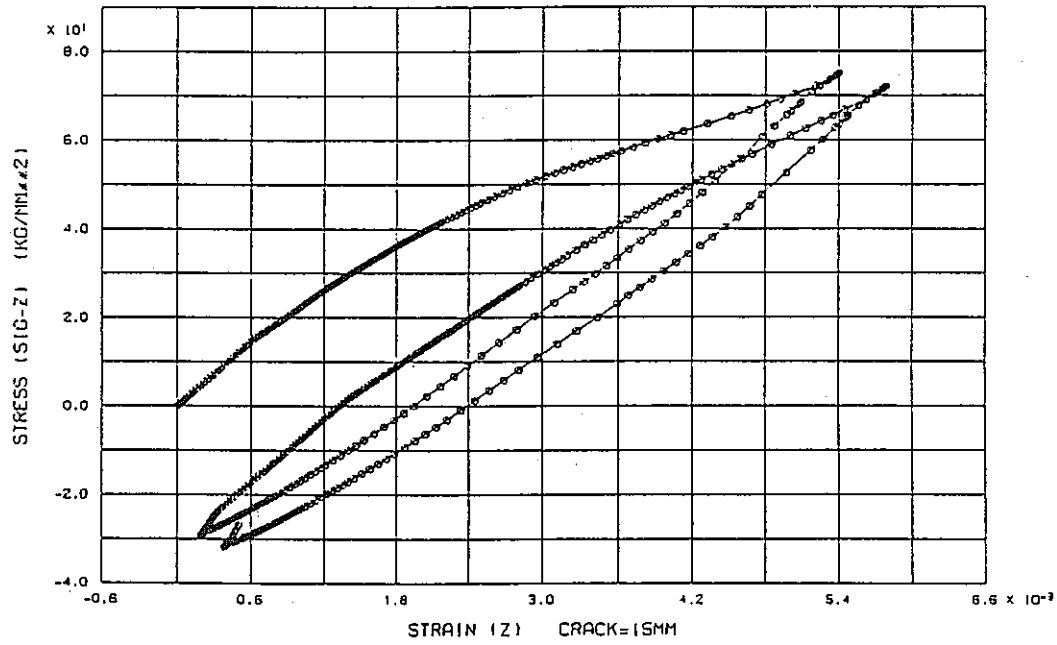

Axial stress and strain histeresis curve (a=15mm)

- Figure 8.f.2 (FINAS) -

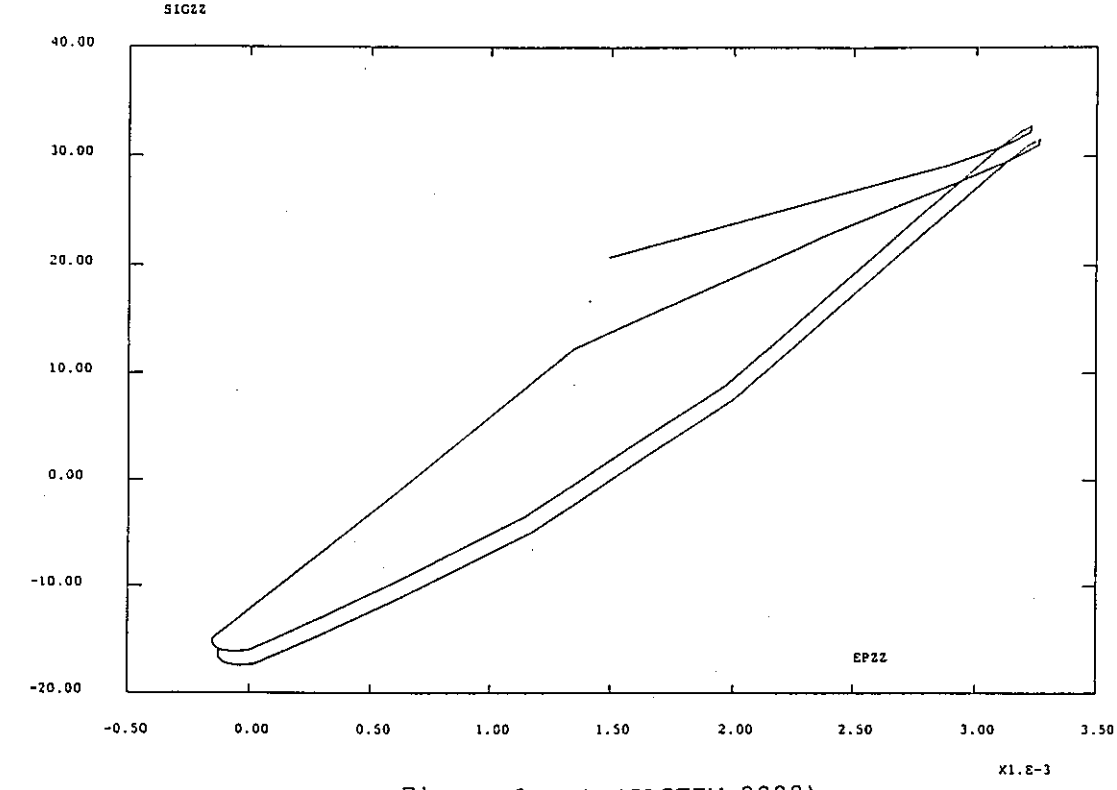

- Figure 8.g.1 (CASTEM 2000) -

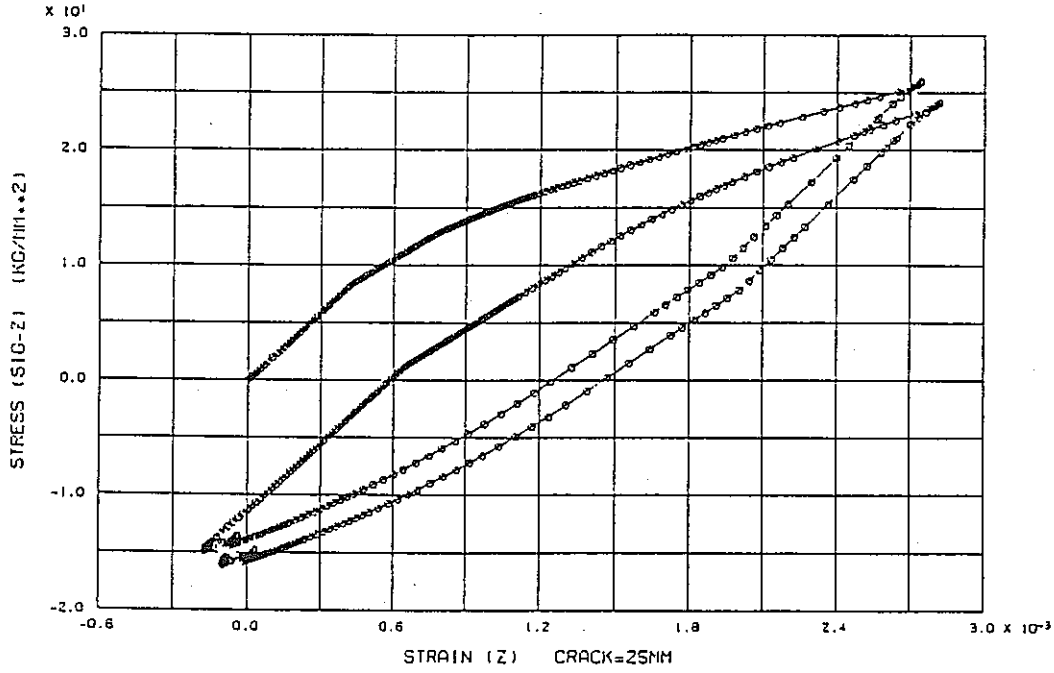

Axial stress and strain histeresis curve (a=25mm)

- Figure 8.g.2 (FINAS) -

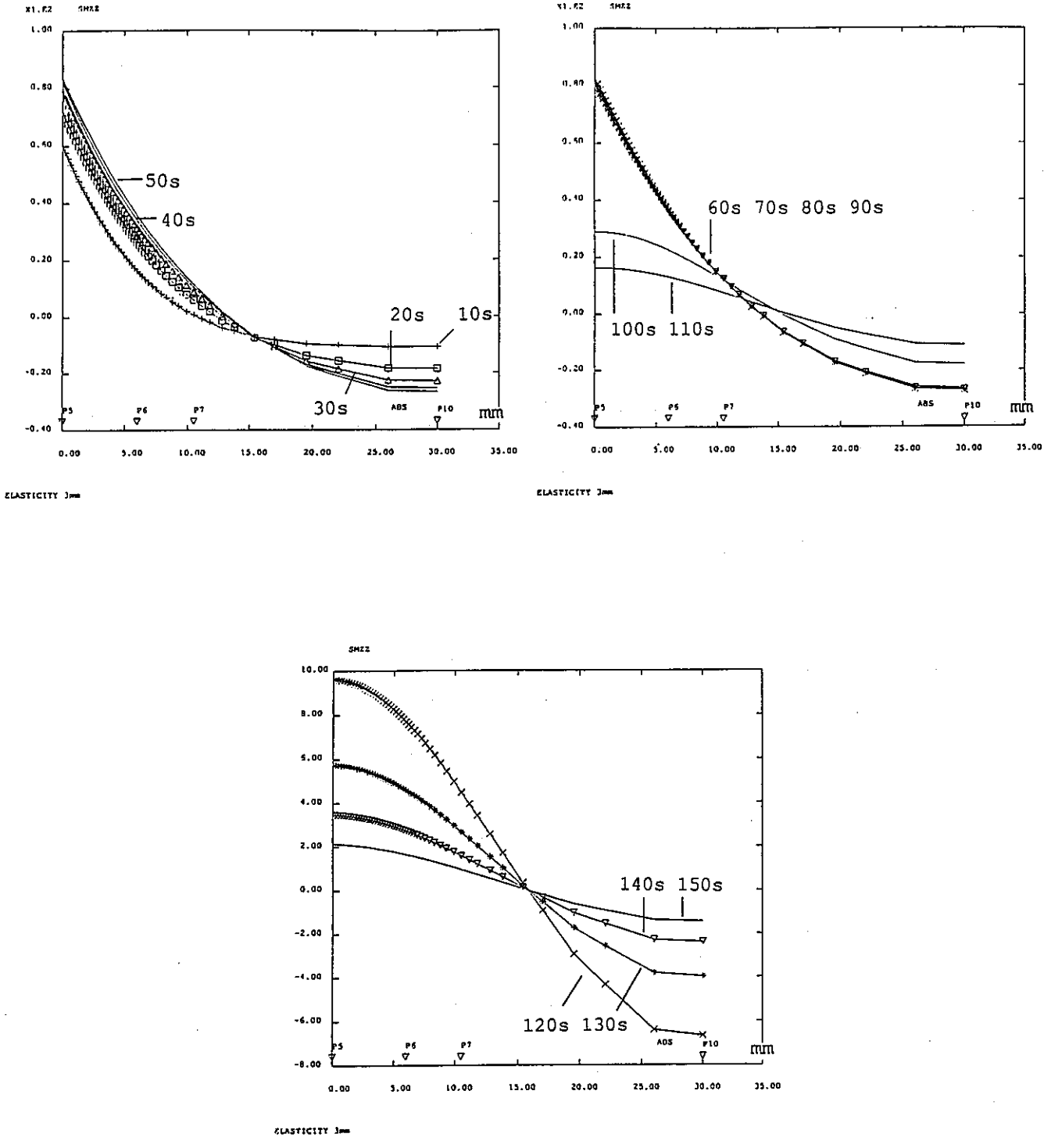

- Figure 9 - SMZZ (kgf/mm2) profiles along the upper edge L1 of the tube
Elasticity - Crack length = 3mm

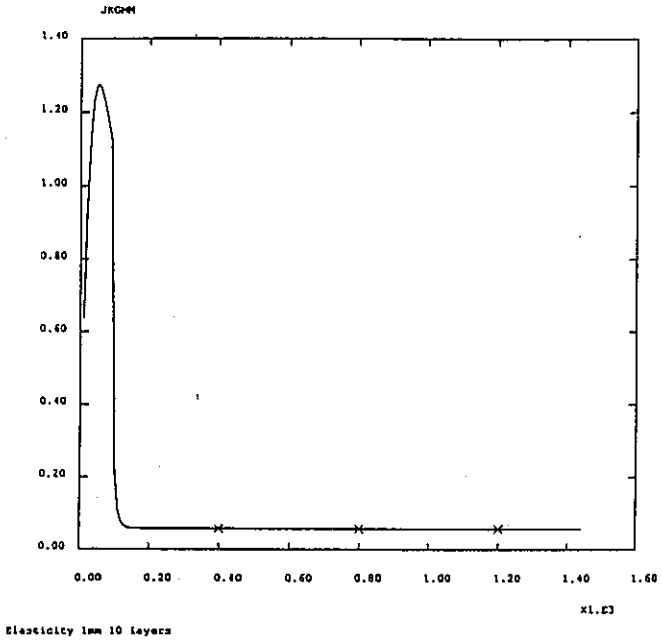

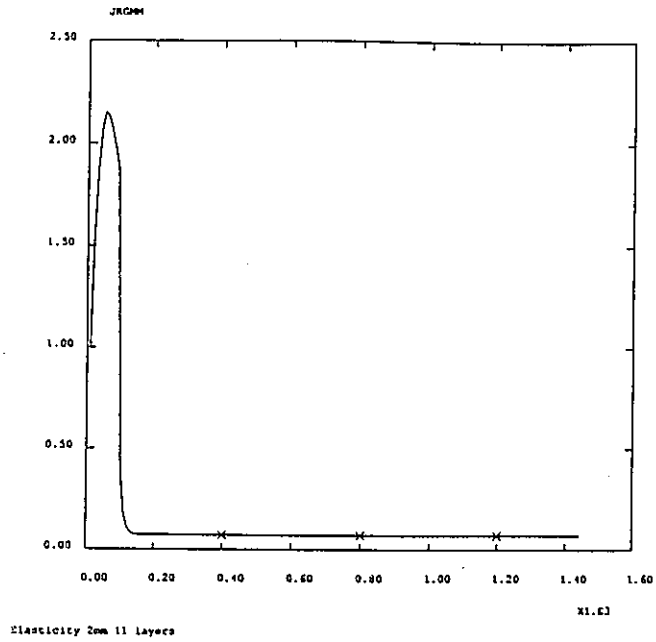

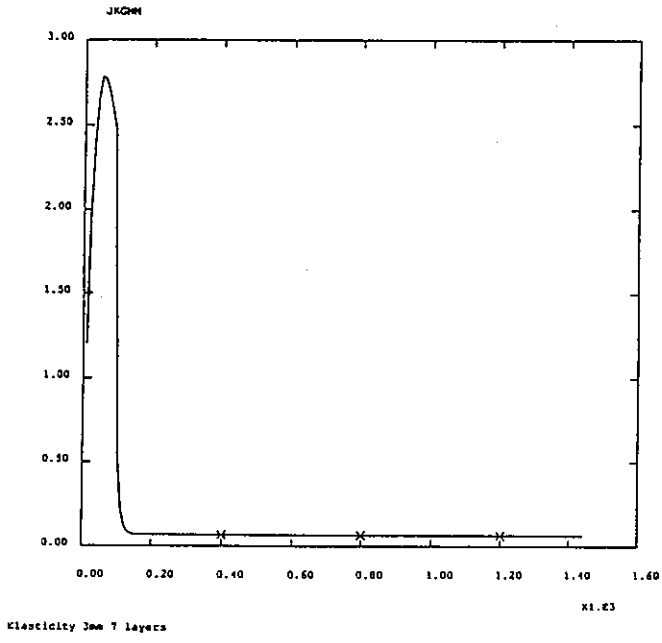

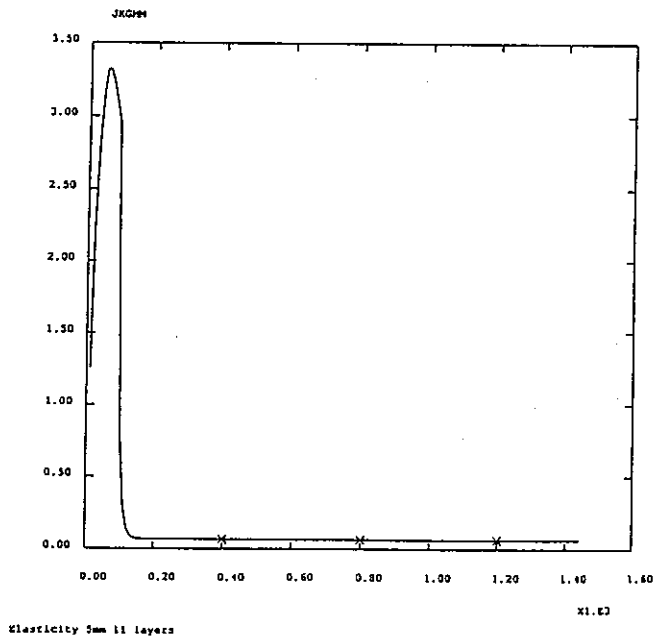

- Figure 10a (CASTEM 2000) -
J(kgf/mm) versus time (seconds) for various crack lengths in Elasticity

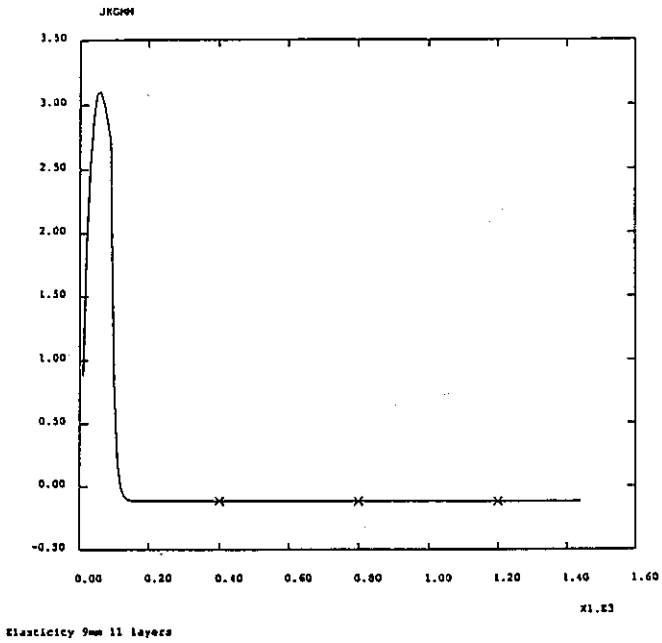

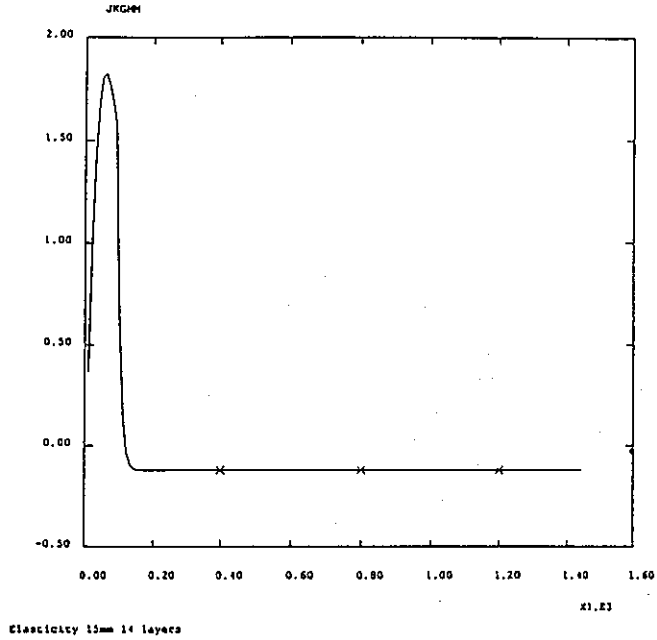

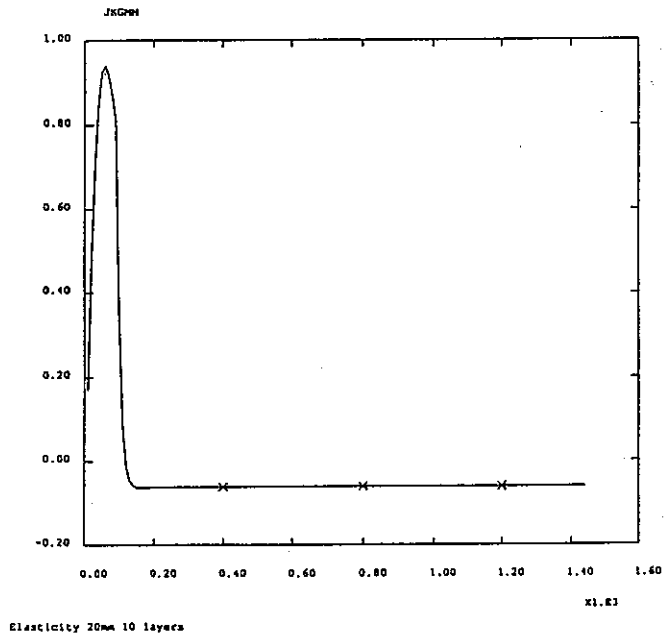

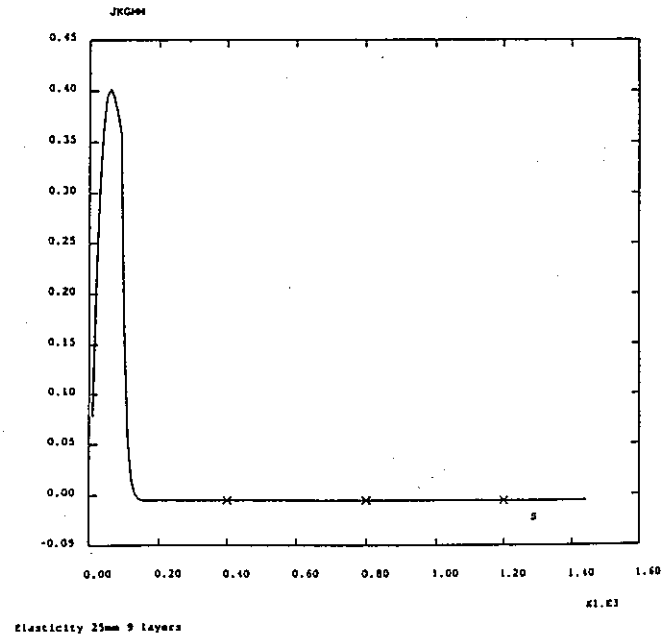

- Figure 10b (CASTEM 2000) -
J(kgf/mm) versus time (seconds) for various crack lengths in Elasticity

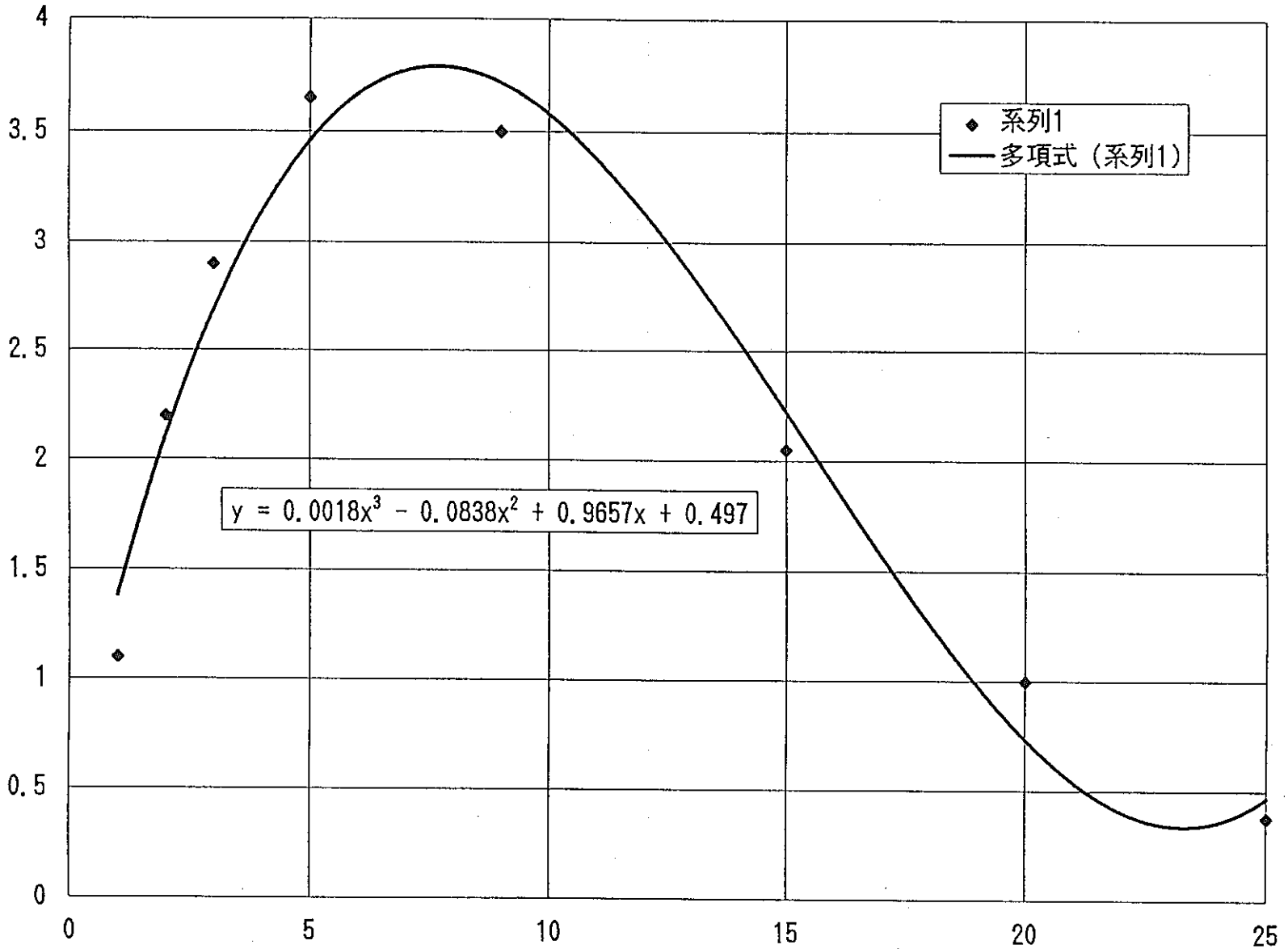

- Figure 11 (CASTEM 2000) -
DJ (kgf/mm) versus crack length (mm) in Elasticity

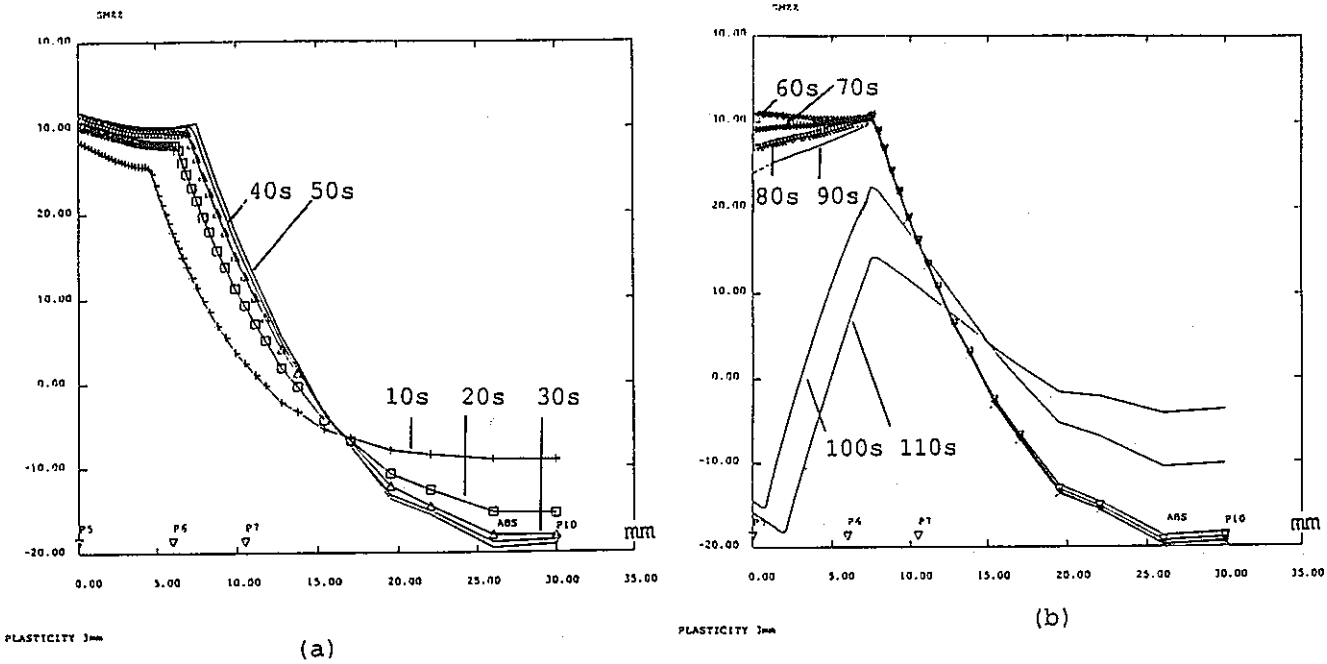

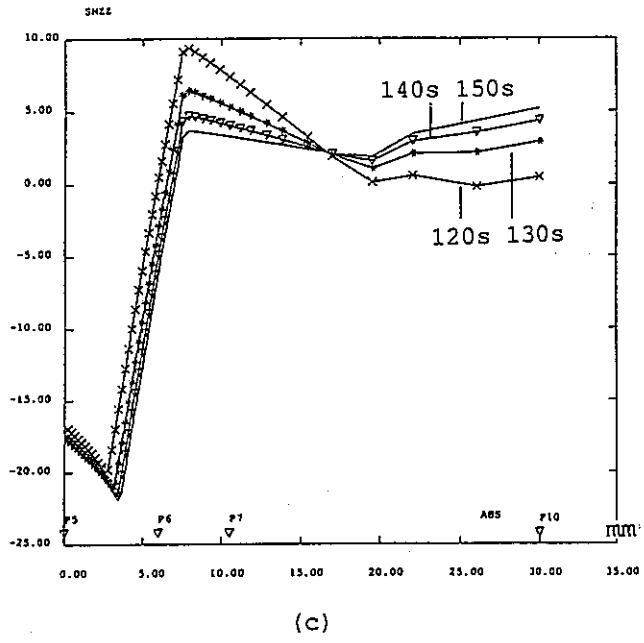

- Figure 12 - SMZZ (kgf/mm2) profiles along the upper edge L1 of the tube
Plasticity - Crack length = 3mm

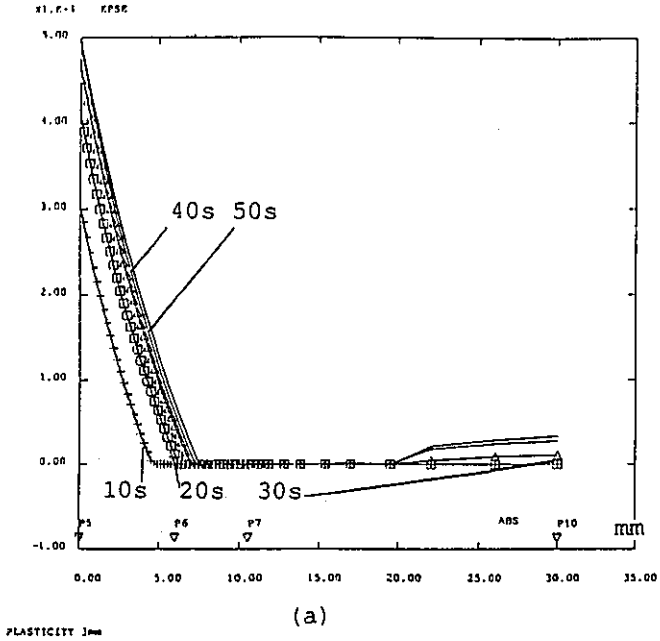

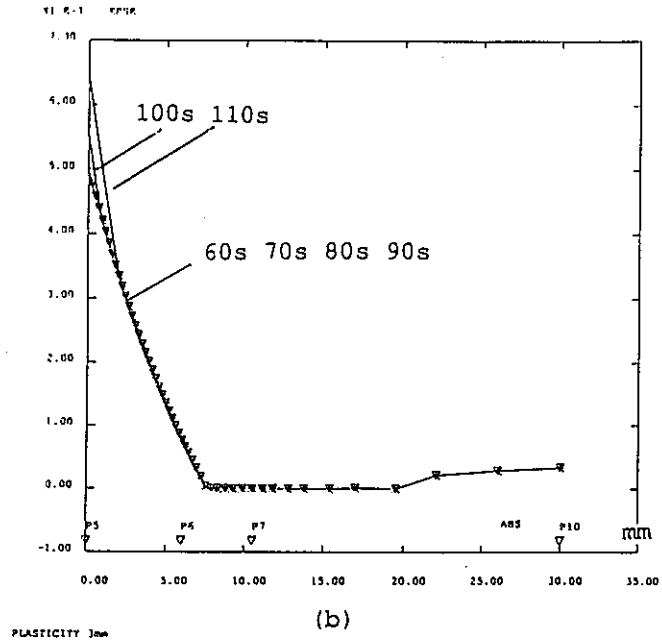

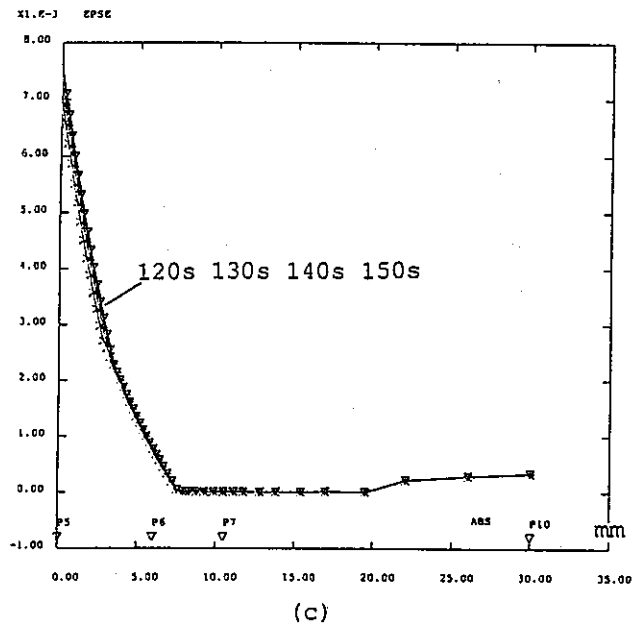

- Figure 13 - Equivalent plastic strain profiles along the upper edge L1 of the tube
Plasticity - Crack length = 3mm

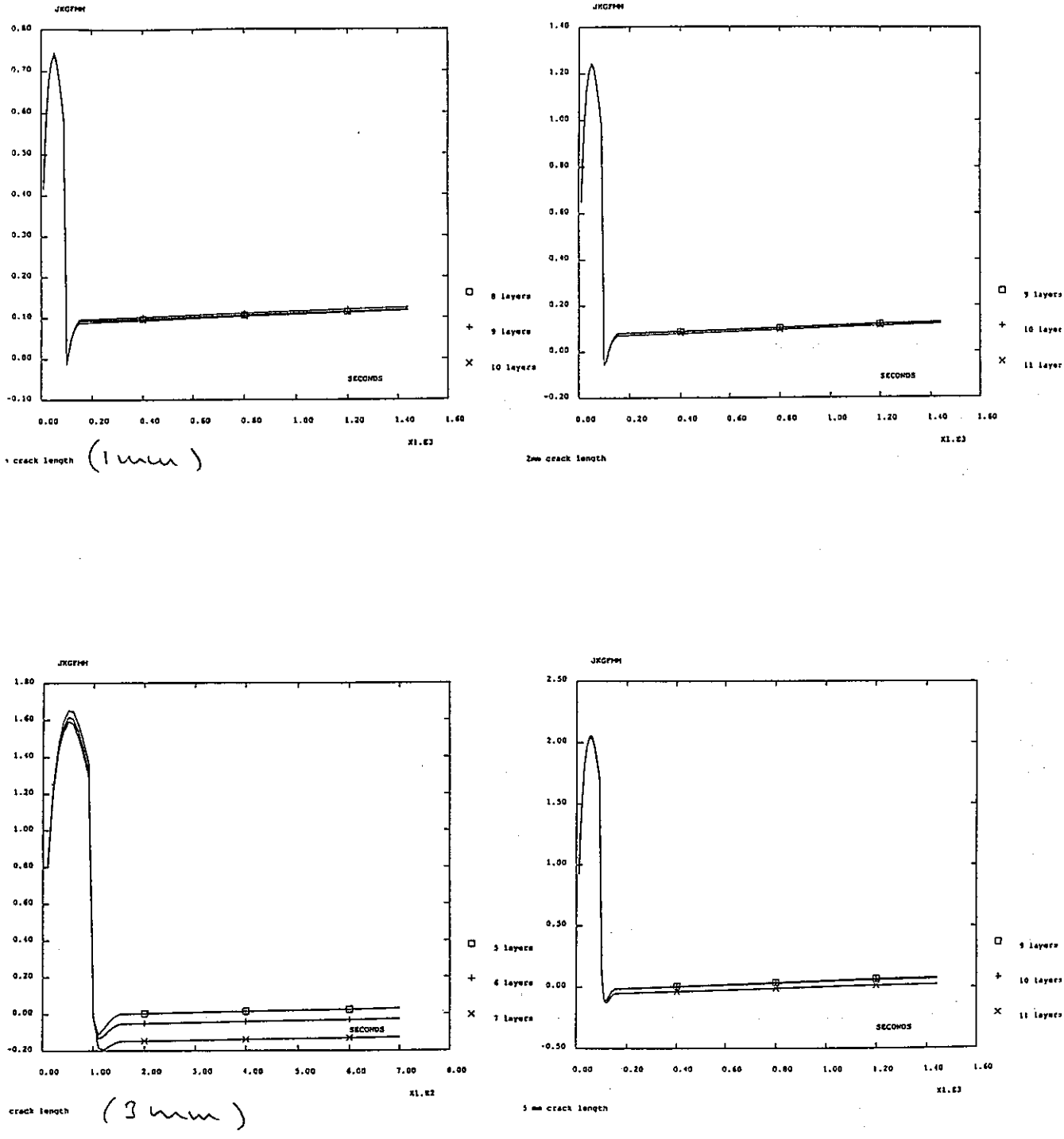

- Figure 14a (CASTEM 2000) -
J(kgf/mm) versus time (seconds) for various crack lengths in Plasticity

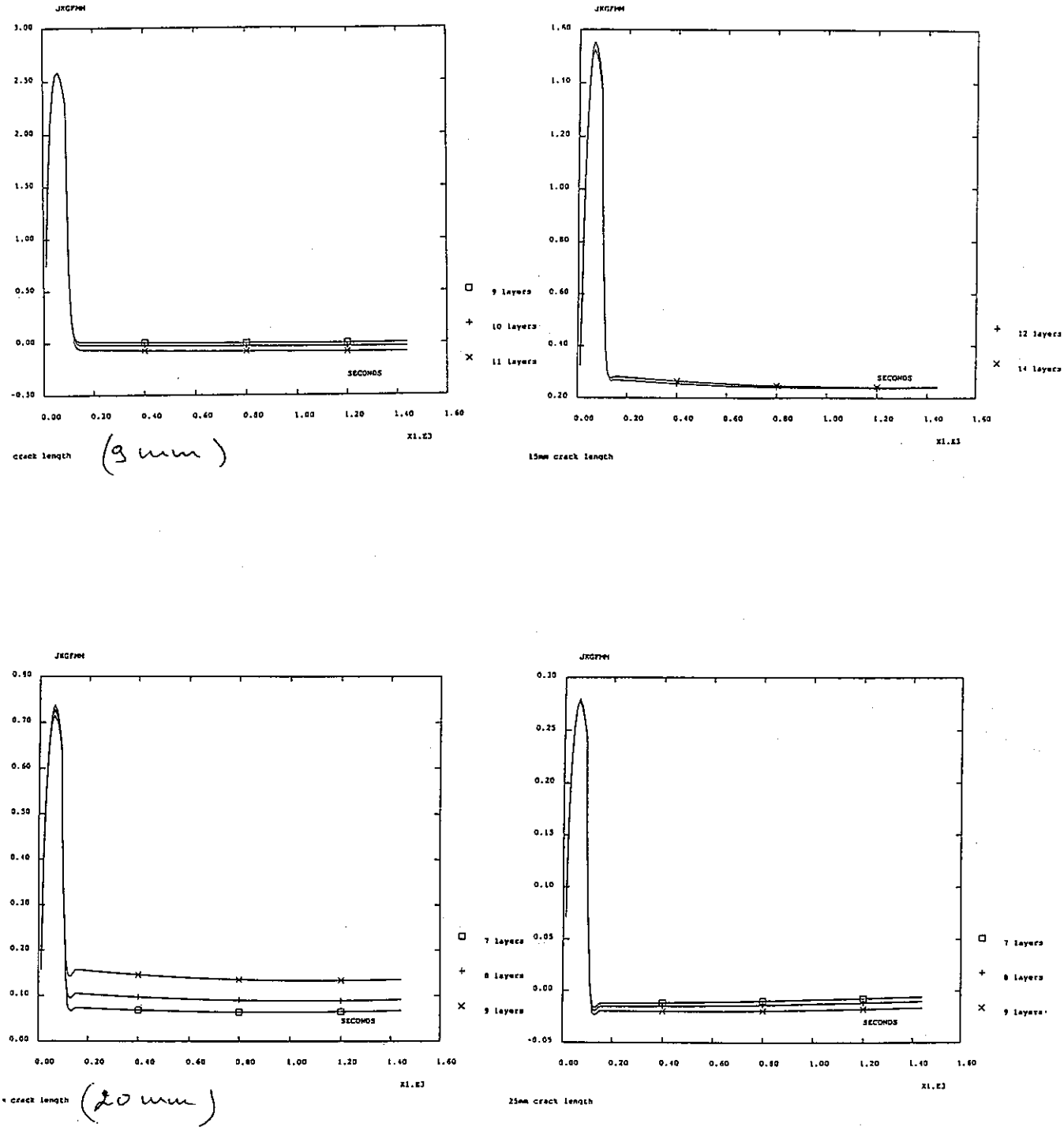

- Figure 14b (CASTEM 2000) -
J(kgf/mm) versus time (seconds) for various crack lengths in Plasticity

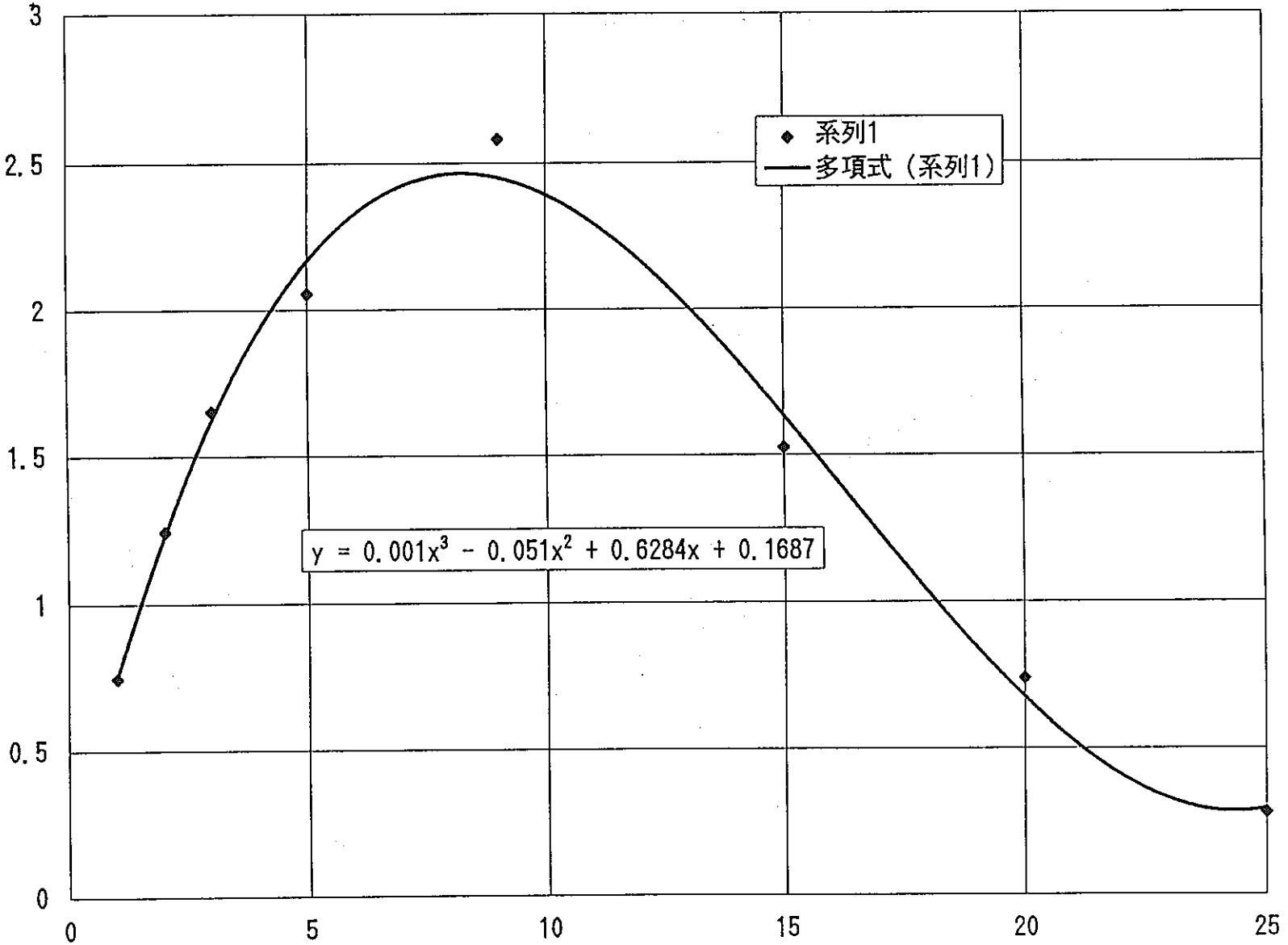

- Figure 15 (CASTEM 2000) -
DJ (kgf/mm) versus crack length (mm) in Plasticity

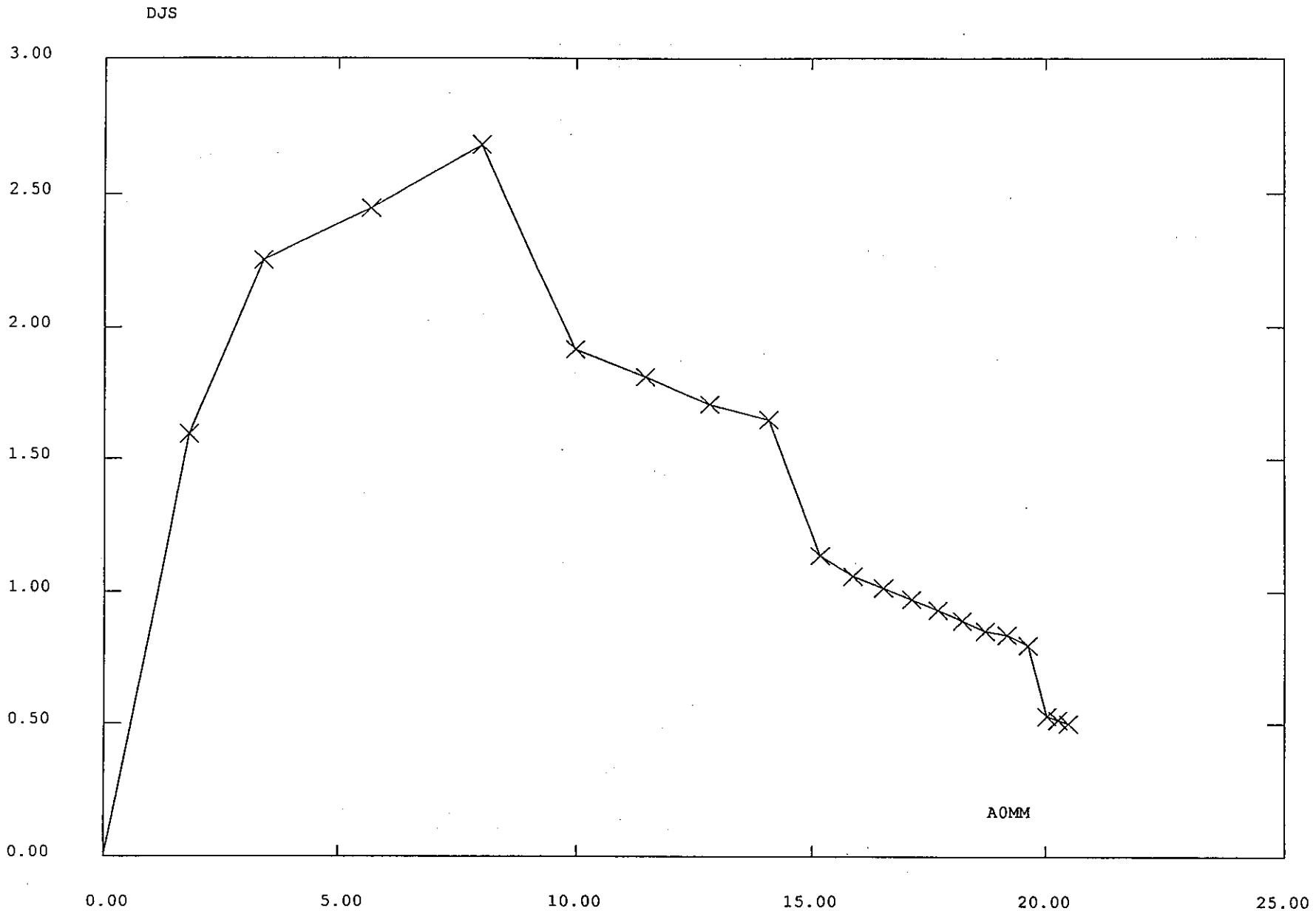

- Figure 16 (A-16 Appendix of the RCCMR) -
DJ (kgf/mm) versus crack length (mm) in Plasticity

PLASTICITY A16

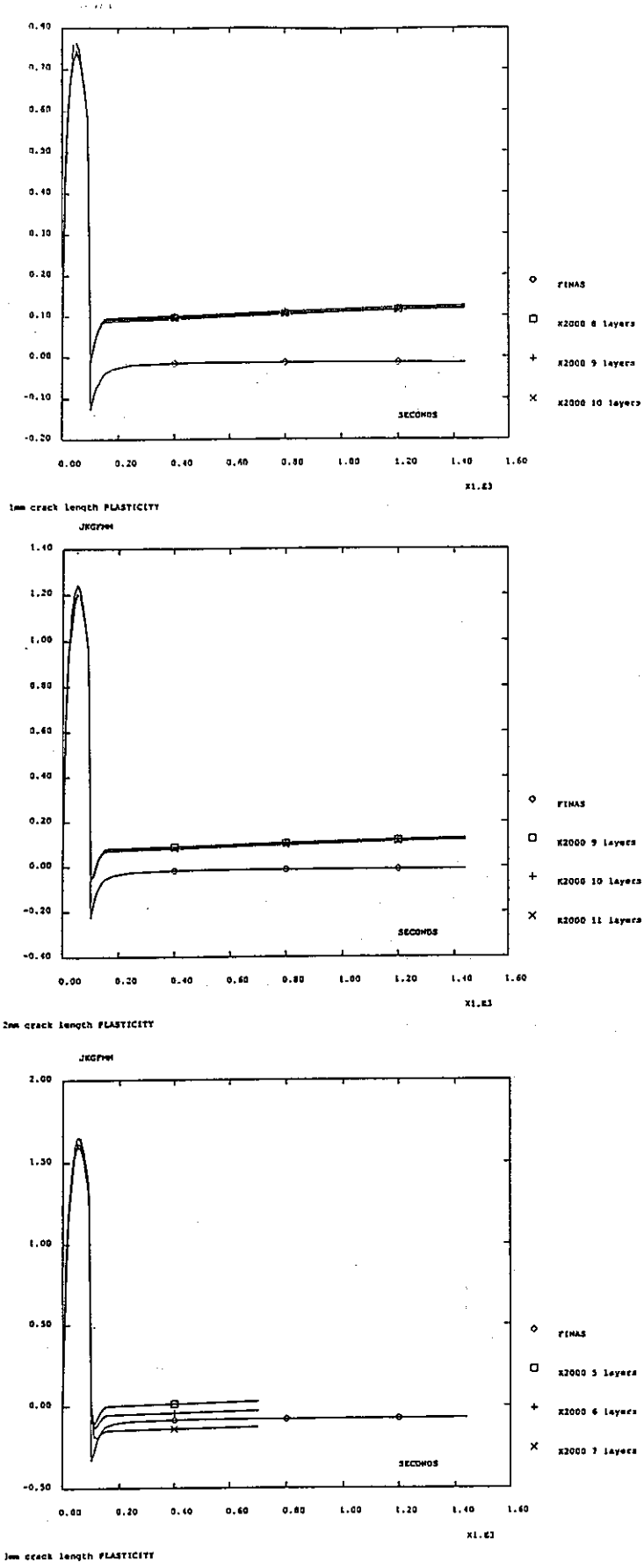

Figure 17a Comparison of Jplastic(K2000) and Jplastic(FINAS) for various crack lengths

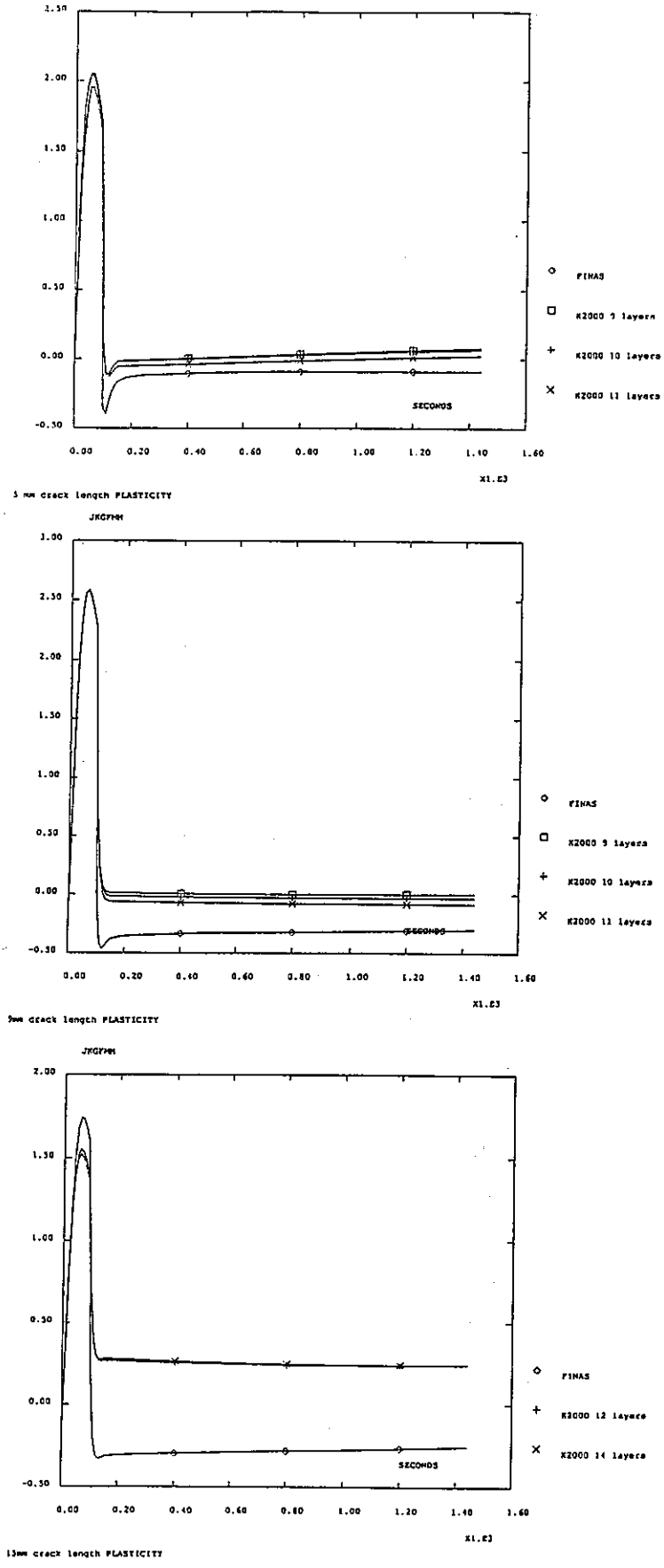

Figure 17b Comparison of Jplastic(K2000) and Jplastic(FINAS) for various crack lengths

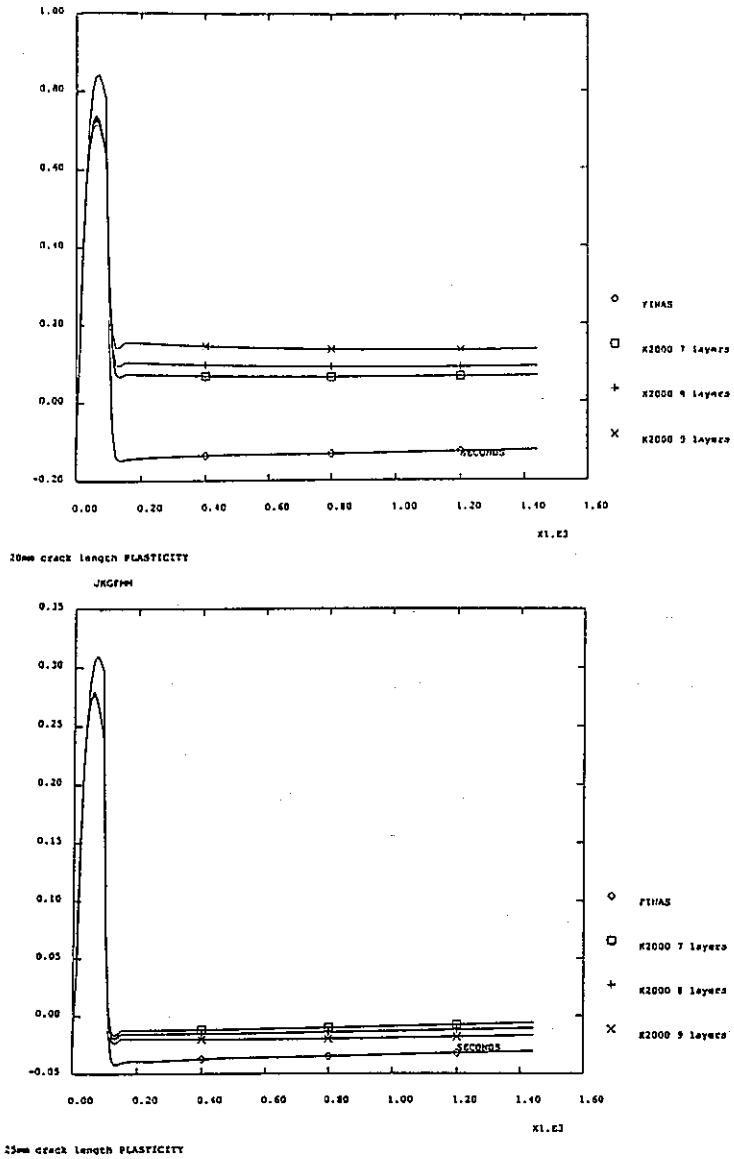

Figure 17c Comparison of Jplastic(K2000) and Jplastic(FINAS) for various crack lengths

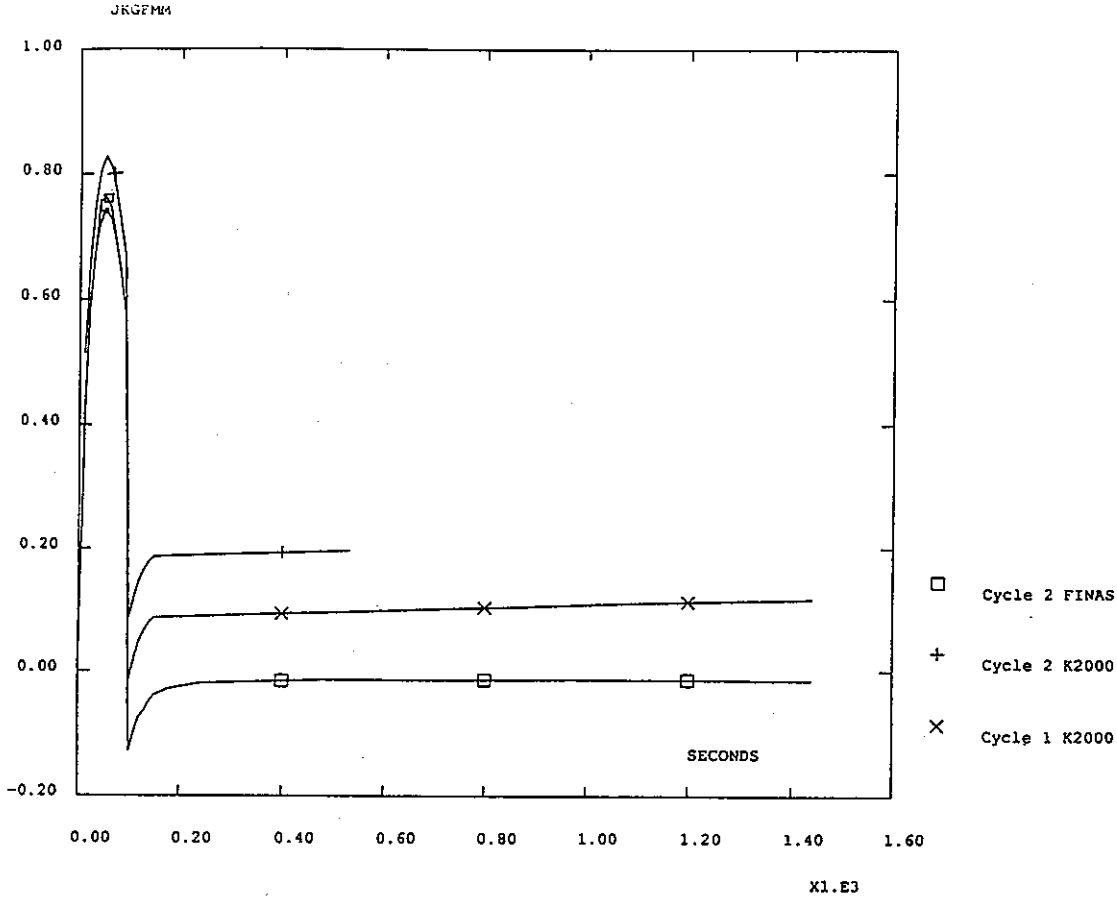

1mm - J - Cycles 1 and 2 - 10 layers - Plasticity

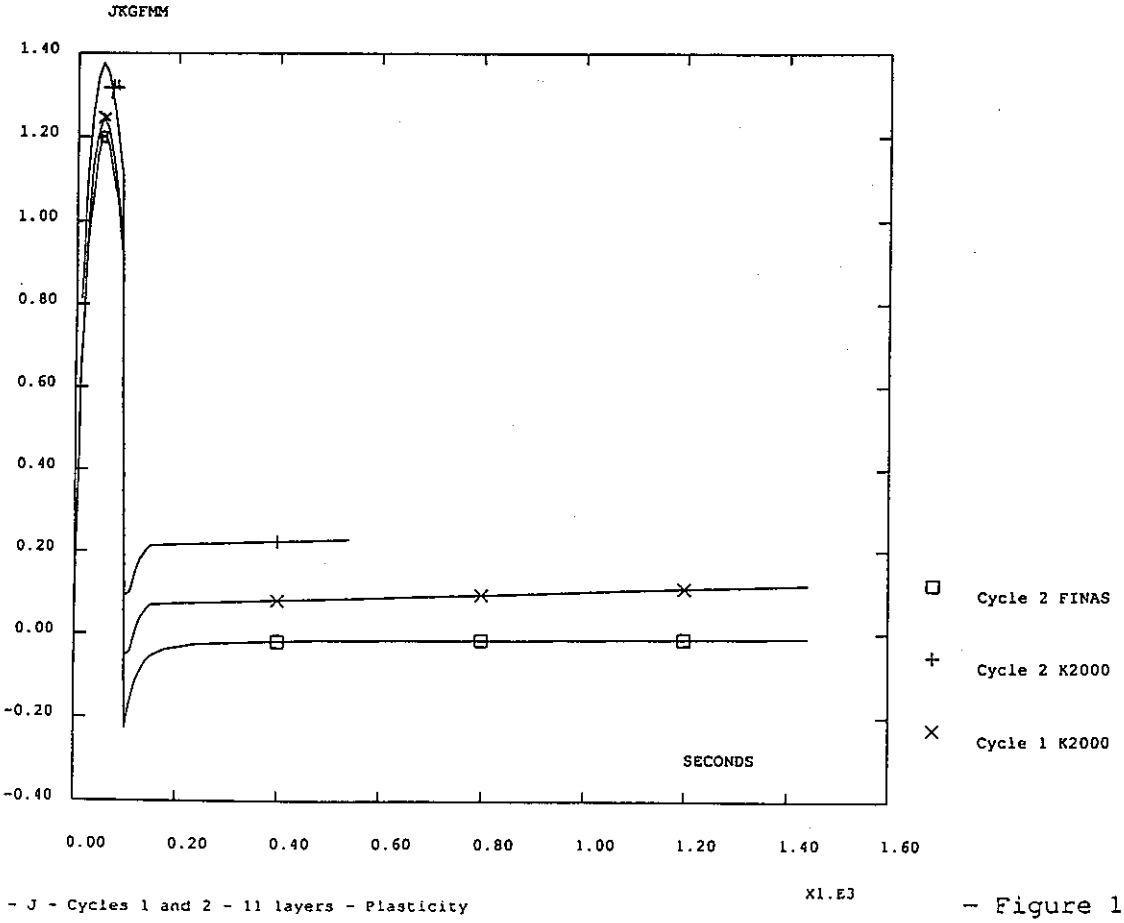

2mm - J - Cycles 1 and 2 - 11 layers - Plasticity

- Figure 17d -

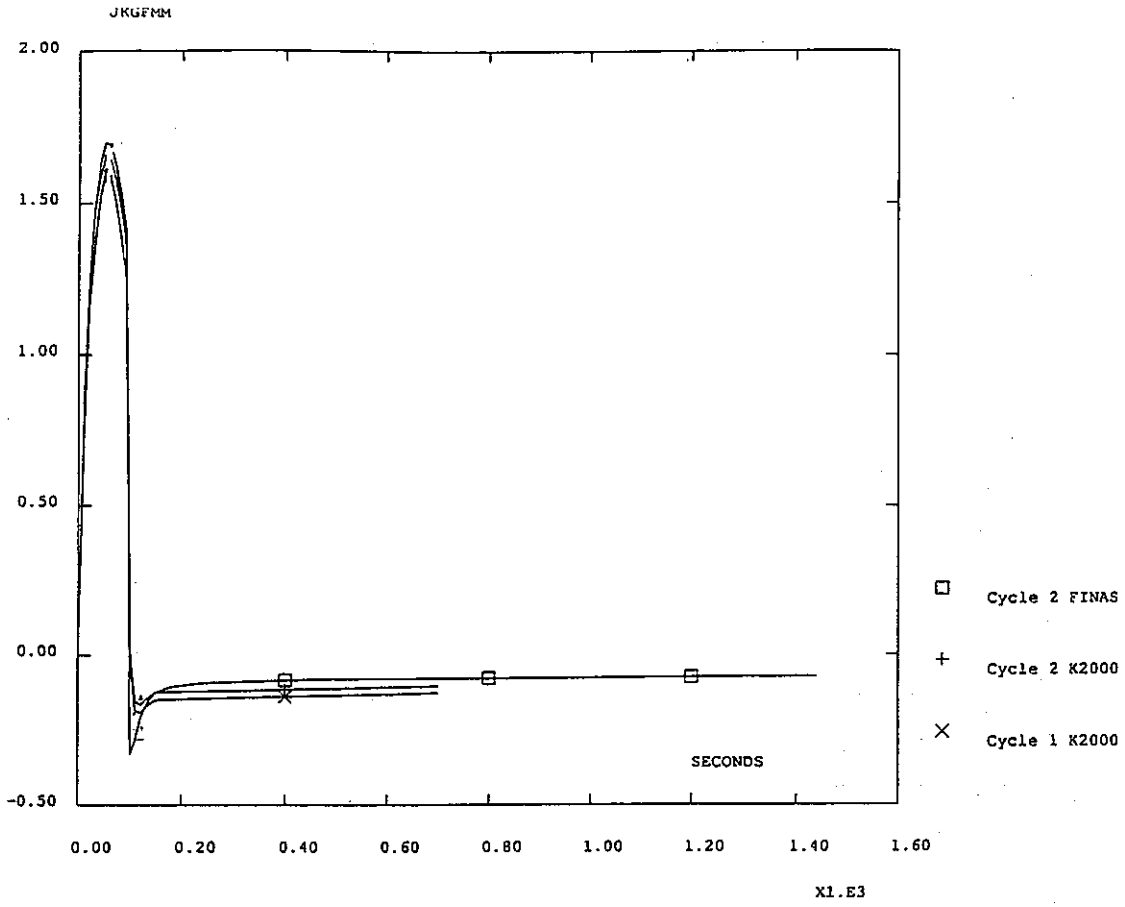

3mm - J - 1 and 2 cycles -7 layers-Plasticity

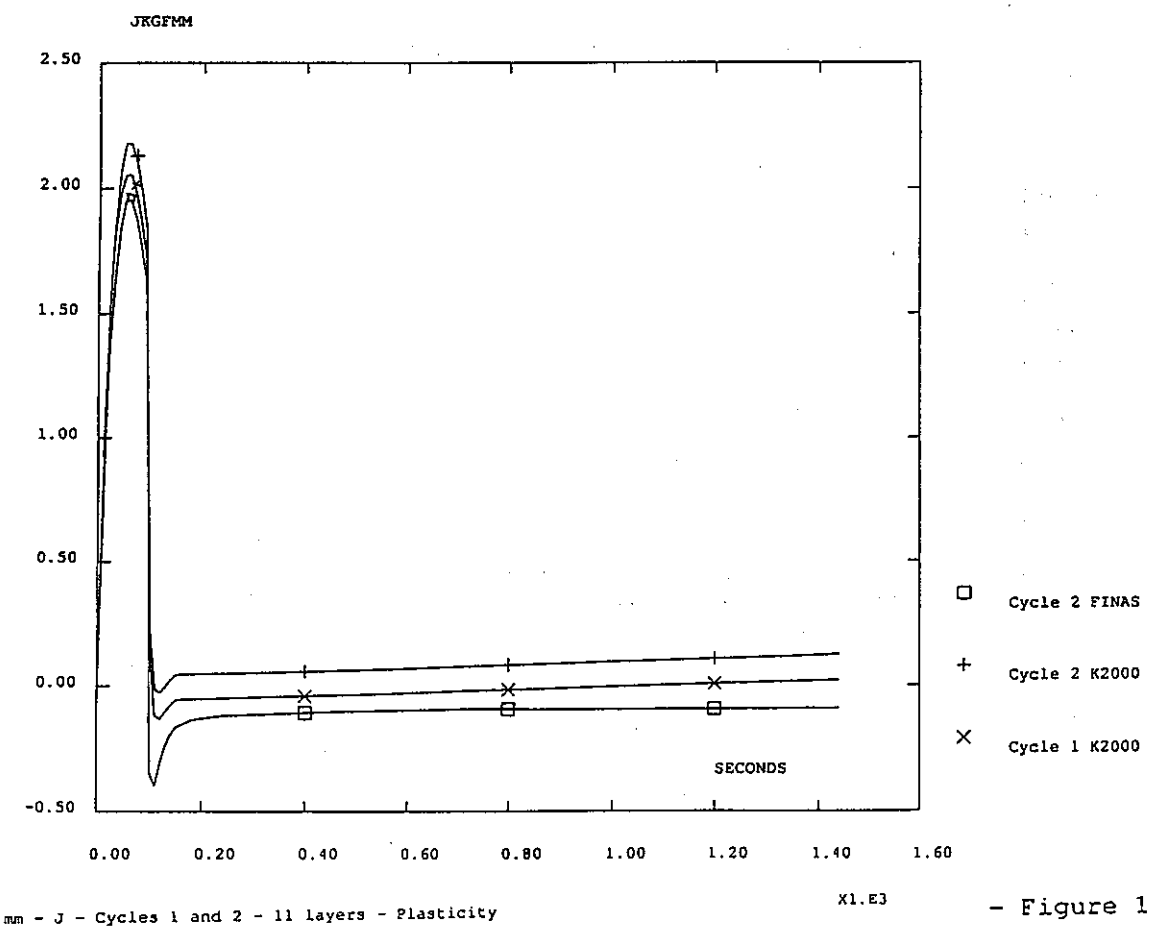

5 mm - J - Cycles 1 and 2 - 11 layers - Plasticity

- Figure 17e -

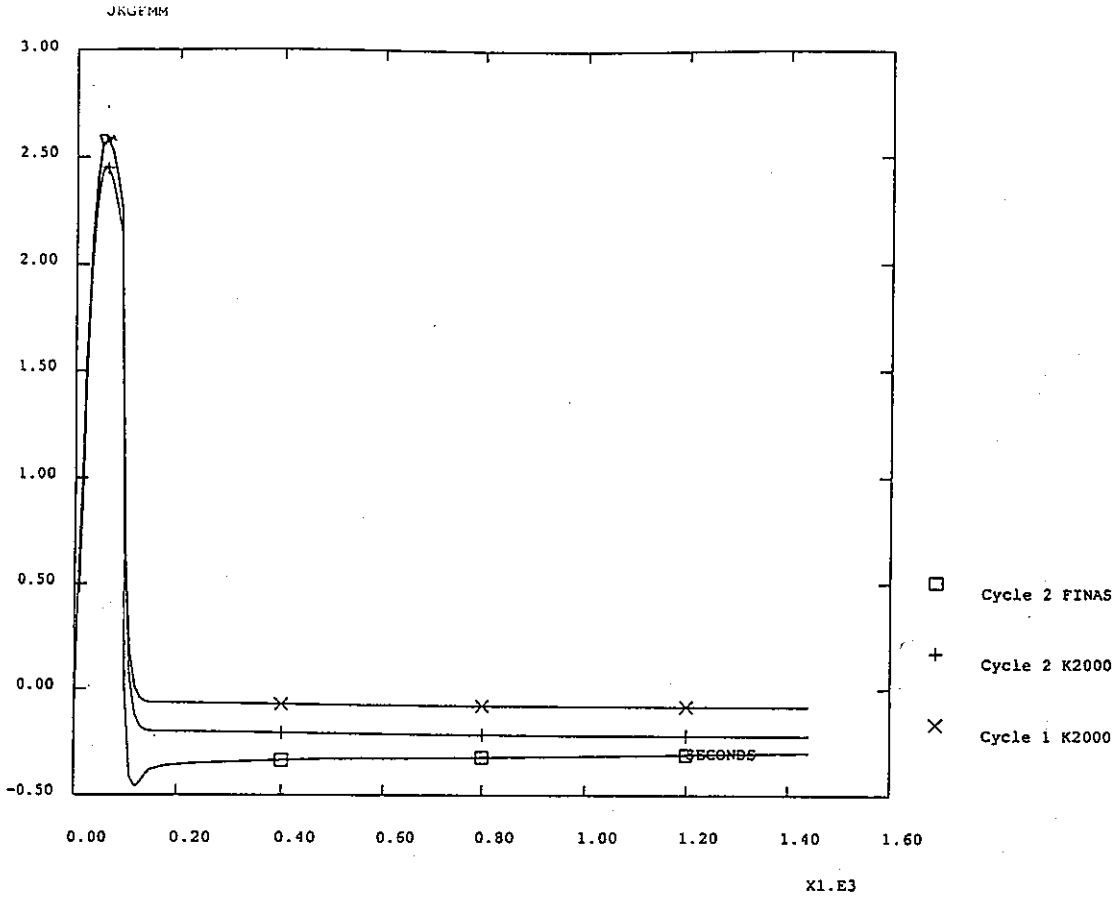

9mm - J - Cycles 1 and 2 - 11 layers - Plasticity

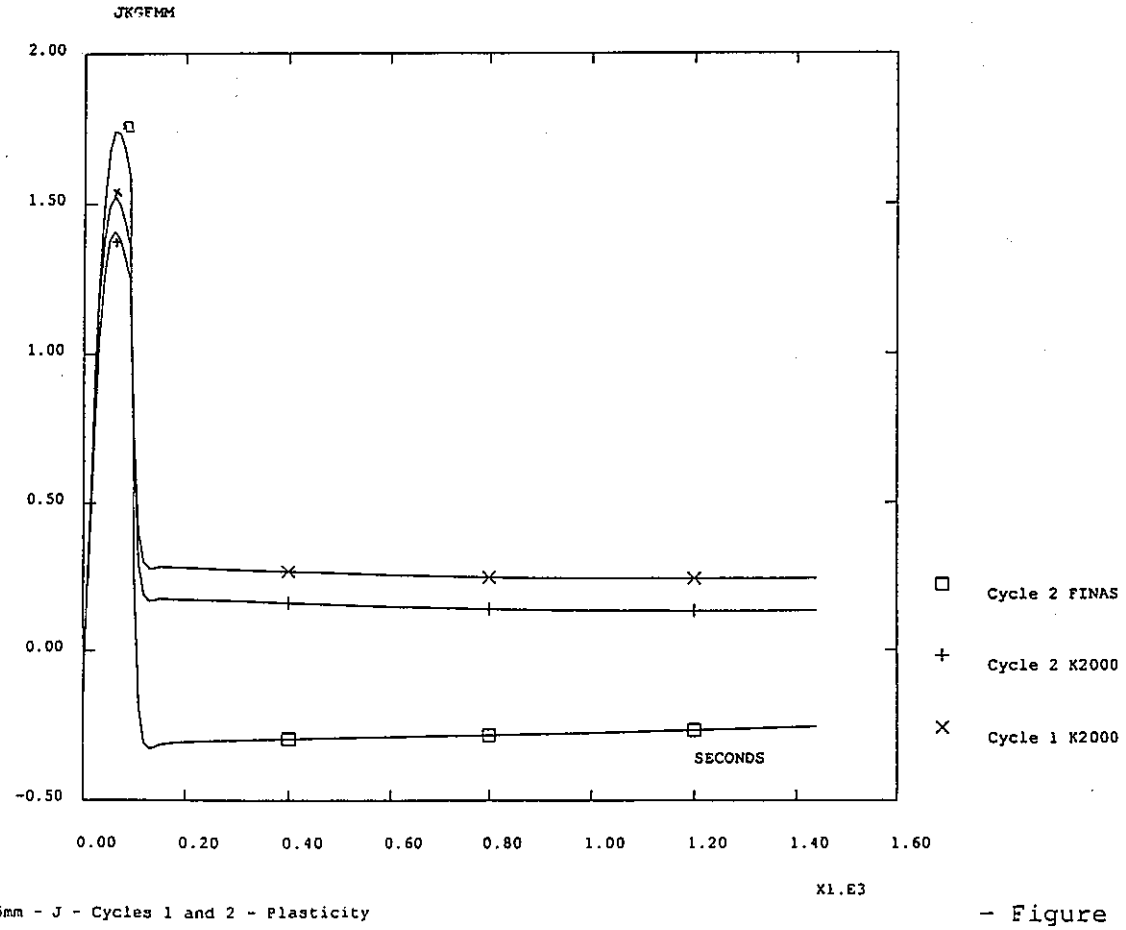

15mm - J - Cycles 1 and 2 - Plasticity

- Figure 17f -

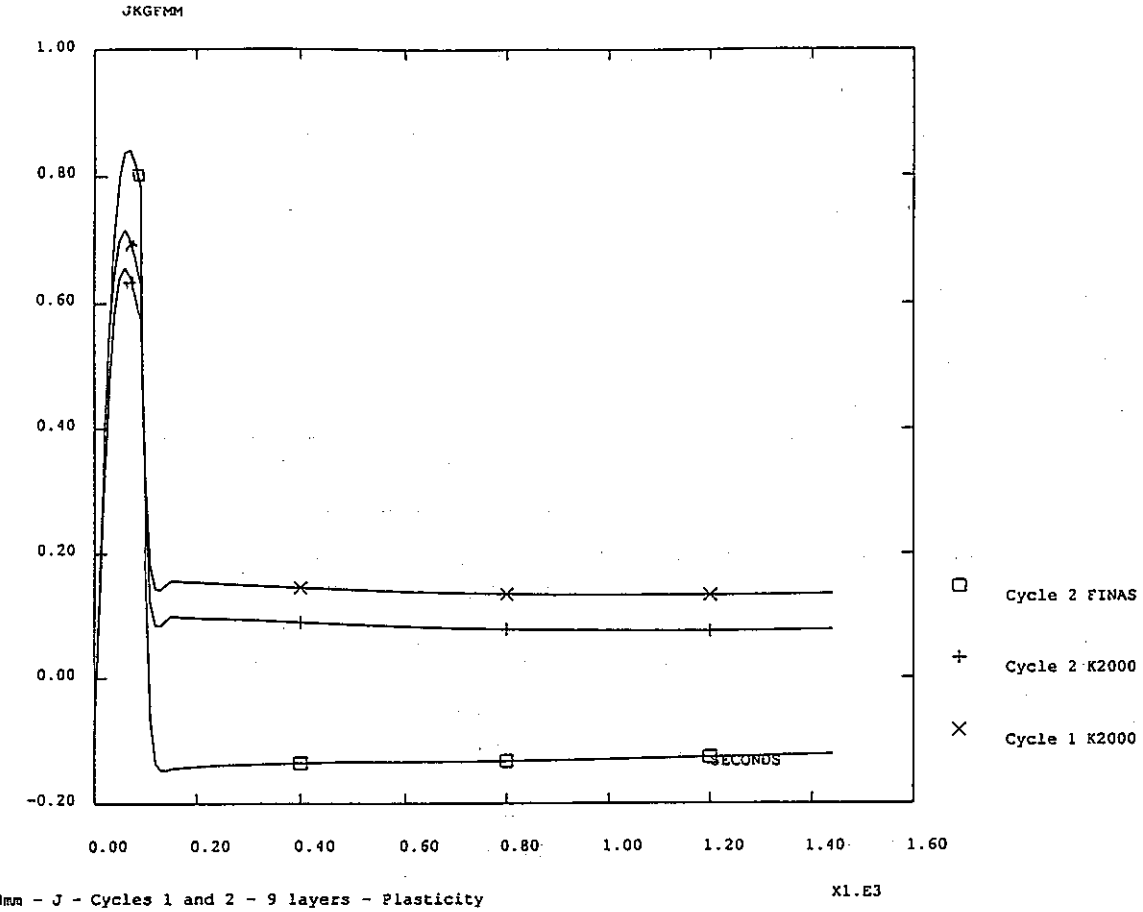

20mm - J - Cycles 1 and 2 - 9 layers - Plasticity

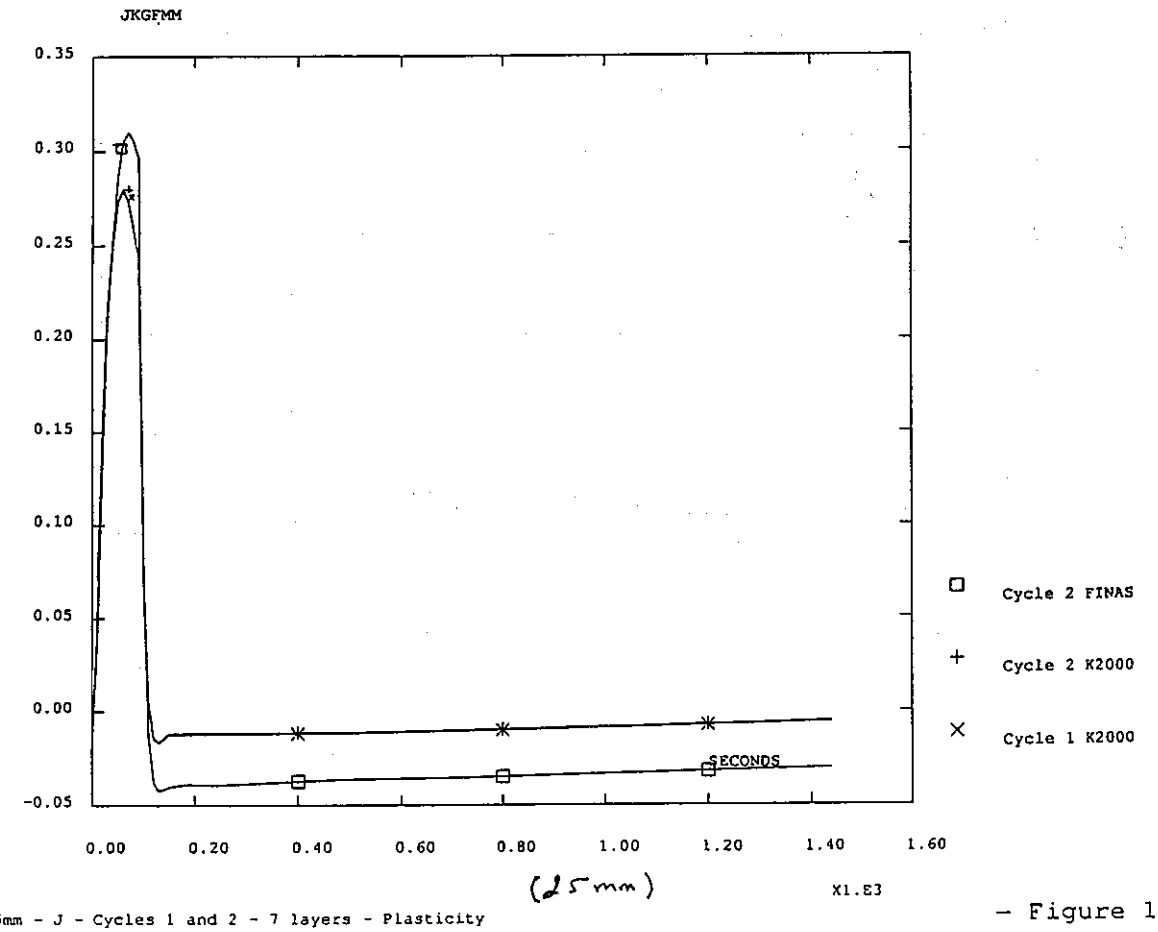

(25mm)

15mm - J - Cycles 1 and 2 - 7 layers - Plasticity

- Figure 17g -

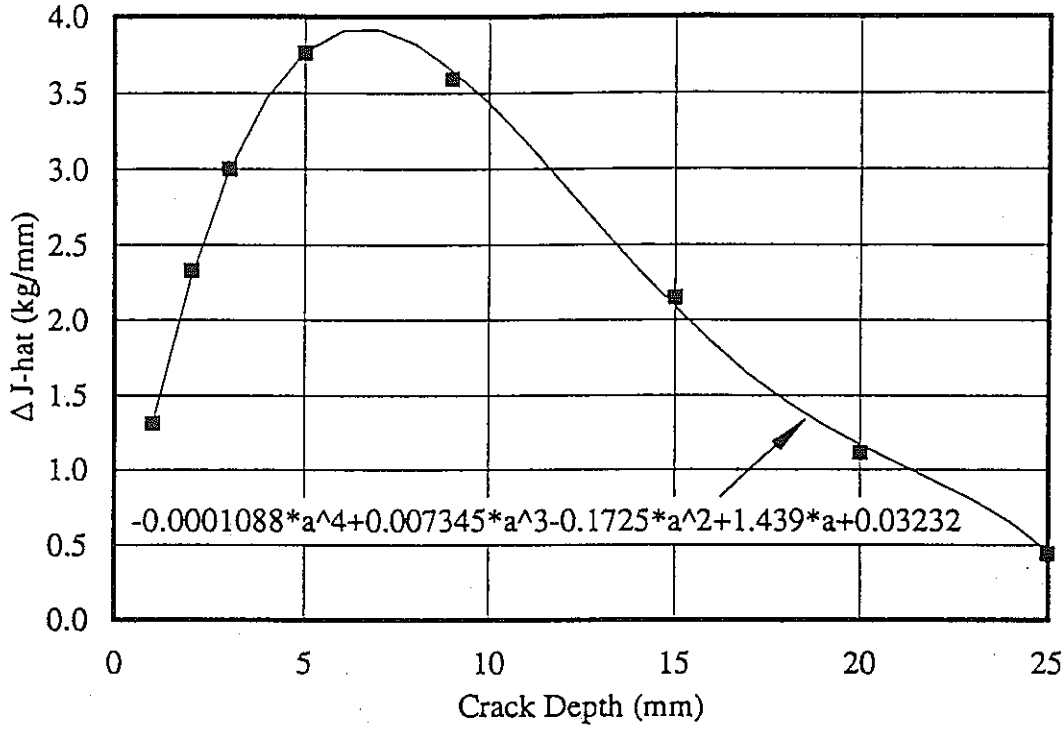

- Figure 17h (FINAS) -
DJ (kgf/mm) versus crack length (mm) in Elasticity

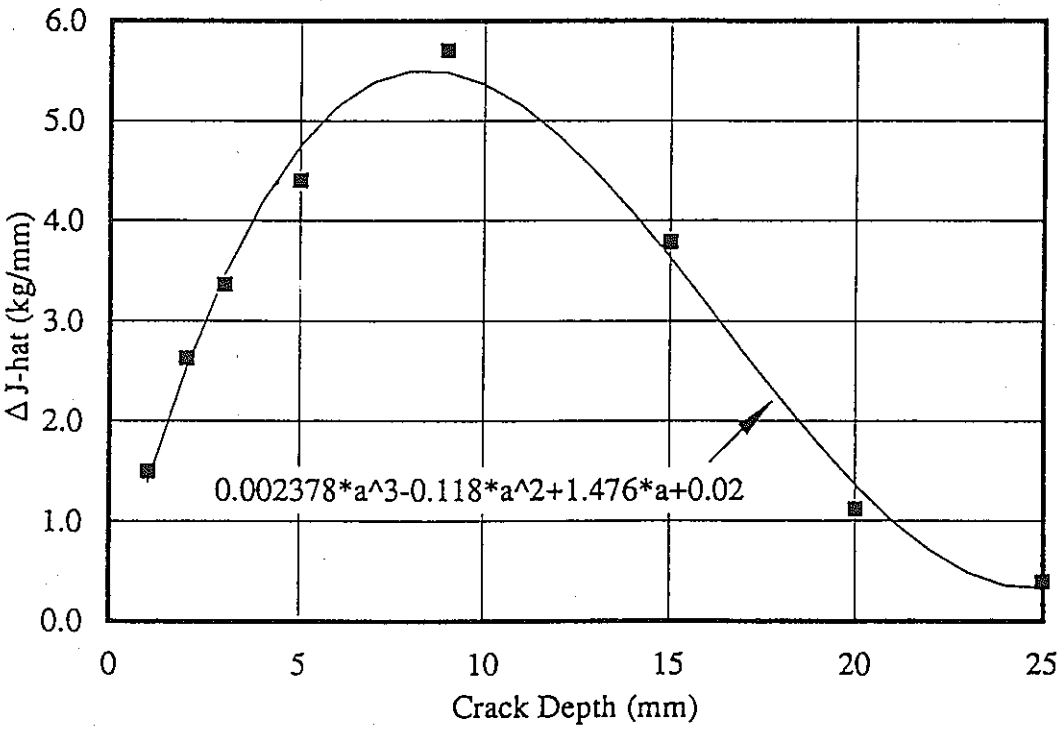

- Figure 17i (FINAS) -
DJ (kgf/mm) versus crack length (mm) in Plasticity

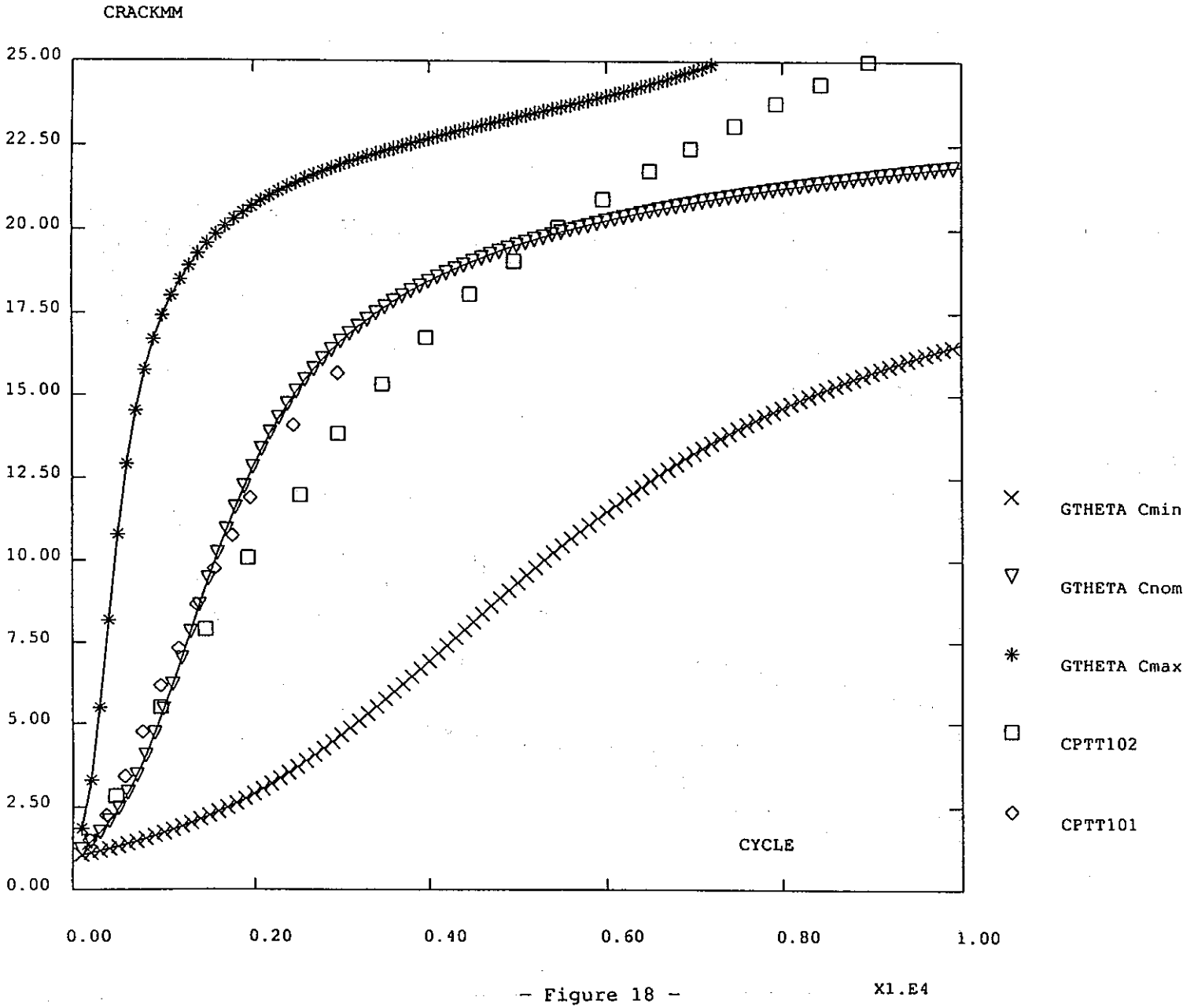

- Figure 18 -

Crack length (mm) versus number of cycles (CASTEM 2000 / Measured Values) in Elasticity

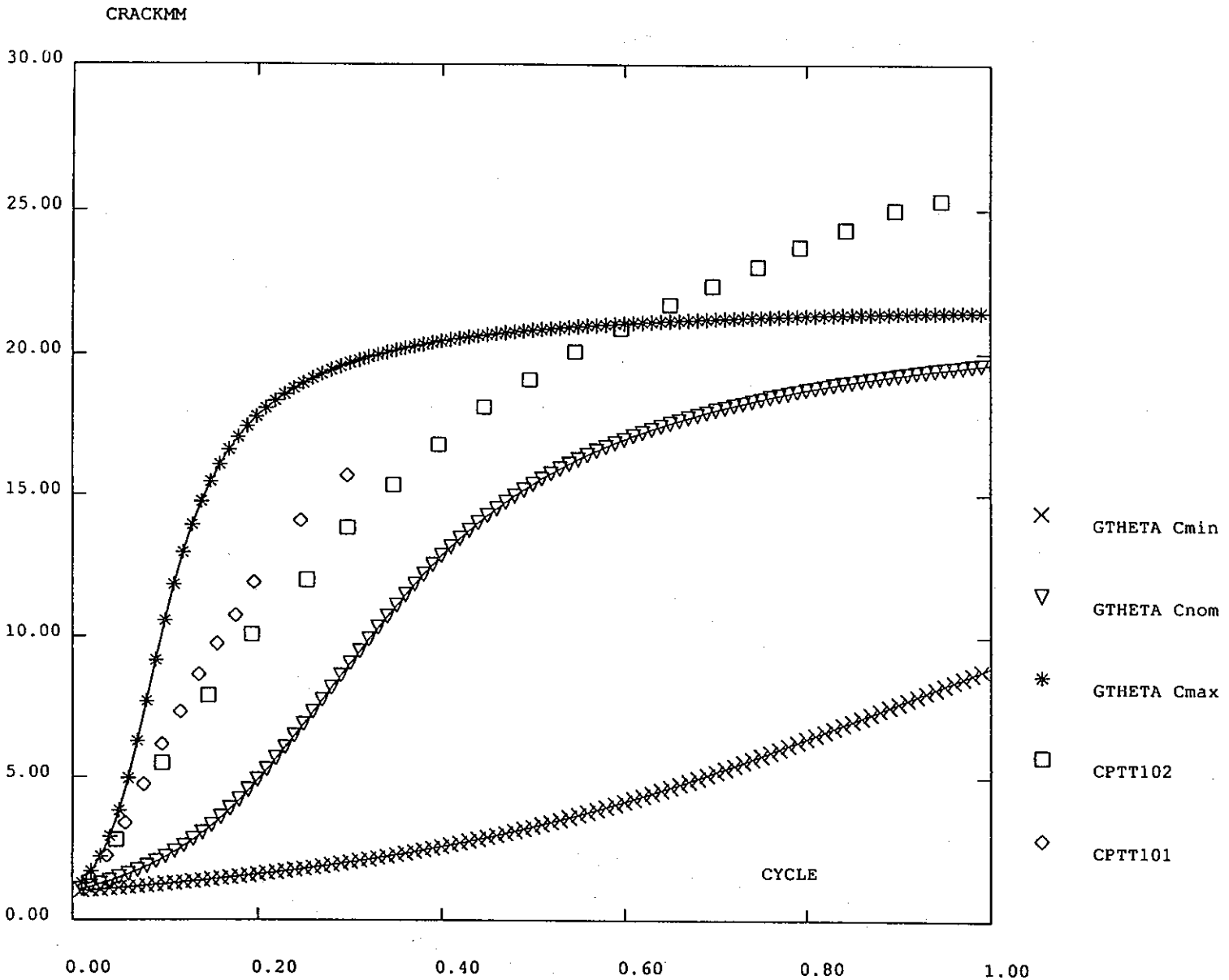

- Figure 19 -
Crack length (mm) versus number of cycles (CASTEM 2000 / Measured Values) in Plasticity

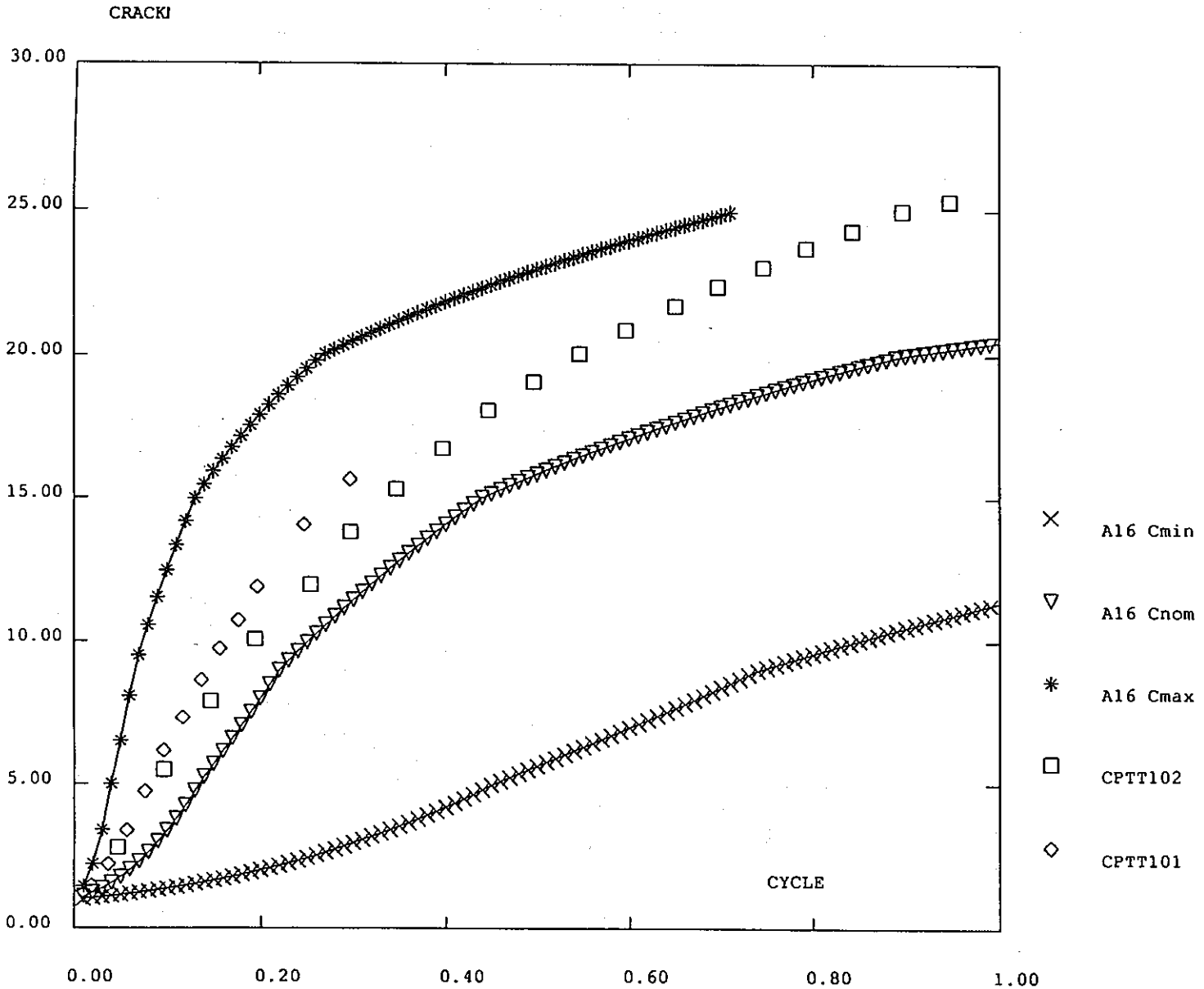

- Figure 20 -

Crack length (mm) versus number of cycles (A-16 Appendix / Measured Values) in Plasticity

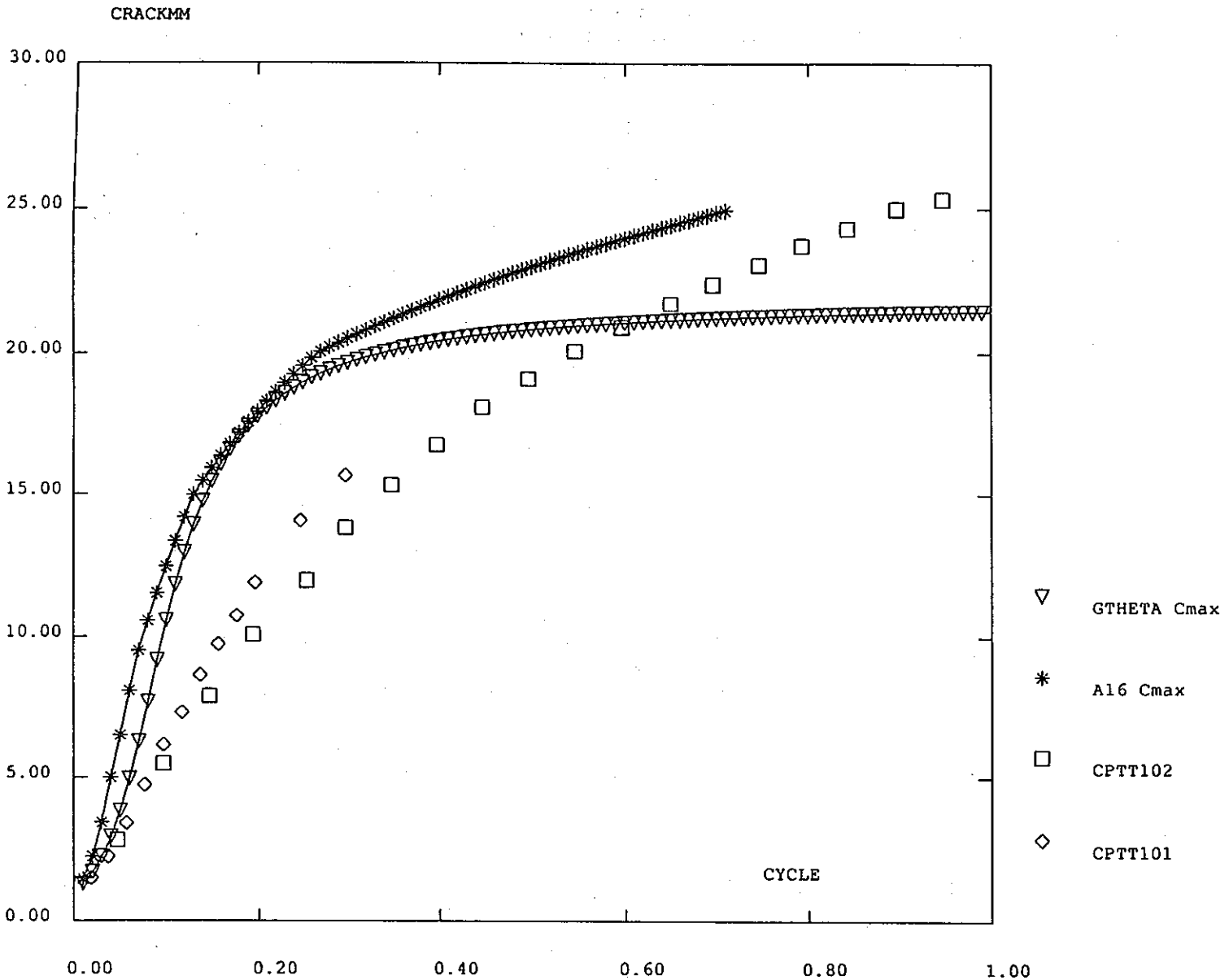

- Figure 21 -

Crack length (mm) versus number of cycles (CASTEM 2000 / A-16 Appendix) for Cmax (PARIS' law) in Plasticity

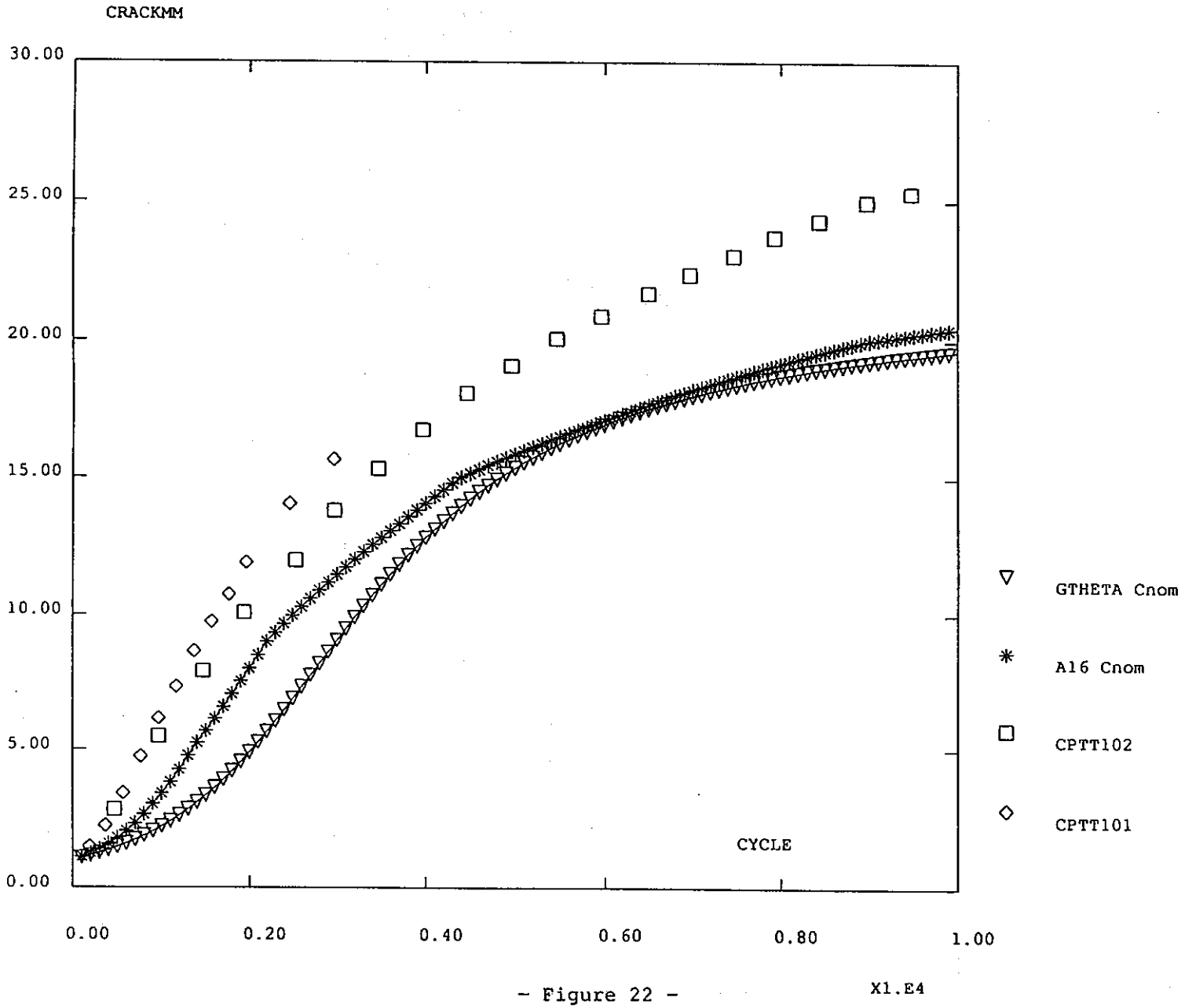

- Figure 22 -
Crack length (mm) versus number of cycles (CASTEM 2000 / A-16 Appendix)
for Cnom (PARIS' law) in Plasticity

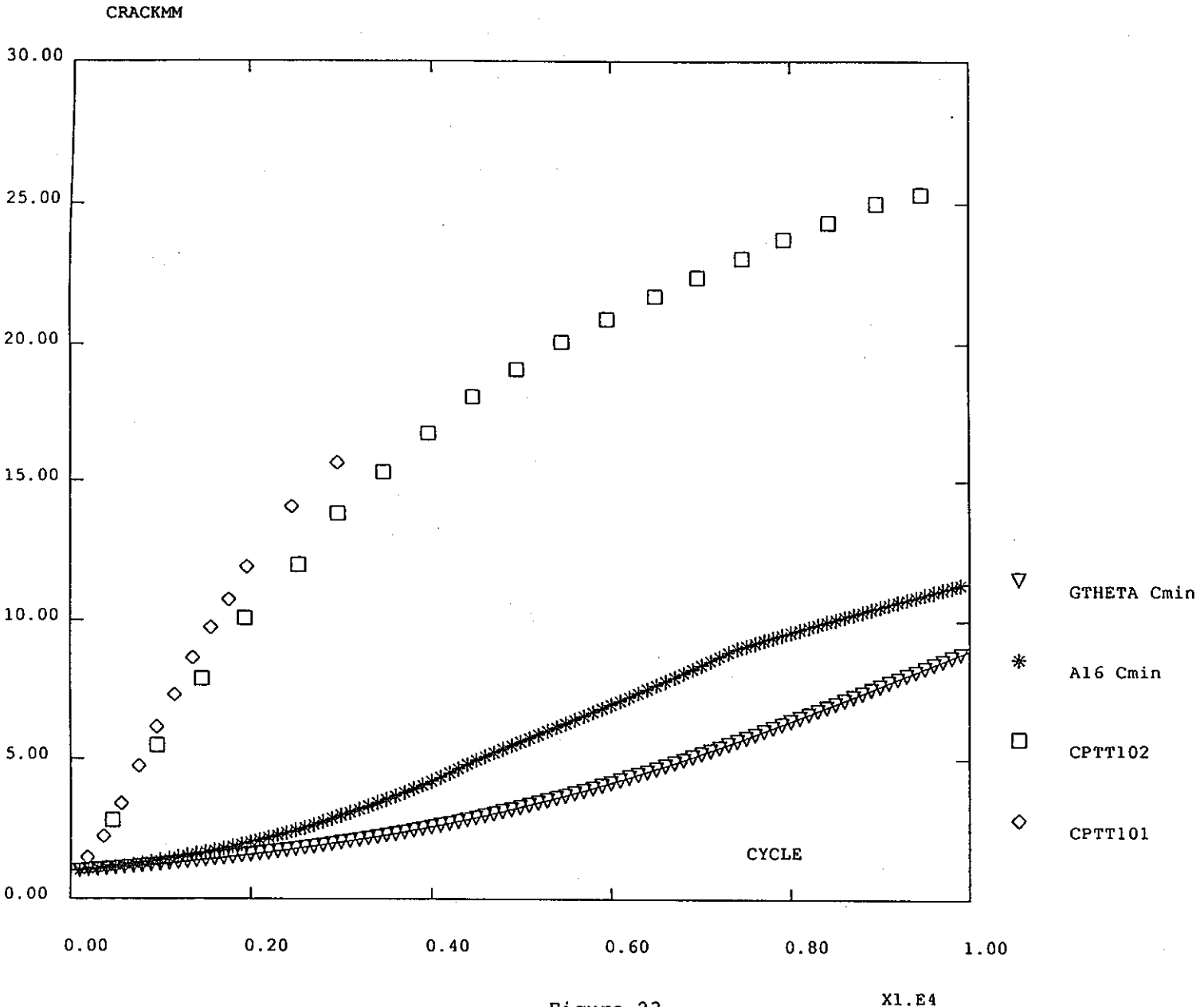

- Figure 23 -
Crack length (mm) versus number of cycles (CASTEM 2000 / A-16 Appendix)
for Cmin (PARIS' law) in Plasticity

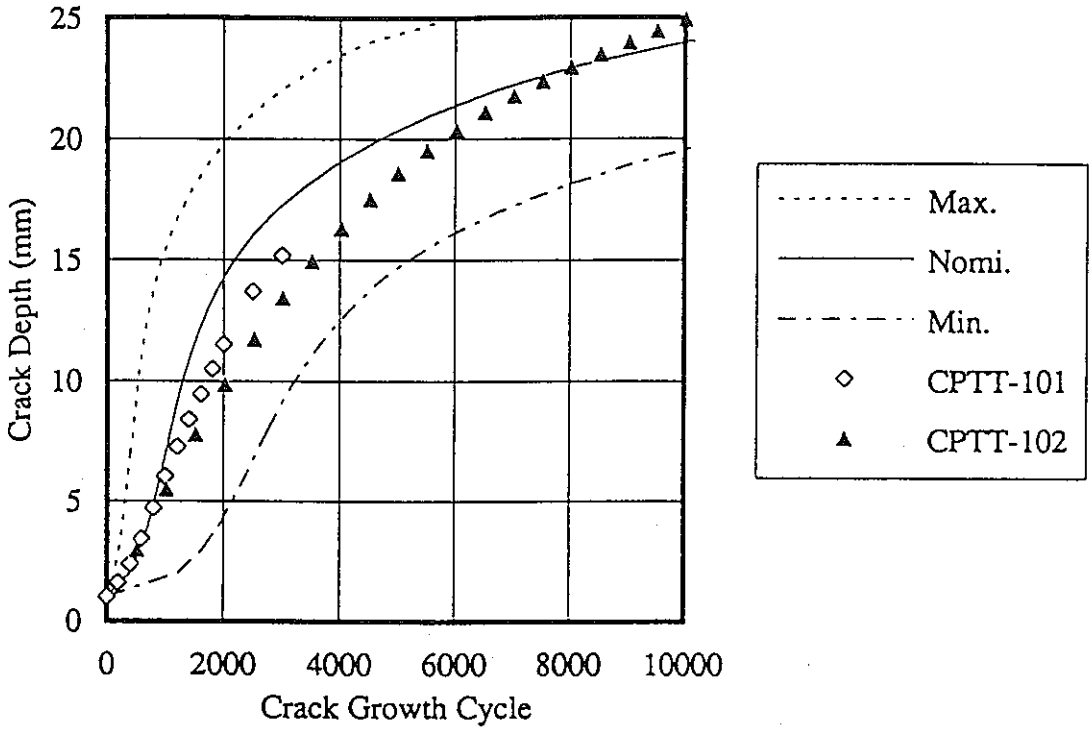

Transition of crack depth calculated with $\Delta \hat{J}_e$

- Figure 24a -
Crack length (mm) versus number of cycles (FINAS / Measured Values) in Elasticity

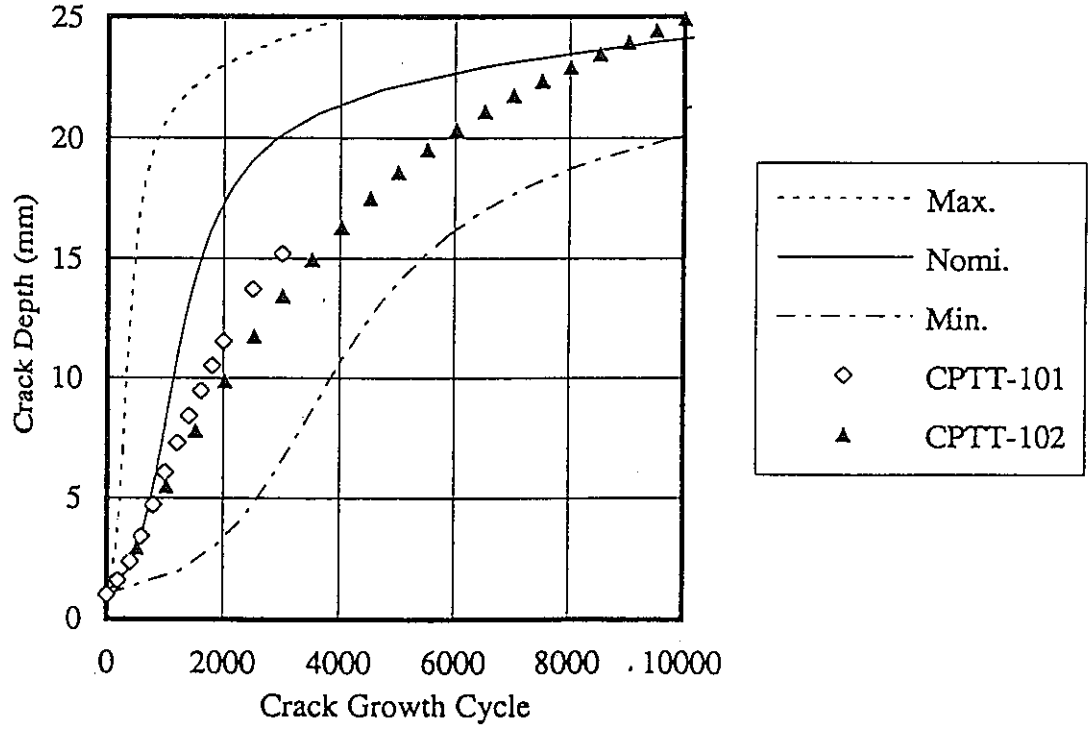

Transition of crack depth calculated with $\Delta \hat{J}_{ep}$

- Figure 24b -
Crack length (mm) versus number of cycles (FINAS / Measured Values) in Plasticity

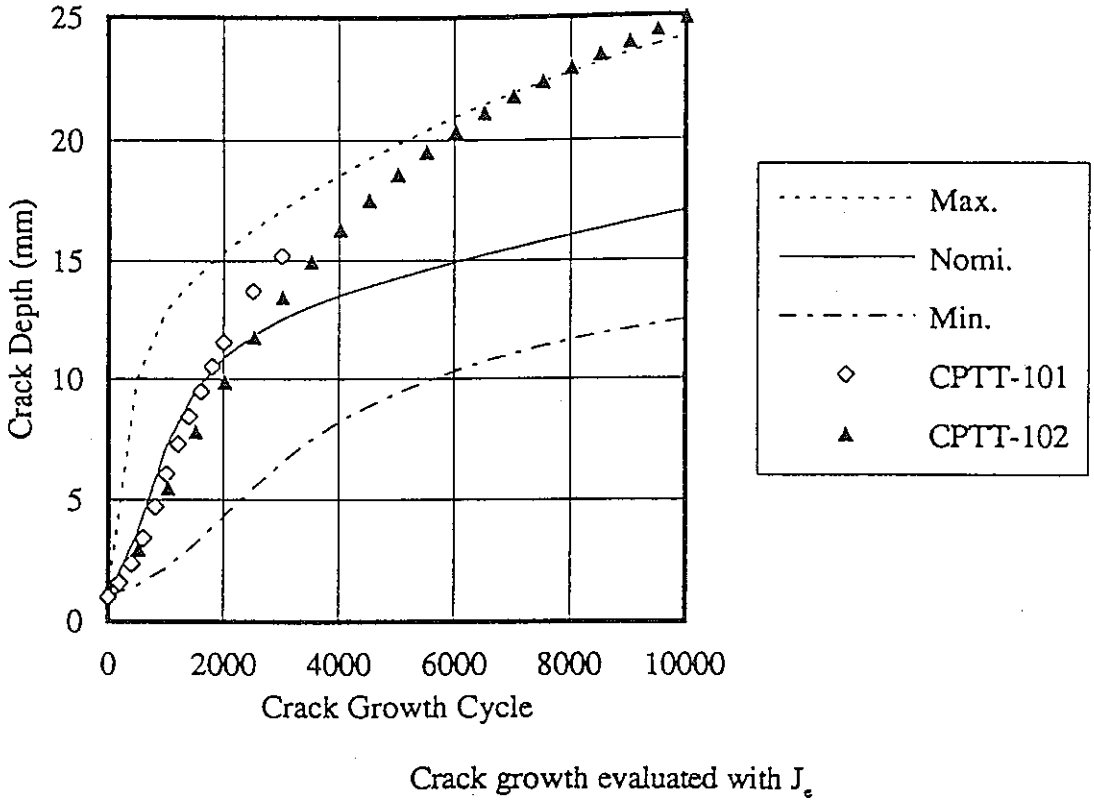

Crack growth evaluated with J_e

- Figure 25a -
Crack length (mm) versus number of cycles (Simplified Methods / Measured Values) in Elasticity

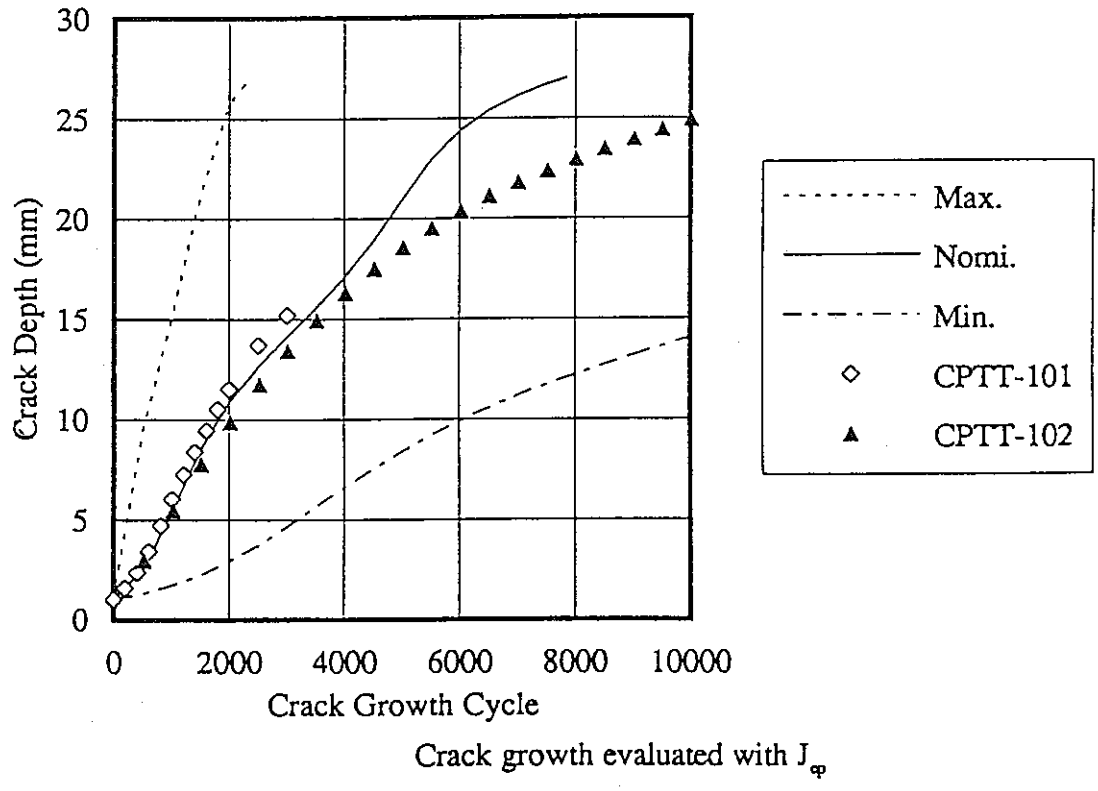

Crack growth evaluated with J_{ep}

- Figure 25b -
Crack length (mm) versus number of cycles (Simplified Methods / Measured Values) in Plasticity